PNNL-25755

Pacific Northwest
NATIONAL LABORATORY
Proudly Operated by Battelle Since 1965

# Review Team Focused Modeling Analysis of Radial Collector Well Operation on the Hypersaline Groundwater Plume beneath the Turkey Point Site near Homestead, Florida

**August 2016**

M Oostrom
L Vail

U.S. DEPARTMENT OF ENERGY

Prepared for the U.S. Department of Energy
under Contract DE-AC05-76RL01830

## DISCLAIMER



PACIFIC NORTHWEST NATIONAL LABORATORY
*operated by*
BATTELLE
*for the*
UNITED STATES DEPARTMENT OF ENERGY
*under Contract DE-AC05-76RL01830*

**Printed in the United States of America**

**Available to DOE and DOE contractors from the**
**Office of Scientific and Technical Information,**
**P.O. Box 62, Oak Ridge, TN 37831-0062;**
**ph: (865) 576-8401**
**fax: (865) 576-5728**
**email: reports@adonis.osti.gov**

**Available to the public from the National Technical Information Service,**
**U.S. Department of Commerce, 5285 Port Royal Rd., Springfield, VA 22161**
**ph: (800) 553-6847**
**fax: (703) 605-6900**
**email: orders@ntis.fedworld.gov**
**online ordering: http://www.ntis.gov/ordering.htm**

This document was printed on recycled paper.
(9/2003)

PNNL-25755

# Review Team Focused Modeling Analysis of Radial Collector Well Operation on the Hypersaline Groundwater Plume beneath the Turkey Point Site near Homestead, Florida

M Oostrom
L Vail

August 2016

Prepared for
Nuclear Regulatory Commission

Pacific Northwest National Laboratory
Richland, Washington 99352

# Summary

Researchers at Pacific Northwest National Laboratory served as members of a U.S. Nuclear Regulatory Commission review team for the Florida Power & Light Company's application for two combined construction permits and operating licenses (combined licenses or COLs) for two proposed new reactor units—Turkey Point Units 6 and 7. The review team evaluated the environmental impacts of the proposed action based on the October 29, 2014 revision of the COL application, including the Environmental Report, responses to requests for additional information, and supplemental information. As part of this effort, team members tasked with assessing the environmental effects of proposed construction and operation of Units 6 and 7 at the Turkey Point site reviewed two separate modeling studies that analyzed the interaction between surface water and groundwater that would be altered by the operation of radial collector wells (RCWs) at the site. To further confirm their understanding of the groundwater hydrodynamics and to consider whether certain actions, proposed after the two earlier modeling studies were completed, would alter the earlier conclusions documented by the review team in their draft environmental impact statement (EIS; NRC 2015), a third modeling analysis was performed. The third modeling analysis is discussed in this report.

The simulations were conducted using the water-salt-energy mode of the STOMP (Subsurface Transport Over Multiple Phases) simulator (White and Oostrom 2006). The applicable governing equations are the component mass-conservation equation for water and salt, and the energy conservation equation. The simulator allows for the consideration of density-driven flow and temperature effects caused by the seepage of warm hypersaline water from the unlined cooling-canal system (CCS) into the saline Biscayne aquifer. The model configuration was based on an earlier cross-sectional model published by Hughes et al. (2010). The two-dimensional (2D) model is 46 km long and extends 35 m vertically. The three-dimensional (3D) model that represents an extension of the 2D model is 2 km wide.

The initial conditions for both the 2D and 3D simulations are obtained using a steady-state simulation with a Biscayne Bay hydraulic head of 0.2 m and a west boundary head of 1.05 m. The long-term (10,000 year) simulations yielded a typical salt intrusion front, extending below the CCS. For the subsequent hypersaline water infiltration simulations, the same boundary conditions as proposed by Hughes et al. (2010) were used for hydraulic heads and temperature.

The main observations from the 2D simulations are as follows:

- CCS operation with warm 70 g/L hypersaline water leads to development of a large subsurface plume.
- Reducing the CCS salt concentration leads to a stable displacement of hypersaline water from the CCS subsurface.
- Increasing the hydraulic head in L-31E Canal limits westward migration of the hypersaline plume.
- Increasing the west boundary hydraulic head (indicative of increased recharge) results in a compression of the hypersaline plume at the west side of the CCS.
- Decreasing the west boundary hydraulic head (indicative of reduced recharge) has the opposite effect, leading to additional migration of the hypersaline plume in the western direction.
- During sea level rise, infiltrating saltwater from the Biscayne Bay pushes the hypersaline water toward the CCS subsurface. Over time, the interface between hypersaline water originating from the CCS and seawater becomes sharper and more vertical.

The main observations from the 3D simulations are as follows:

- Periodic extraction using the RCW system leads to fluctuating salt concentrations in the wells.
- During pumping, the concentrations initially increase because of advective transport of hypersaline water through the Upper Higher Flow Zone; the concentrations then decrease because of the influence of extracted Biscayne Bay saltwater.
- Between pumping episodes, the concentrations slightly increase due to diffusion of hypersaline water eastward; the well salt concentrations do not change significantly from year to year.
- RCW pumping increases the concentration gradients between the hypersaline plume below the CCS and Biscayne Bay saltwater in the upper parts of the aquifer and removes some of the hypersaline water from the Fort Thompson formation; the extracted volumes originate largely from the Biscayne Bay (>95 %); pumping rate reduction (up to 10% of maximum) and duration reduction (50 %) do not considerably influence well concentrations. This result indicates that the proposed RCW operation with 86,400 gal/min withdrawal rate over 60 days per year completely dominates flow and transport adjacent to the RCWs because reasonable variations in the rate and duration do not considerably influence well concentrations.
- Boundary condition modifications (i.e., L-31E Canal head and west boundary head increases) applied to the west of the CCS do not influence RCW extraction behavior.
- Seawater rise in Biscayne Bay leads to decreasing RCW saltwater concentration over time because the increasing Biscayne Bay hydraulic head displaces hypersaline water toward the CCS subsurface.
- Operation of remediation wells in the Lower Higher Flow Zone below the Interceptor Ditch does not influence extracted RCW salt concentrations.
- Salt concentrations in the remediation wells are predicted to increase to CCS levels within a year.
- Freshening of the CCS surface water results in reduced RCW salt concentrations with relatively minor (<1 g/L) fluctuations.

There is no question that some perturbations of the baseline boundary conditions result in significantly altered environmental baselines. However, while the operation of the RCWs would change the incremental impacts of the RCWs on the salinity distribution of the aquifer, the alterations would remain at levels that may only be detectable within the immediate vicinity of the RCWs. While the numerical model analysis suggest the slight westward movement of hypersalinity assumed in the conceptual model from the operation of the RCWs, it does not demonstrate any plausible upward impelling force above the RCWs that would result in hypersalinity moving into the Bay as a result of the RCWs. As the review team has acknowledged in the EIS, when the water surface elevation in the cooling canals exceeds that in the Bay, the water will follow the gradient of the impelling force into the Bay and may contribute to salinity in the Bay. Both of the above effects also apply for other tracers, including nutrients and tritium.

Although the primary focus of the review reported here is on the incremental effects of the RCWs on the Biscayne Bay, the review team also acknowledges the cumulative impacts of other changes, including those from sea level rise and possible future regulatory actions. While the scenarios considered in this analysis tended to be bounding for sea level rise and possible regulatory actions, they also provide a basis for assessing the cumulative impacts. The review team has no jurisdiction over the proposed regulatory actions considered and assumes that mitigation actions proposed by state and county agencies would improve the baseline environment. As long as the incremental effect of the RCWs remains minor, the cumulative effects would also remain minor.

The minor localized alterations in salinity distribution suggest that the operation of the RCWs is unlikely to interfere with any of the proposed mitigation actions.

# Acknowledgments

The authors acknowledge the valuable comments and suggestions in scoping, performing, and documenting the analysis provided by Eric Stabenau and Kevin Kotun, South Florida Natural Resource Center, National Park Service; Dan Barnhurst, New Reactor Office, Nuclear Regulatory Commission; and Paul Thorne, Pacific Northwest National Laboratory.

# Acronyms and Abbreviations

| | |
|---|---|
| °C | degree(s) Celsius |
| 2D | two-dimensional |
| 3D | three-dimensional |
| CCS | cooling-canal system |
| cm | centimeter(s) |
| COC | Conditions of Certification |
| EIS | environmental impact statement |
| FPL | Florida Power & Light Company |
| ft | foot(feet) |
| g | gram(s) |
| gal | gallon(s) |
| IWF | industrial wastewater facility |
| J | joule(s) |
| kg | kilogram(s) |
| L | liter(s) |
| LHFZ | Lower Higher Flow Zone |
| m | meter(s) |
| RCW | radial collector well |
| RTF | Review Team Focused |
| s | second(s) |
| STOMP | Subsurface Transport Over Multiple Phases |
| UHFZ | Upper Higher Flow Zone |

# Contents

# Figures

# Tables

# 1.0 Introduction

Pacific Northwest National Laboratory researchers served as members of a U.S. Nuclear Regulatory Commission review team for the Florida Power & Light Company's (FPL's) 2009 application for two combined construction permits and operating licenses (combined licenses or COLs) for two proposed new reactor units—Turkey Point Units 6 and 7. The review team evaluated the environmental impacts of the proposed action based on the October 29, 2014 revision of the COL application (FPL 2014a), including the Environmental Report (ER) (FPL 2014b), responses to requests for additional information, and supplemental information. As part of this effort, team members tasked with assessing the environmental effects of proposed construction and operation of Units 6 and 7 at the Turkey Point site reviewed two separate modeling studies that analyzed how the interaction between surface water and groundwater would be altered by the operation of proposed radial collector wells (RCWs) at the site. The team performed a third modeling analysis to further confirm their understanding of the groundwater hydrodynamics and to consider whether certain actions, proposed after the two earlier modeling studies were completed, would alter the earlier conclusions documented by the review team in the draft environmental impact statement (EIS, NRC 2015). This third modeling analysis is the subject of this report. The two earlier analyses are discussed in Appendix G.2.1 and G.2.2 of the draft EIS (NRC 2015).

## 1.1 Purpose and Scope

2D and 3D models of the subsurface of the Turkey Point cooling-canal system (CCS, also referred to as the IWF) were developed to assess the behavior of hypersaline saltwater emanating from the CCS. The 2D simulations were conducted to investigate the effects of CCS salinity, L-31E Canal head, Interceptor Ditch head, boundary conditions, and sea level rise. The 3D model was developed to evaluate potential impacts of RCW pumping on the movement of water between the CCS, the underlying Biscayne aquifer, and the Biscayne Bay. Numeric modeling and site potentiometric surface and boundary conditions were essential elements of the assessment.

### 1.1.1 Numerical Modeling

Numerical models are computer codes used to analyze the response of complex physical systems. Numerical models employ mathematical representations of physical processes to transform a specific set of initial conditions, boundary conditions, and process parameters into a time series of state variables at specific locations and times. Numerical models provide reliable enforcement of irrefutable principles such as conservation of mass for complex heterogeneous domains. By consistently applying assumptions that are explicitly codified in the model and its inputs, a clearer understanding of the complex systems behavior can be achieved. Systematic perturbation of assumptions about initial conditions, boundary conditions, and model parameter provide a basis for assessing the sensitivity of assumptions and uncertainty in the overall assessment.

Numerical modeling is often a necessary element of National Environmental Policy Act assessments that involve complex physical systems such as aquifers. However, numerical models rarely are sufficient as the sole basis of an assessment. The conceptual understanding that provides the framework for the model has limitations. It is the responsibility of the analyst looking at the model results to understand the implications of these limitations on the assessment.

Multiple distinct models can be used in multiple roles to assist on the same assessment. In the Turkey Point hydrologic modeling assessment described herein three distinct models were used in three distinct ways. Numerical models with different spatial scales and resolutions, models including different process

representations, and models with different goals give the analyst a stronger basis for making an assessment. It should be noted that numerical models are never perfect representations of any system and that a prudent analyst will also consider the role of monitoring and mitigation in making an impact determination in case the actual system does not fit within the assessment envelope considered. Models help the analyst determine whether monitoring is likely to detect such outliers in a timely manner. Models also help the analyst determine if the proposed mitigation will be effective.

### 1.1.2 Site Potentiometric Surface and Boundary Conditions

The impelling force that drives subsurface water movement is defined by the potentiometric surface—the level to which fresh water in a confined aquifer would rise were it completely pierced with wells. The potentiometric surface of the Biscayne aquifer beneath the Turkey Point site is complicated by the presence of freshwater, seawater, and hypersaline water. While these fluids are not immiscible, their density differences help to maintain an interface between them. The density differences influence the shape of the potentiometric surface. Water moves from higher potentiometric head toward lower potentiometric head proportionally to the viscosity of the fluid and intrinsic permeability of the subsurface matrix material. The potentiometric surface will shift as the water transports and the boundary conditions change.

The RCW system for Turkey Point is described in Chapter 3 of the EIS (NRC, in progress). RCWs behave more like tile drainage systems than like conventional wells. In a conventional well, all the water must move laterally into a small cross-sectional area causing significant drawdowns at the well where a RCW moves the volume vertically through a much larger cross-sectional area. For instance, the nominal increase in cross-sectional area of a conventional 6 in. well screened over 100 ft relative to the surface area of a RCW with 100 ft radial arms is a 400 factor increase. This results in smaller perturbations in the potentiometric surface and emphasizes vertical water motion over lateral water motion. RCWs are placed at shallow depths beneath surface waterbodies that effectively provide an unconstrained source of water or a boundary condition unaffected by withdrawal from the RCWs. Differences on stratigraphy and hydraulic conductivity also influence the potentiometric surface around RCWs.

A variety of boundary conditions exist at the Turkey Point site, including potentiometric boundary conditions and salinity boundary conditions. Biscayne Bay represents both a specified potentiometric boundary condition and a specified salinity boundary condition to the upper surface of the conceptual model. The Bay potentiometric boundary condition varies in response to tides, storm surge, and sea level rise. The industrial wastewater facility (IWF) cooling canals, Interceptor Ditch, and L-31 Canal also represent potentiometric and salinity boundary conditions on the upper surface of the conceptual model. These boundary conditions may also vary over time and space.

The western vertical boundary is also represented by a specified potentiometric and salinity boundary condition. Wet periods cause this boundary condition to rise and dry periods cause this boundary to fall.

Two types of wells, the RCWs and remediation wells, also represent specified flux sink boundary conditions. The RCWs are the focus of this assessment. As discussed in Section 2.3, the remediation wells are proposed to abate the westward migration of the hypersaline plume. The exact design of this proposed remediation system is not known at this time.

All of the boundary conditions experience differing degrees of normal variability. For instance, a significant rainfall event will increase the potentiometric head in the western boundary, decrease the salinity in the cooling canals, increase the head in the cooling canals, increase head in the L-31 Canal, increase recharge, and decrease salinity in Biscayne Bay. Also, boundary conditions are linked to varying degrees. For instance, an increase in the Bay water surface elevation can influence the elevation of water

in the cooling canals. Including these linkages and time-varying boundary conditions can make it more difficult for the analyst to understand the results because of too many confounding factors. One of the benefits of numerical models is that they allow selective and limited interactions of boundary conditions to reduce the confounding issues in interpreting the model results.

The spatial distribution of the salinity at the initiation of operation is the dominant initial condition. The location of the hypersaline plume and the freshwater-seawater interface are initial conditions. As discussed in Section 2.3, a variety of regulatory actions related to the IWF may alter the initial conditions before the proposed Units 6 and 7 would ever require operation of the RCWs. The initial conditions developed through a sequence of processes that occurred in the past. Prior to operation of the RCWs and the IWF a freshwater-saltwater interface formed based on patterns of freshwater flow from the aquifer to the ocean. As inland water demands and recharge patterns changed the saltwater interface moved farther inland. During this period, the IWF was constructed and the denser hypersaline water that occurred at times moved downward under the unlined cooling canals and displaced the less dense water below, thereby resulting in a hypersaline plume that extends all the way down to the base of the aquifer.

The hypersaline groundwater plume formed beneath the cooling-canal system that was used for Turkey Point Units 1, 2, 3, 4, and 5. The proposed Units 6 and 7 would rely primarily on reclaimed water from a regional wastewater treatment plant and discharge blowdown into a very deep formation called the Boulder Zone. Therefore, the review team determined that under normal operation the cooling system impact of Units 6 and 7 on the shallow subsurface aquifer and cooling canals would be de minimis. However, the proposed design for Units 6 and 7 also includes an RCW system as a backup in case of a loss of access to reclaimed water. The RCWs are designed to encourage downward movement of water from Biscayne Bay into a set of shallow laterals. However, the review team determined that even a very shallow depression in the potentiometric head in the aquifer around the RCW will result in some lateral movement in the groundwater.

## 1.2 Report Contents and Organization

The ensuing sections of this report contain brief descriptions of the site being modeled, the simulator used to model site behaviors, the 2D and 3D model configurations, the associated parameter values, and how the initial and bounding conditions were derived for the simulations. Section 7.0 provides a tabulated overview of the simulations by case number and title as a lead into the presentation of the 2D and 3D simulation results in Sections 8.9 and 9.0. A discussion of the results is provided in Section 10.0. Conclusions of the overall assessment are provided in Section 11.0.

# 2.0 Site Description

The 2D model configuration was based on an earlier cross-sectional model published by Hughes et al. (2010). The 2D model (Figure 2.1) has a length of 46 km and a vertical extent of 35 m. The 3D model represents an extension of the 2D model and has a width of 2 km. Both models extend approximately 15.5 km farther offshore than shown in Figure 2.1, allowing for the evaluation of Biscayne Bay effects. The models represents part of the Turkey Point power plant large CCS overlying a permeable limestone aquifer. At its maximum extent (south of the 2D model cross section), the CCS has 40 canals, 32 of which transport warm water toward the south (i.e., discharge canals), and 8 of which return water to the plant (i.e., return canals). In the model cross section used by Hughes et al. (2010) and for this modeling effort, 22 discharge and 8 return canals are intersected by the cross section used. The 60 m wide canals are separated by 27 m wide berms. The cooling water salinity is considerably higher than the natural salt concentrations in groundwater in the aquifer, which likely leads to unstable density-dependent convection. The cooling water temperatures are also higher than those of the aquifer water, which potentially reduces the density effects. A more detailed description of the CCS can be found in Section 2.3 of the Turkey Point Units 6 and 7 EIS (NRC 2016). Water exchange between the CCS and groundwater occurs because the canals are unlined. An Interceptor Ditch (Figure 2.1), located west of the CCS, is used to create an artificial groundwater gradient that inhibits shallow flow of the hypersaline water from the CCS to the west. Another prominent feature is the L-31E Canal, located just west of the Interceptor Ditch. The subsurface of the model area consists of an unconfined surficial aquifer characterized by the presence of two relatively thin very high-permeability zones (Cunningham et al. 2006) with hydraulic conductivities larger than 1,000 m/day.

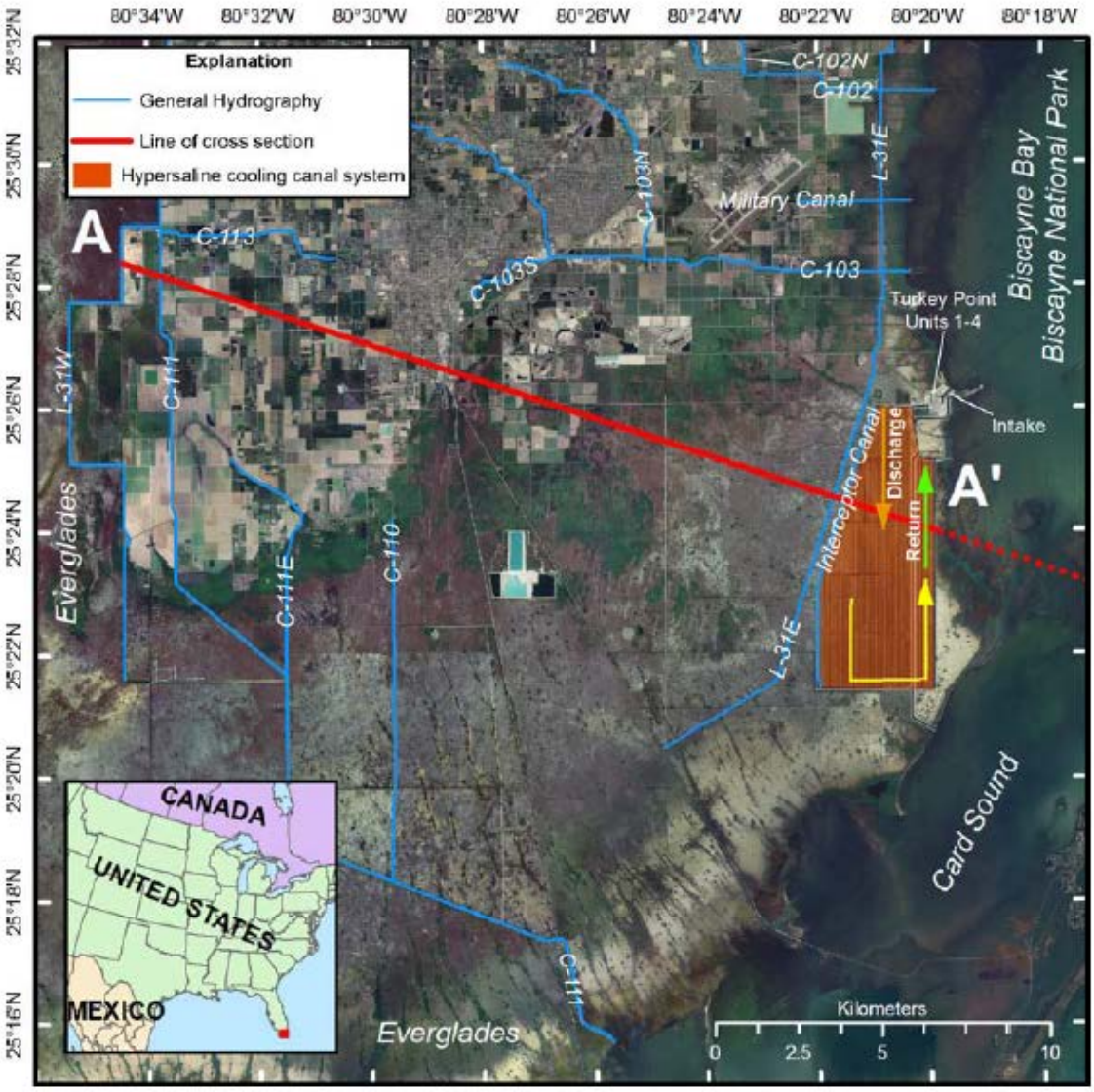


**Figure 2.1**. Cross-sectional model of the Turkey Point CCS (after Hughes et al. 2010). Note that the model extends approximately 15,500 m farther offshore than shown in the figure. The general hypersaline CCS flow direction is indicated with arrows.

# 3.0 Numerical Simulator

The simulations were conducted using the water-salt-energy mode of the STOMP (Subsurface Transport Over Multiple Phases) simulator (White and Oostrom 2006). The applicable governing equations are the component mass-conservation equation for water and salt, and the energy conservation equation. The simulator allows for the consideration of density-driven flow and temperature effects caused by the seepage of warm hypersaline water from the unlined canals of the CCS into the saline Biscayne aquifer. The governing partial differential equations are discretized with the integrated-volume finite difference method by integrating over a control volume. Using Euler backward time differencing, which yields a fully implicit scheme, a series of nonlinear algebraic expressions is derived. The algebraic forms of the nonlinear governing equations are solved with a multi-variable, residual-based Newton-Raphson iterative technique, in which the Jacobian coefficient matrix is composed of the partial derivatives of the governing equations with respect to the primary variables.

# 4.0 Model Configuration and Discretization

The layered configuration of the Biscayne aquifer and assignment of hydraulic properties to the layers were based on work performed by FPL and documented in the Final Safety Analysis Report and reports related to the power uprate for FPL Units 3 and 4. Figure 4.1 shows the geologic layering of the current model, including the thin Upper Higher Flow Zone (UHFZ) and the Lower Higher Flow Zone (LHFZ) of the Miami Limestone. Other units are the remainder of the Miami Limestone, the Key Largo, and the Fort Thompson formations. The model includes 22 discharge canals and 8 return canals, consistent with the cross section shown in Figure 4.1. The easternmost discharge canal is the Grand Canal, which is approximately 4 m deeper than the adjacent canals. The hydraulic conductivities assigned to the model layers are shown in Table 5.2 (see Section 5.0). For the 3D model, the same stratigraphy was used throughout the computational domain. In the current model configuration, the two "higher flow zones" were defined to be 1 m thick based on borehole data, rather than the 3 m thickness used by Hughes et al. (2010).

The 3D model configuration is shown in Figure 4.2. The model has a total width of 2 km, although the numerical model only comprises the right half of the total domain using the center line as a line of symmetry. The 3D model incorporates three RCWs, located 1,500, 1,700, and 1,900 m into the Biscayne Bay. Each RCW has a horizontal length of 150 m in the right half of the computational domain and all RCW laterals are installed in the UHFZ. The RCWs are assumed to operate continuously or for 60 days per year at a maximum pumping rate of 86,400 gal/min. The model also has the option to use up to 10 vertical remediation wells with open intervals located below the Interceptor Ditch in the LHFZ). FPL plans to install and operate these wells along the western side of the CCS to remove hypersaline water and limit its migration to the west. The extracted water will be pumped at a maximum combined rate of 12,000,000 gal/day. The 2D domain was discretized into 876 × 45 grid cells for a total of 39,420 nodes. Considerable refinement of the model grid was applied below the CCS. For the 1 km width of the 3D model, 72 grid cells were used, resulting in a total of 2,838,420 nodes.

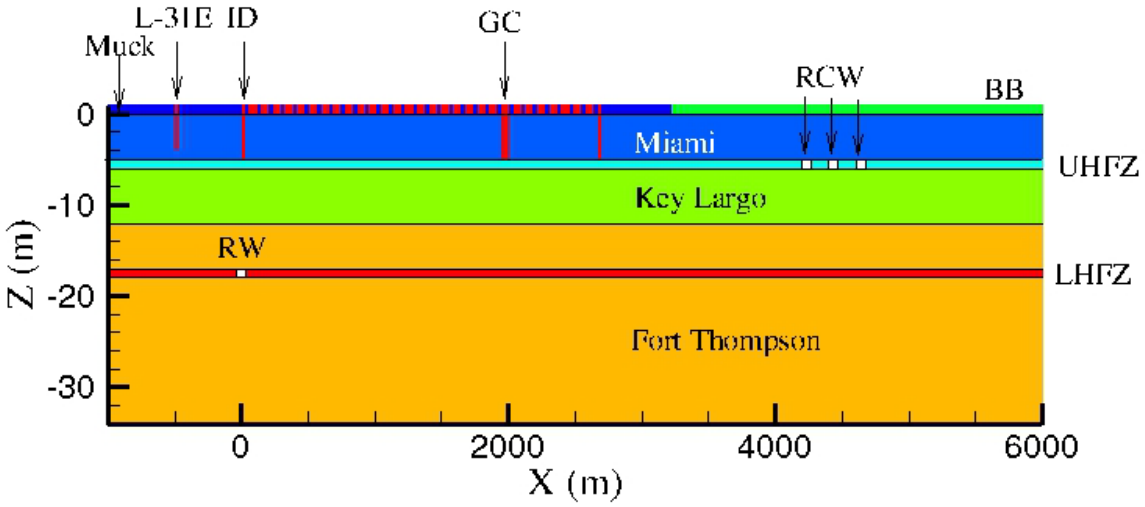


**Figure 4.1**. Geologic Layering and Location of the CCS (including the Grand Canal; GC) L-31E Canal, Interceptor Ditch (ID), Biscayne Bay (BB), Radial Collector Wells (RCW), and Remediation Wells (RW)

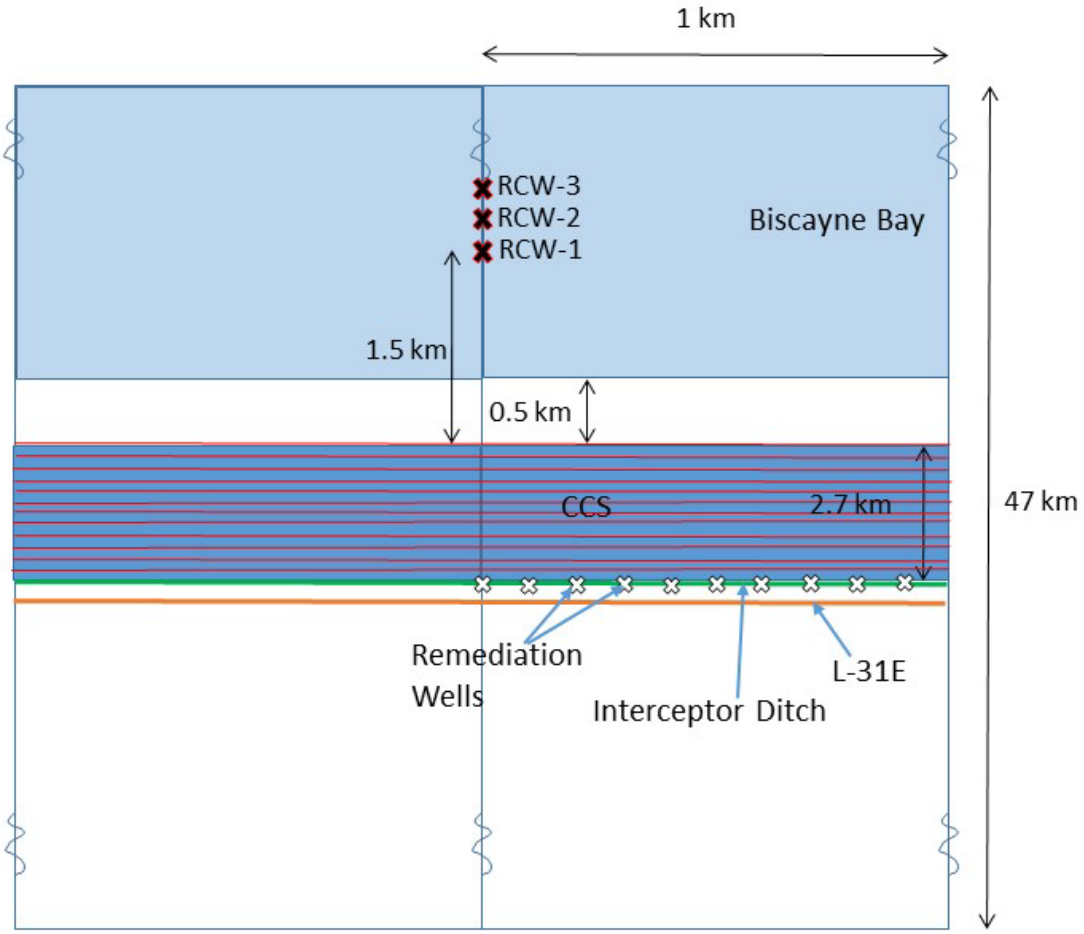


**Figure 4.2**. Top View of the Symmetrical 3D Model

# 5.0 Parameter Values

The fluid and aquifer properties are summarized in Table 5.1. The density-concentration relationships were obtained from Millero and Huang (2009). The hydraulic conductivities of the layers are listed in Table 5.2.

**Table 5.1**. Model Parameter Values

| Model Parameter | Value |
|---|---|
| Reference Temperature (°C) | 20 |
| Land Surface Temperature (°C) | 24.4 |
| Seawater Temperature (°C) | 26.2 |
| Cooling-Canal System Temperature (°C) | 35.6 |
| Longitudinal Dispersivity (m) | 1 |
| Transverse Dispersivity (m) | 0.1 |
| Molecular Diffusion Coefficient Salt ($m^2/s$) | 1.477e-09 |
| Porosity | 0.2 |
| Particle Density ($kg/m^3$) | 2650 |
| Specific Heat Fluid (J/(kg°C)) | 4.183 |
| Specific Heat Sediment (J/(kg°C)) | 835.0 |
| Thermal Conductivity Fluid (J/(m°Cs)) | 0.61 |
| Thermal Conductivity Sediment (J/(m°Cs)) | 3.59 |
| Seawater Concentration (g/L) | 35.0 |
| Cooling-Canal Salt Concentration (g/L) | 70.0 |

**Table 5.2**. Hydraulic Conductivity of the Model Layers (FPL 2015)

| Layer Name | Horizontal Hydraulic Conductivity (cm/s) | Vertical Hydraulic Conductivity (cm/s) |
|---|---|---|
| Muck | 0.0044 | 0.00044 |
| Miami Limestone | 0.088 | 0.00590 |
| Upper High Flow Zone | 30.0 | 3.700 |
| Key Largo | 5.90 | 0.740 |
| Fort Thompson | 0.33 | 0.033 |
| Lower High Flow Zone | 1.70 | 0.170 |

# 6.0 Initial and Boundary Conditions

The initial conditions for both the 2D and 3D simulations were obtained using a steady-state simulation with a Biscayne Bay hydraulic head of 0.2 m and a west boundary head of 1.05 m. The long-term (10,000 year) simulations yielded a typical salt intrusion front, extending below the CCS. For the subsequent hypersaline water infiltration simulations, the same boundary conditions as those proposed by Hughes et al. (2010) were used (Table 6.1) for hydraulic heads and temperature. Between the L-31E Canal and the west boundary, a no-flux boundary was established for the model surface without the consideration of spatial and temporal variations in local recharge. Instead, regional groundwater flow was assumed to enter solely from the west boundary.

**Table 6.1**. Overview of Imposed Boundary Condition for Hydraulic Head, Temperature, and Salt Concentration.

| Feature | Hydraulic Head (m) | Temperature (ºC) | Salt Concentration (g/L) |
|---|---|---|---|
| West Boundary | 1.05 | 24.4 | 0 |
| L-31E Canal | 0.48 | 24.4 | 0 |
| Interceptor Ditch | 0.43 | 24.4 | 0 |
| Discharge Canals | 0.39 | 35.6 | 70 |
| Return Canals | 0.09 | 34.2 | 70 |
| Biscayne Bay | 0.20 | 28.2 | 35 |

# 7.0 Overview of the 2D and 3D Simulations

Overviews of the conducted 2D and 3D simulations are provided in Table 7.1 and Table 7.2, respectively. The 2D and 3D Base Case simulations involve a 25-year infiltration event of 70 g/L hypersaline water. Each sensitivity simulation has a duration of 40 years.

**Table 7.1**. Overview of 2D Sensitivity Simulations

| Name | Variation with Base Case | Results Figures | Comments |
|---|---|---|---|
| 2D-1 | 0 g/L salt concentration in CCS | 8,4, 8.5, 8.6 | Representative of freshwater. |
| 2D-2 | 34 g/L salt concentration in CCS | 8.7, 8.8, 8.9 | Seawater concentration. Consistent with proposed freshening targets mentioned in Section 2.3 of the EIS. |
| 2D-3 | 90 g/L salt concentration in CCS | 8.10, 8.11, 8.12 | Extreme hypersaline. No freshening. |
| 2D-4 | Head in CCS doubled | 8.13, 8.14, 8.15 | Potentiometric head increase in CCS. Increase consistent with freshening. |
| 2D-5 | Seawater rise in Biscayne Bay of 0.5 m over 40 years | 8.16, 8.17, 8.18 | Plausible sea level rise. |
| 2D-6 | Seawater rise in Biscayne Bay of 1.5 m over 40 years | 8.19, 8.20, 8.21 | Plausible sea level rise. |
| 2D-7 | Head in L-31E Canal increased by 0.5 m | 8.22, 8.23, 8.24 | Shallow hydraulic control of westward migration proposed by Miami-Dade County Department of Environmental Resources Management. |
| 2D-8 | Head at west boundary increased by 1.0 m | 8.25, 8.6, 8.27 | Rehydration of inland including Model Lands. |
| 2D-9 | Head at west boundary decreased by 1.0 m | 8.28, 8.29, 8.30 | Drought of inland and Model Lands. |

**Table 7.2**. Overview of 3D Simulations

| Name | Description | Results Figures |
|---|---|---|
| 3D Base Case | 86,400 gal/min divided evenly over three wells (RCW-1, RCW-2, and RCW-3). Wells operate 60 days per calendar year. Total system operation time 20 years. CCS operating with 70 g/L salt concentration. | 9.1, 9.3 |
| 3D-1 | As Base Case but no pumping | 9.2, 9.3 |
| Pumping Scenarios | | |
| 3D-2 | As Base Case but with half the extraction rate (43,200 gal/min) | 9.4 |
| 3D-3 | As Base Case but with one-tenth of the extraction rate (8,640 gal/min) | 9.5 |
| 3D-4 | As Base Case but with 30 days per year of operation | 9.6 |
| 3D-5 | As Base Case but only two operational cycles during the first two years and no pumping afterwards | 9.7 |
| 3D-6 | As Base Case but with continuous pumping | 9.8 |
| Variations in Boundary Condition Scenarios | | |
| 3D-7 | As Base Case but with 0.5 m elevated head in L-31E Canal | 9.9, 9.10, 9.11 |
| 3D-8 | As 3D-7 but without pumping | 9.10b, 9.11 |
| 3D-9 | As Base Case but with 1 m increased head at west boundary | 9.12, 9.13a, 9.14 |
| 3D-10 | As 3D-9 but without pumping | 9.13b, 9.14 |
| 3D-11 | As Base Case but with 1 m decreased head at west boundary | 9.15, 9.16a, 9.17 |
| 3D-12 | As 3D-11 but without pumping | 9.16b, 9.17 |
| 3D-13 | As Base Case but with 1.5 m sea level rise over 40 years | 9.18, 9.19a, 9.20 |
| 3D-14 | As 3D-13 but without pumping | 9.19b, 9.20 |
| 3D-15 | As Base Case but with 0.5 m sea level rise over 40 years | 9.21, 9.22a, 9.23 |
| 3D-16 | As 3D-15 but without pumping | 9.22b, 9.23 |
| Consideration on Remedial Pumping West of CCS | | |
| 3D-17 | As Base Case but with 4 remediation wells continuously operating at 12,000,000 gal/day | 9.24, 9.25 |
| Scenarios after Aquifer Refreshing | | |
| 3D-18 | Pumping after refreshing with 34 g/L salt water from CCS for 25 years. 86,400 gal/min divided evenly over three wells (RCW-1, RCW-2, and RCW-3). Total system time 20 years. CCS operating with 34 g/L salt concentration. | 9.26 |
| 3D-19 | As 3D-18 but without pumping. | 9.27 |
| 3D-20 | As 3D-18 but with 1.5 m sea level rise over 40 years | 9.28 |
| 3D-21 | As 3D-18 but with 1 m decreased head at west boundary, 1m increased head in CCS, and 1.5 m sea level rise over 40 years | 9.29 |
| 3D-22 | Initial conditions with pristine aquifer. CCS operating for 20 years with 34 g/L salt concentration. Pumping as in 3D-18. | 9.30 |

# 8.0 2D Simulation Results

2D simulations results showing salt concentration distributions for the Base Case and sensitivity simulations are presented in the following sections.

## 8.1 Base Case Simulation

Salt concentration distributions at various times are shown in Figure 8.1. Figure 8.1a shows that less than 30 days after initiation of the CCS operation, hypersaline water emanating from the Grand Canal has migrated all the way to the bottom of the aquifer. Downward migration as a result of density differences from the other shallower canals is considerably slower. Unstable convective flow patterns develop from the plumes descending downwards from the individual canals, and fresher groundwater is forced upward in the areas between the plumes. After 1 year, most of subsurface below the CCS has become hypersaline and the plume starts to migrate laterally in the Fort Thompson formation below the LHFZ. Although this transport might be considered to be reasonably fast, it is much slower than what is reported by Hughes et al. (2010) for a homogeneous subsurface with a hydraulic conductivity of 10,000 m/day. After 5 years of operation, differences in salt concentrations are relatively low; the approximate plume growth at the bottom of the aquifer is 25 m/yr both toward the west and the east. The influence of the UHFZ and LHFZ on the plume behavior is small and no obvious additional spreading is observed in either layer.

The temperature distribution plots in Figure 8.2 show that heat propagates considerably slower than salt due to heat exchange in the subsurface. The thermal plumes are also more diffuse. The lateral extent of the thermal plume is less than the overall hypersaline salt plume. The thermal results are consistent with the findings of Hughes et al. (2010), showing that the effects of temperature on hypersaline water transport are far less pronounced than the salt concentration effects.

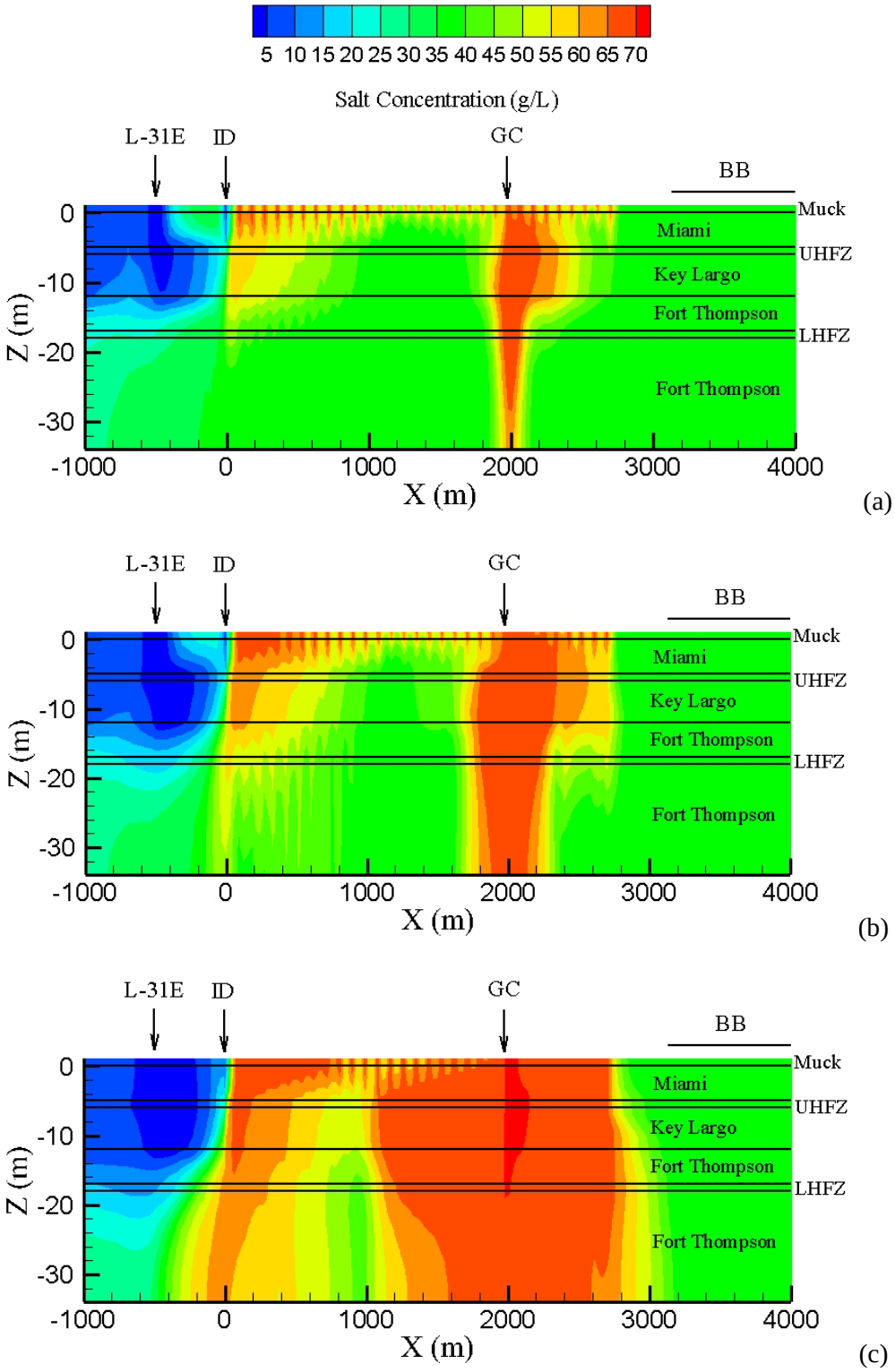


**Figure 8.1**. Salt Concentrations for the Base Case Simulation after (a) 30 Days, (b) 90 Days, (c) 1 Year, (d) 5 Years, (e) 10 Years, and (f) 25 Years

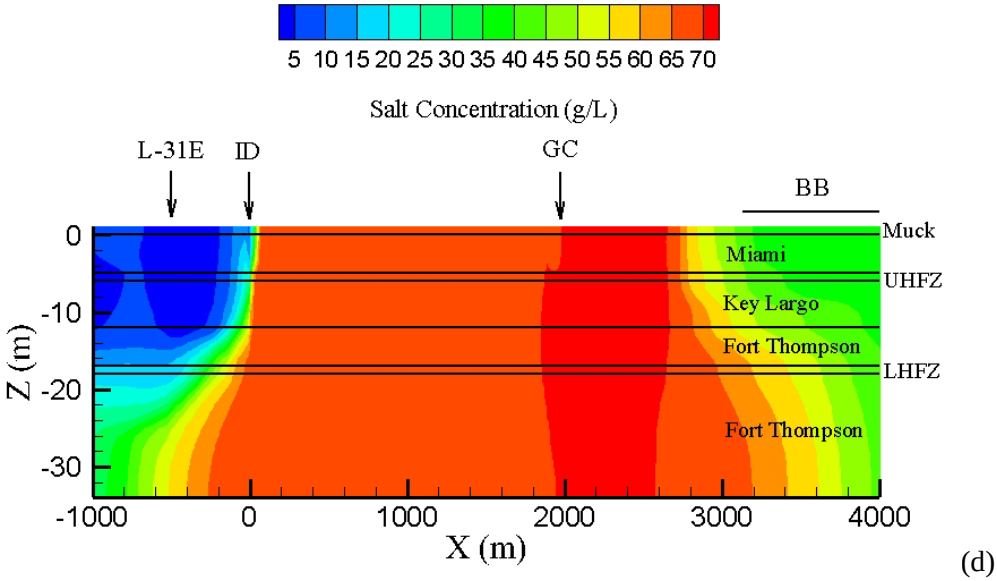


(d)

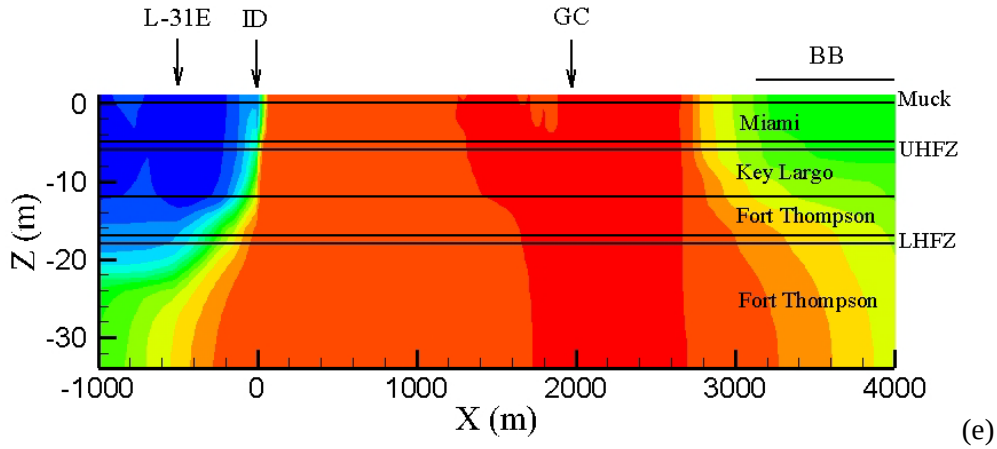


(e)

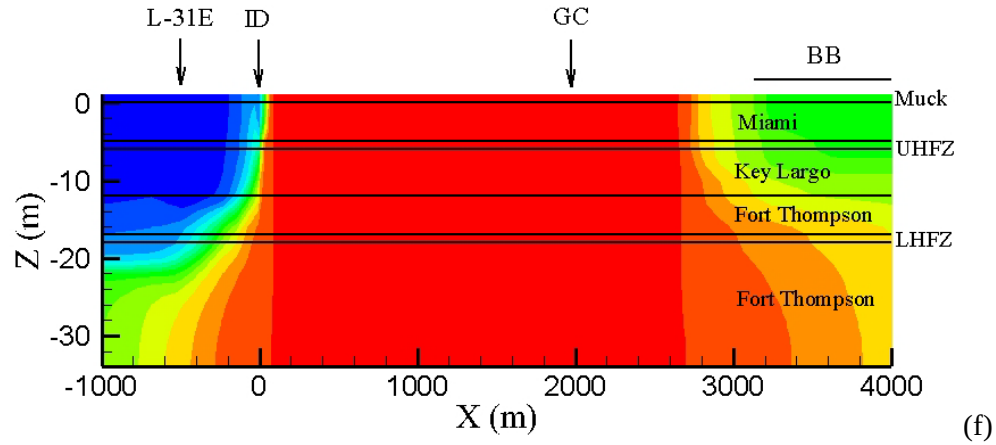


(f)

**Figure 8.1**. (contd)

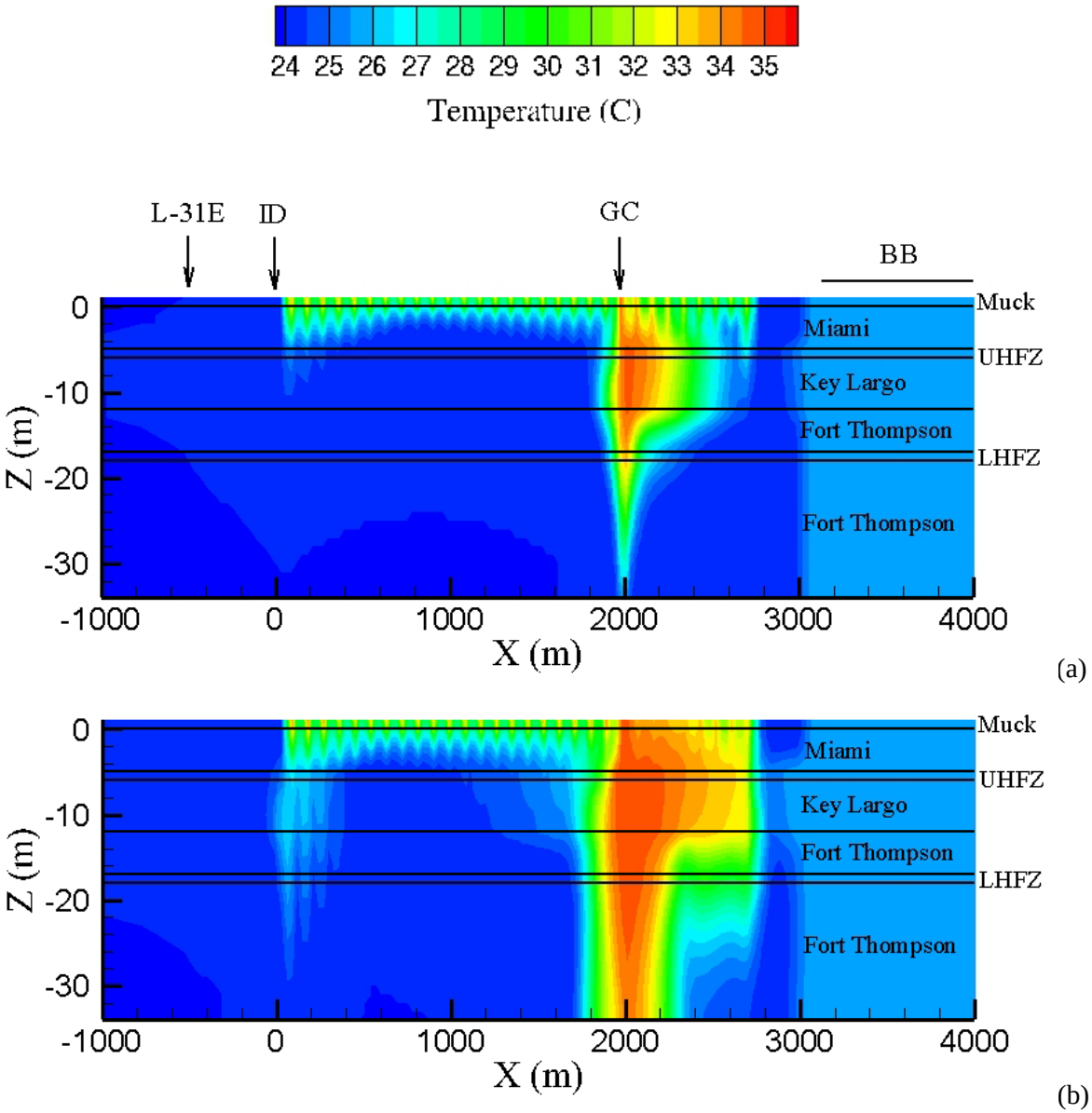


**Figure 8.2**. Temperature for the Base Case Simulation after (a) 30 Days, (b) 180 Days, (c) 1 Year, and (d) 25 Years

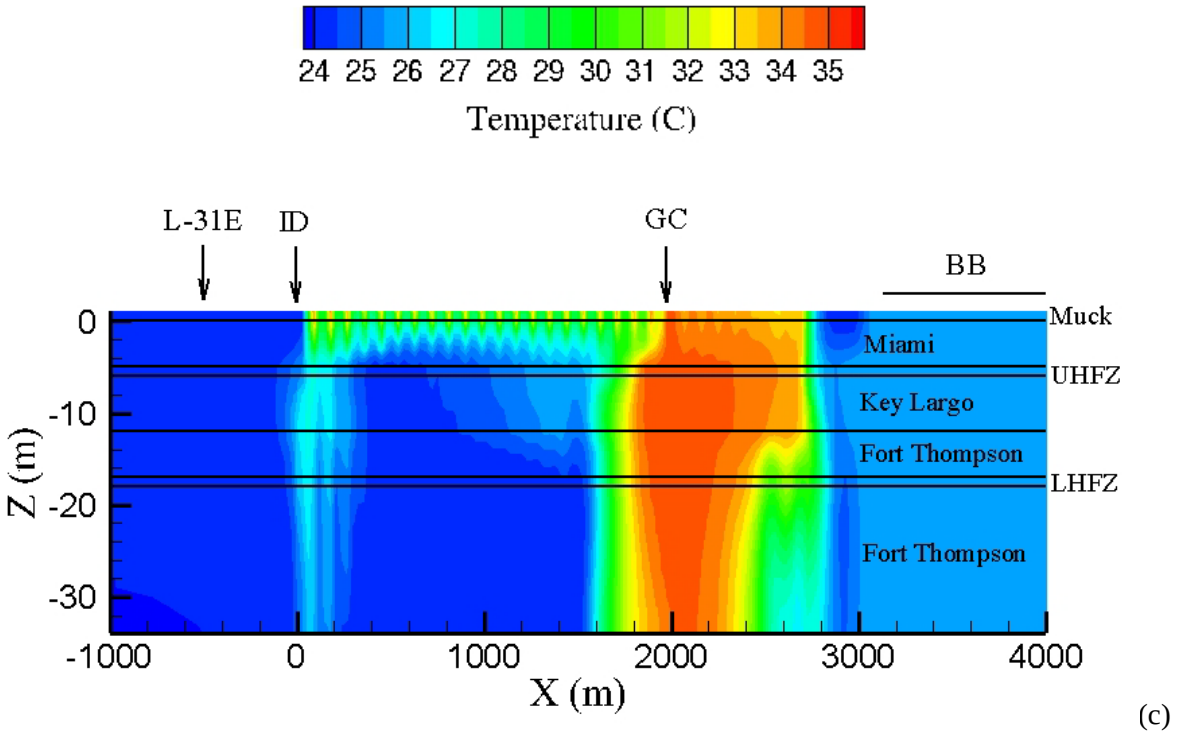


(c)

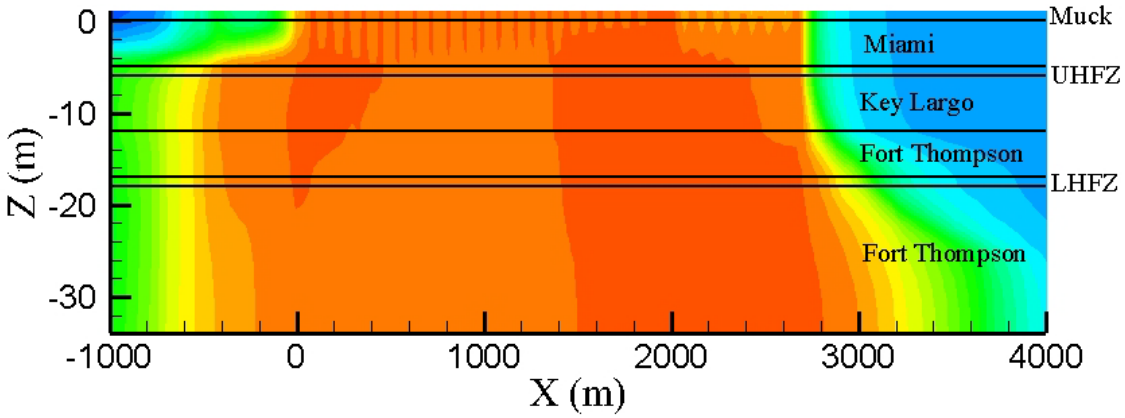


(d)

**Figure 8.2**. (contd)

## 8.2 2D Sensitivity Simulations

A list of the 2D sensitivity simulations is provided in Table 7.1. The salt concentration initial conditions of these simulations are shown in Figure 8.3 for a larger area ranging from -5,000 < *x* < 10,000 m, and a zoomed-in area ranging from -1,000 < *x* < 4,000 m. Included in Figure 8.3 and the sensitivity simulation result plots are the 19,000 salinity lines (black solid lines). For each sensitivity case, salt concentration distributions are shown after *t* = 1, 10, and 40 years for both the large and zoomed-in areas. In addition, salt concentration differences with the concentrations shown in both Figure 8.3 plots are shown for the distribution at *t* = 40 years.

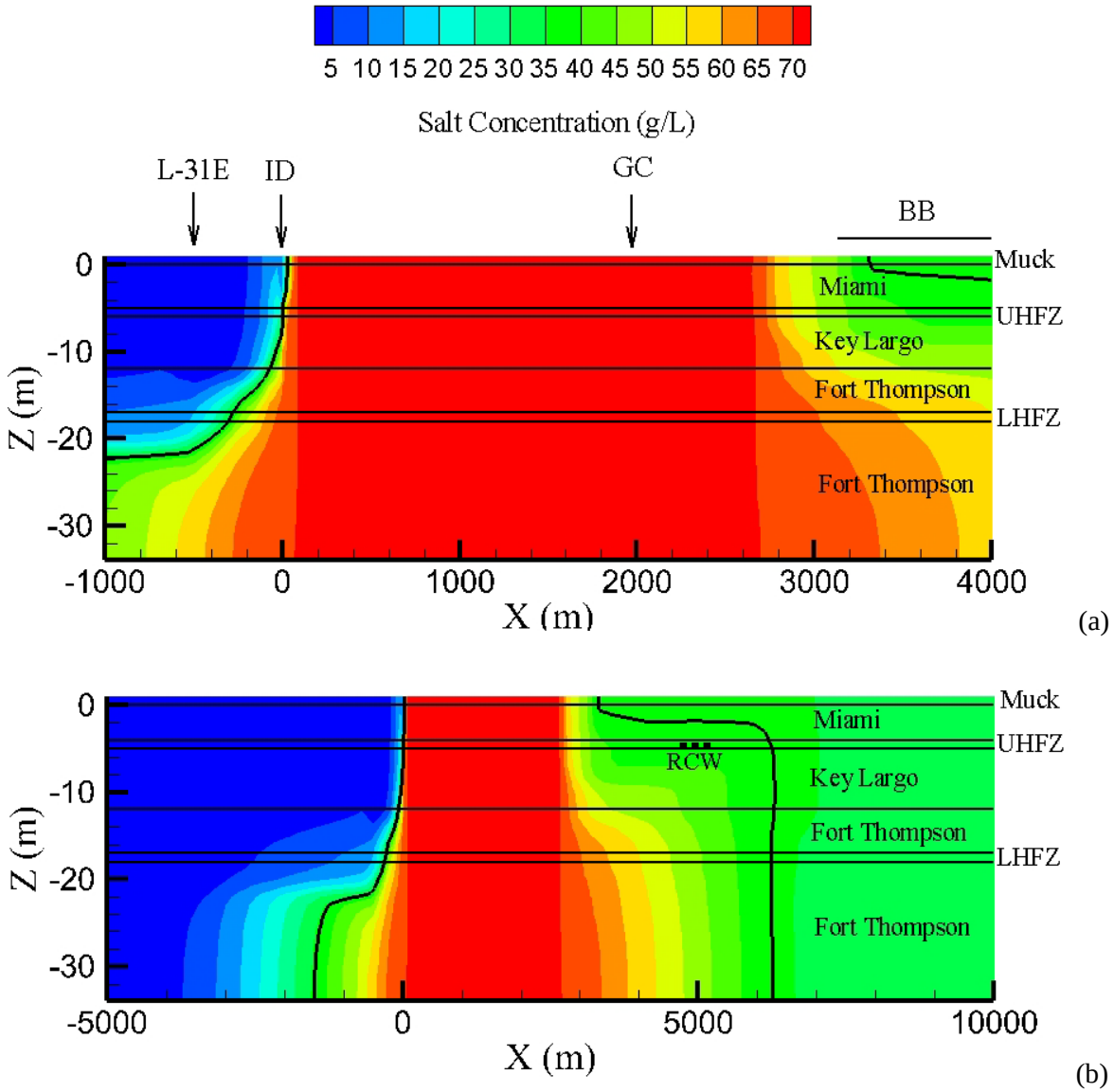


**Figure 8.3**. Base Case Salt Concentrations (g/L) 25 Years after CCS Initiation for the (a) -1,000 < *x* < 4,000 m Range, and (b) -5,000 < *x* < 10,000 m Range. The salt distributions depicted in this figure are the initial conditions for the 2D sensitivity simulations.

The results of the 2D simulations are summarized here by case number/name and the associated figures, presented by case number/name, appear in the following sections. For Case 2D-1(0 g/L salt concentration

in the CCS), the results are shown in Figure 8.4, Figure 8.5, and Figure 8.6. Below the CCS, hypersaline water is displaced with much lighter freshwater. The displacement is therefore stable, resulting in a relatively uniform displacement front (Figure 8.4a). Over time, the subsurface below the CCS is mostly salt free, and the freshwater-seawater interface is pushed toward the east. Over a larger area (Figure 8.5), it can be seen that some of the original hypersaline water is still present in the lower layers of the subsurface both west and east of the CCS. The difference plots in Figure 8.6 confirm the effectiveness of the displacement.

Displacement with 34 g/L saltwater emanating from the CCS (Case 2D-2) also results in removal of the hypersaline water, but the process is considerably slower than for Case 2D-1 (Figure 8.7, Figure 8.8, and Figure 8.9). Hypersaline water in the lower parts of the Fort Thompson remains below the CCS for several years and only after more than 10 years of operation, has most hypersaline water been pushed to either the west or east. The difference plots (Figure 8.9) show that after 40 years of operation, the groundwater below the CCS is not hypersaline anymore.

The opposite of Cases 2D-1 and 2D-2 is observed when high concentration hypersaline water is infiltrating from the CCS (Case 2D-3; Figure 8.10, Figure 8.11, and Figure 8.12). In this case, a denser fluid displaces a less dense fluid, causing instable flow patterns, as can be observed in Figure 8.10a and Figure 8.11a. Over time, the overall plume width is considerably larger than for the Base Case (Figure 8.3), especially below the Biscayne Bay. At the west side of the CCS, the regional west to east water flow limits the growth of the plume. At the east side of the CCS, there is no groundwater flow restricting expansion of the plume.

Doubling the CCS hydraulic head (Case 2D-4; Figure 8.13, Figure 8.14, and Figure 8.15) increases the driving force of the infiltrating hypersaline water. As a result, the plume is able to expand mostly toward the east and exhibits more limited growth toward the west. The limited plume expansion toward the west can be explained by the stabilizing regional water flow migrating toward the CCS coming from the west.

Cases 2D-5 and 2D-6 assess the effects of sea level rise in the Biscayne Bay, showing a 0.5 m and 1.5 m rise, respectively, over a 40-year time span. For the smaller sea level rise, the results show that most of the changes occur at the east side of the CCS (Figure 8.16, Figure 8.17, and Figure 8.18), and the increasing seawater head pushes the hypersaline water toward the CCS subsurface. The case with the sea level rise (Case 2D-6; Figure 8.19, Figure 8.20, and Figure 8.21) shows results similar to Case 2D-5, but the rise occurs at a faster pace. For both cases, the interface between hypersaline and Biscayne Bay seawater becomes sharp and nearly vertical, illustrating the competing forces of the CCS hypersaline water infiltration and the increasing head of the Biscayne Bay.

A head increase in the L-31E Canal by 0.5 m (Case 2D-7; Figure 8.22, Figure 8.23, and Figure 8.24) sharpens the hypersaline-freshwater interface at the west and prevents plume growth in the western direction. The modification does not have an impact on the salt concentration distribution east of the CCS. A part of the original hypersaline plume at the west side is initially separated from the main plume below the CCS and dissipates slowly over time.

Changes in the west boundary hydraulic head reflect changes in recharge west of the CCS. For Case 2D-8, the head is increased (Figure 8.25, Figure 8.26, Figure 8.27), resulting in a shrinking hypersaline plume over time in the lower Fort Thompson. When the head is decreased (Case 2D-9), the plume slowly extends toward the west and toward the top of the aquifer (Figure 8.28, Figure 8.29, and Figure 8.30). For both west boundary modifications, the influence on the salt distribution east of the CCS is minimal.

### 8.2.1 Case 2D-1: 0 g/L Salt Concentration in CCS

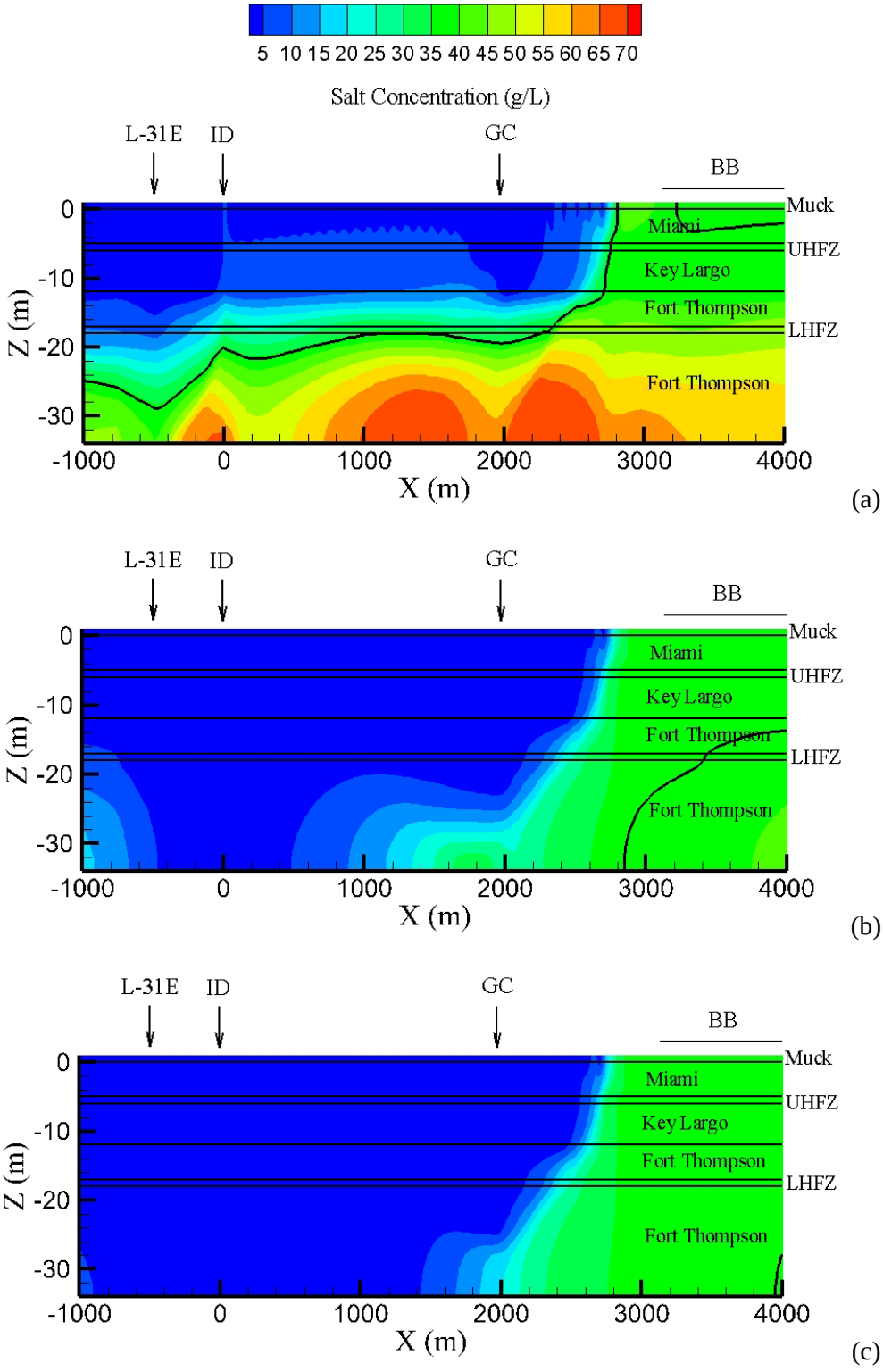


**Figure 8.4**. Salt Concentrations (g/L) over -1,000 < *x* < 4,000 m Range for Case 2D-1 (CCS Salt Concentrations at 0 g/L) at (a) 1 Year, (b) 10 Years, and (c) 40 Years

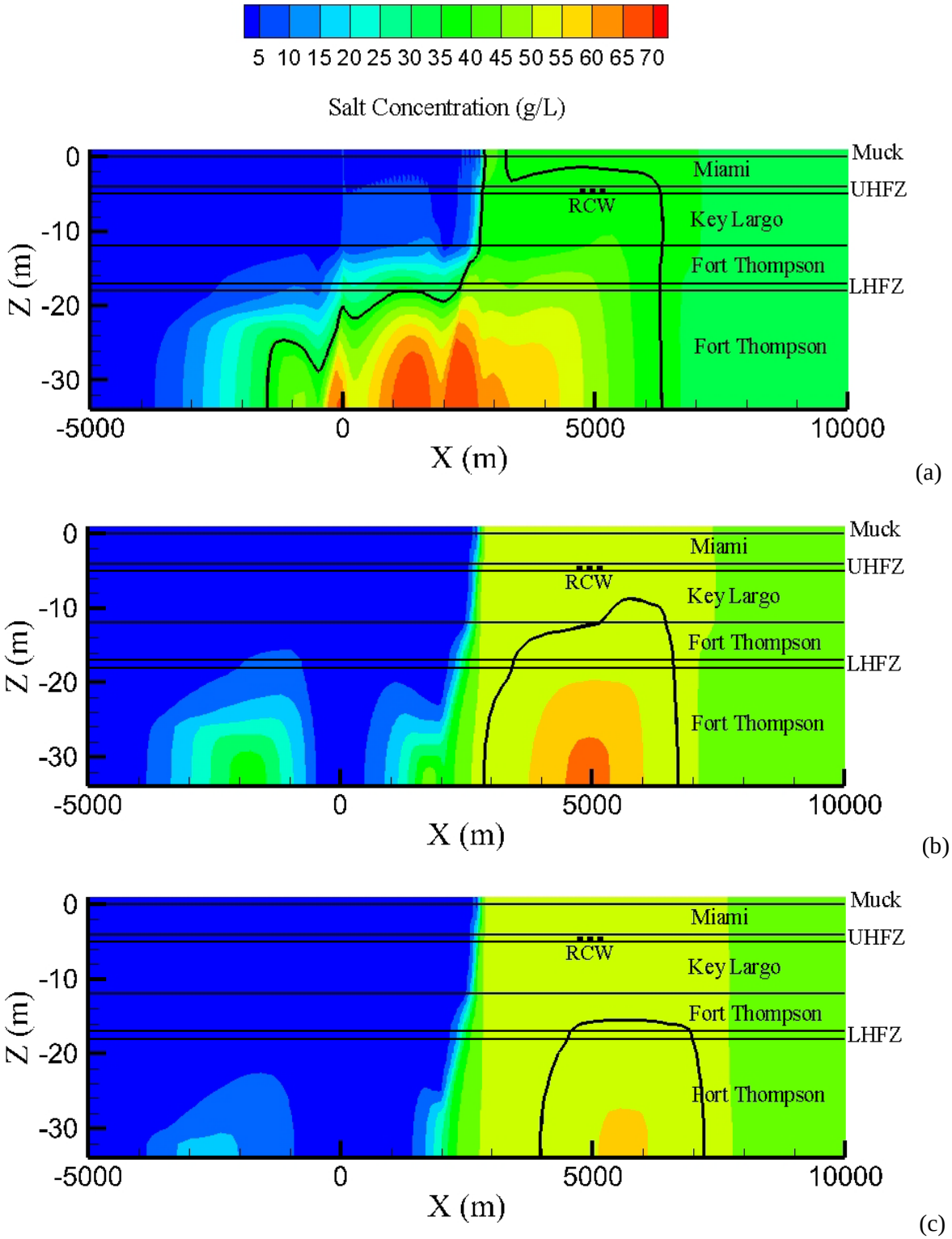


**Figure 8.5**. Salt Concentrations (g/L) over -5,000 < *x* < 10,000 m range for Case 2D-1 (CCS Salt Concentrations at 0 g/L) at (a) 1 Year, (b) 10 Years, and (c) 40 Years

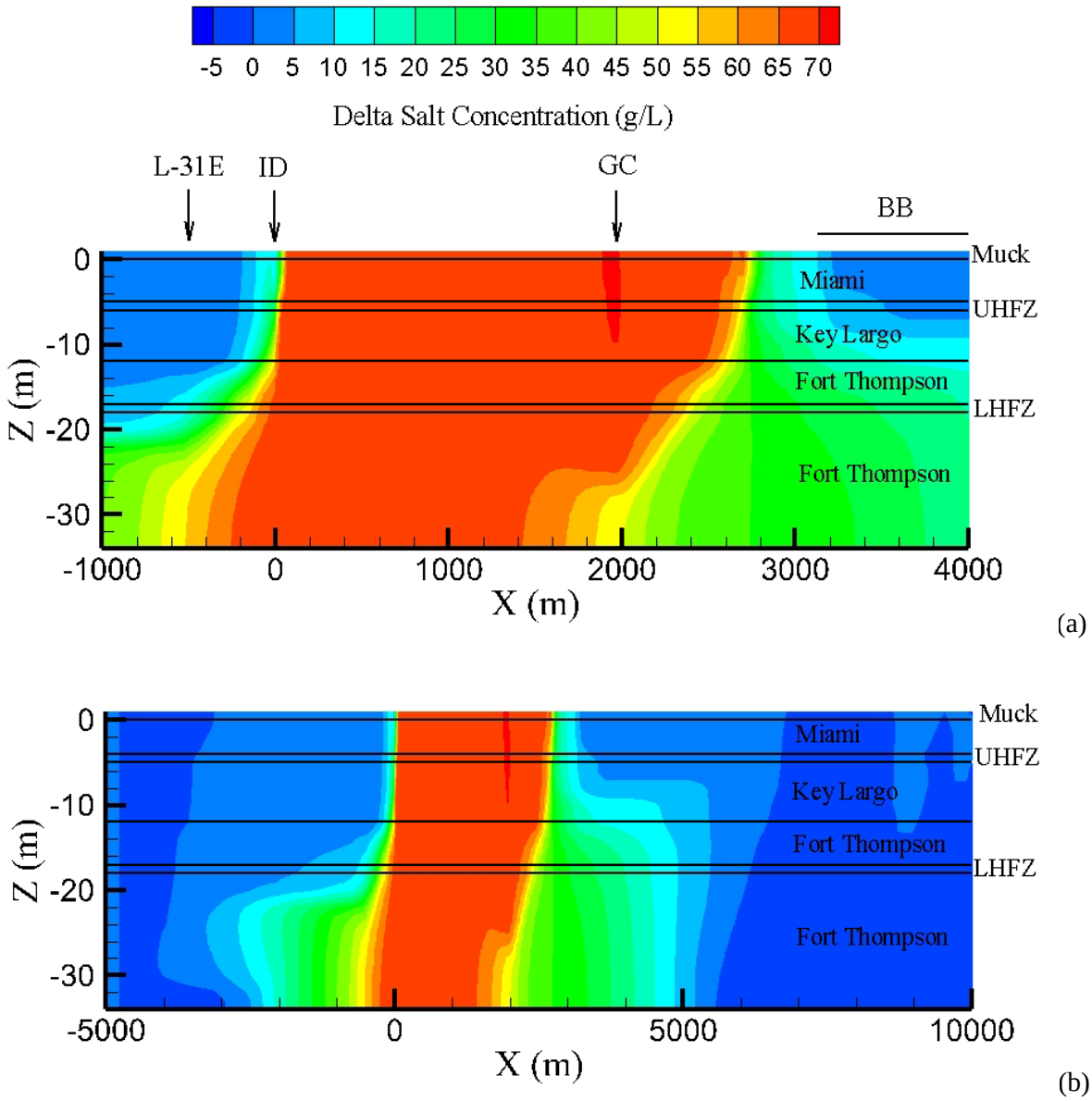


**Figure 8.6**. Differences in Salt Concentrations (g/L) between Base Case and Case 2D-1 at t = 40 Years for (a) -1,000 < *x* < 4,000 m Range, and (b) -5,000 < *x* < 10,000 m Range

### 8.2.2 Case 2D-2: 34 g/L Salt Concentration in CCS

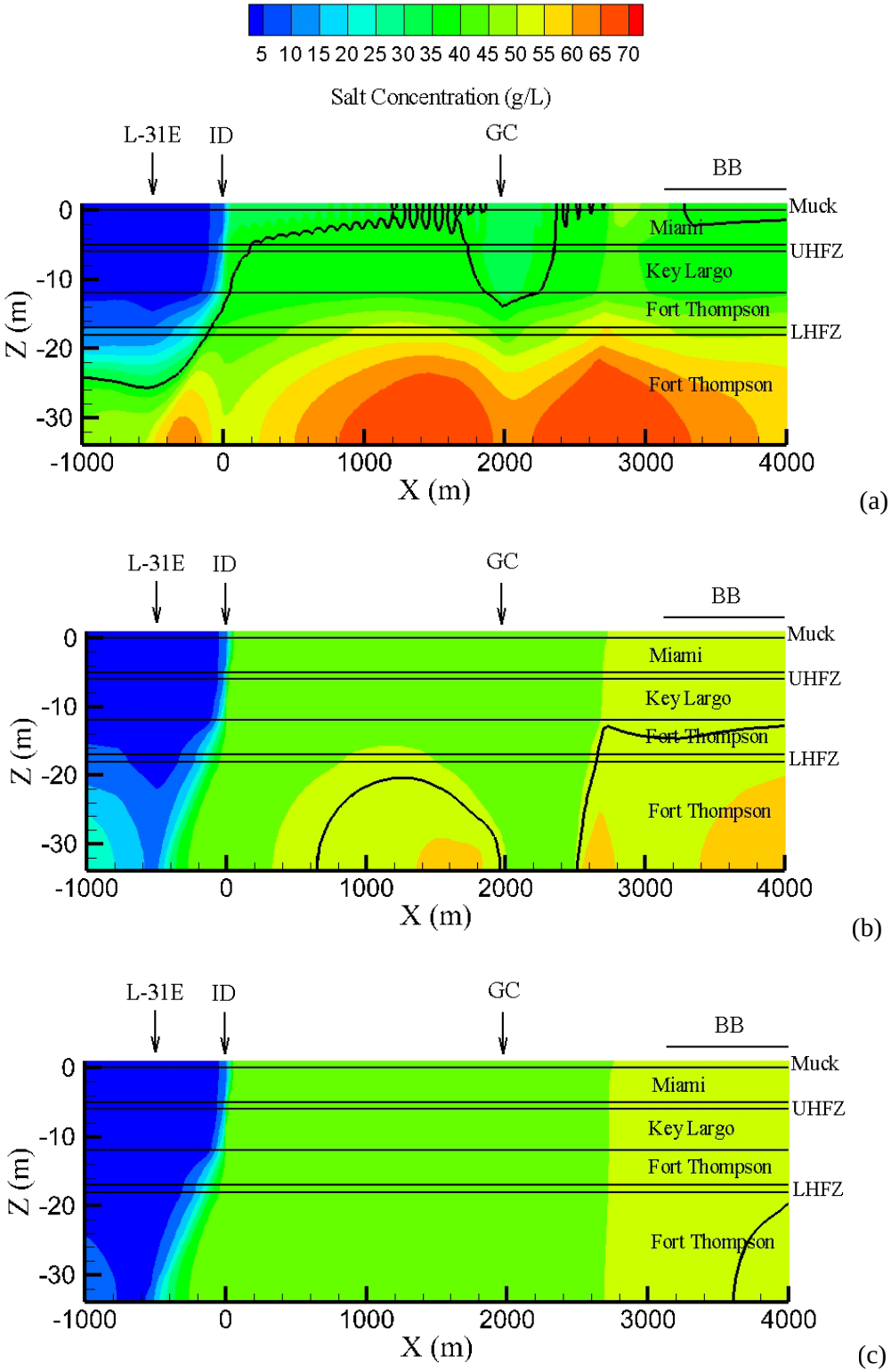


**Figure 8.7**. Salt Concentrations (g/L) over -1,000 < *x* < 4,000 m Range for Case 2D-2 (CCS Salt Concentrations at 34 g/L) at (a) 1 Year, (b) 10 Years, and (c) 40 Years

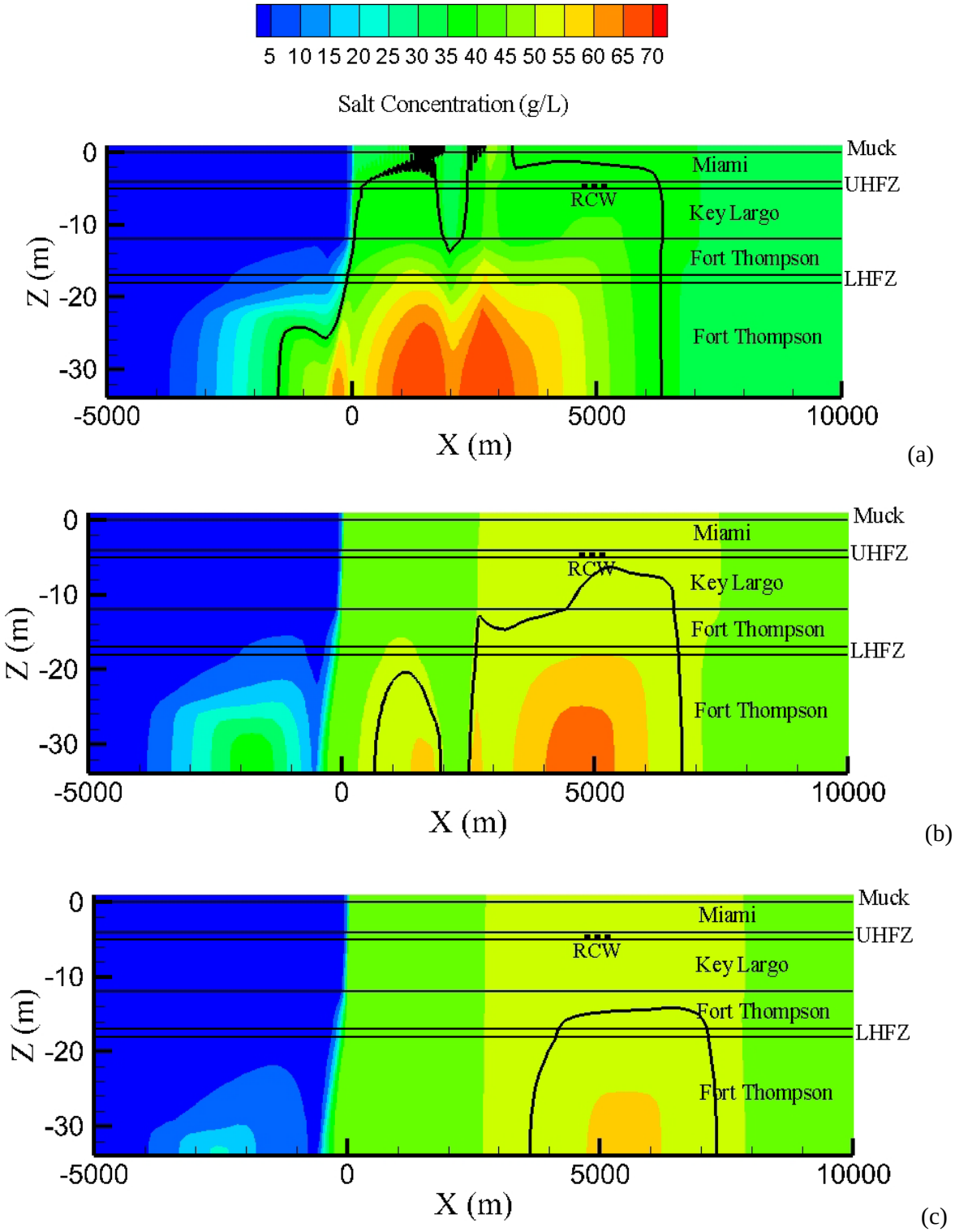


**Figure 8.8**. Salt Concentrations (g/L) over -5,000 < *x* < 10,000 m Range for Case 2D-2 (CCS Salt Concentrations at 34 g/L) at (a) 1 Year, (b) 10 Years, and (c) 40 Years

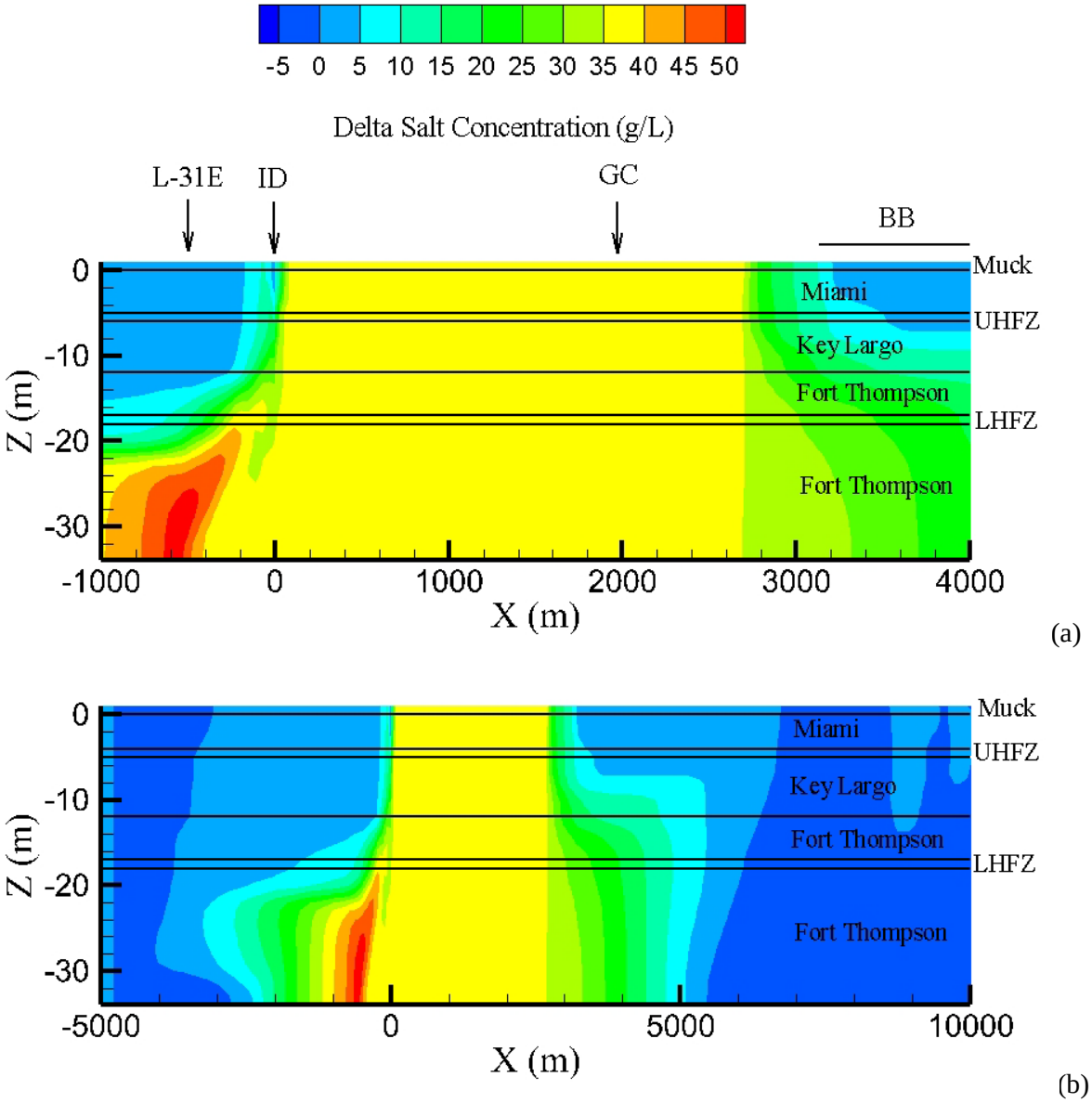


**Figure 8.9**. Differences in Salt Concentrations (g/L) between Base Case and Case 2D-2 at $t$ = 40 Years for (a) -1,000 < $x$ < 4,000 m Range, and (b) -5,000 < $x$ < 10,000 m Range

### 8.2.3 Case 2D-3: 90 g/L Salt Concentration in CCS

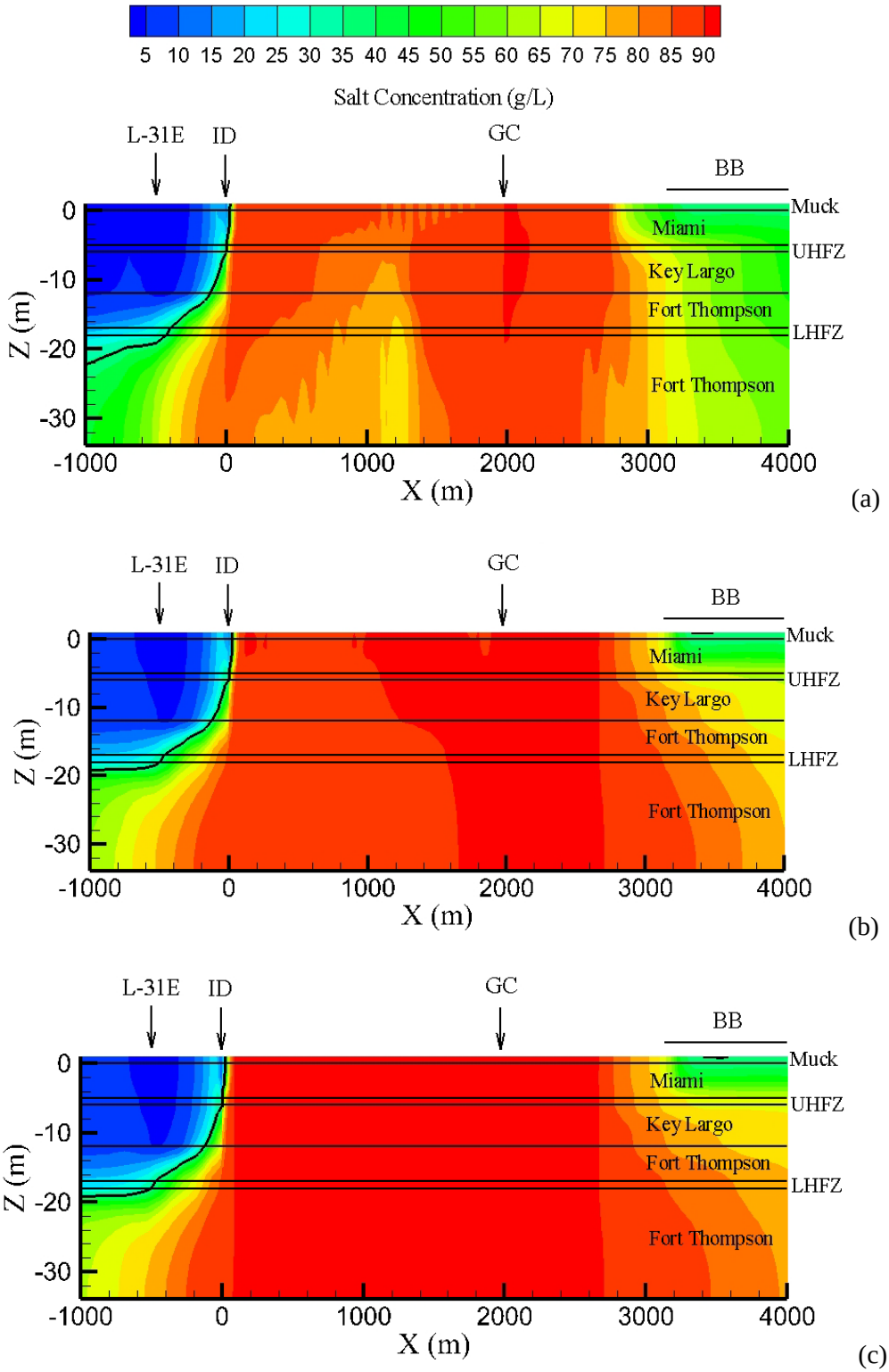


**Figure 8.10**. Salt Concentrations (g/L) over -1,000 < *x* < 4,000 m Range for Case 2D-3 (CCS Salt Concentrations at 90 g/L) at (a) 1 Year, (b) 10 Years, and (c) 40 Years

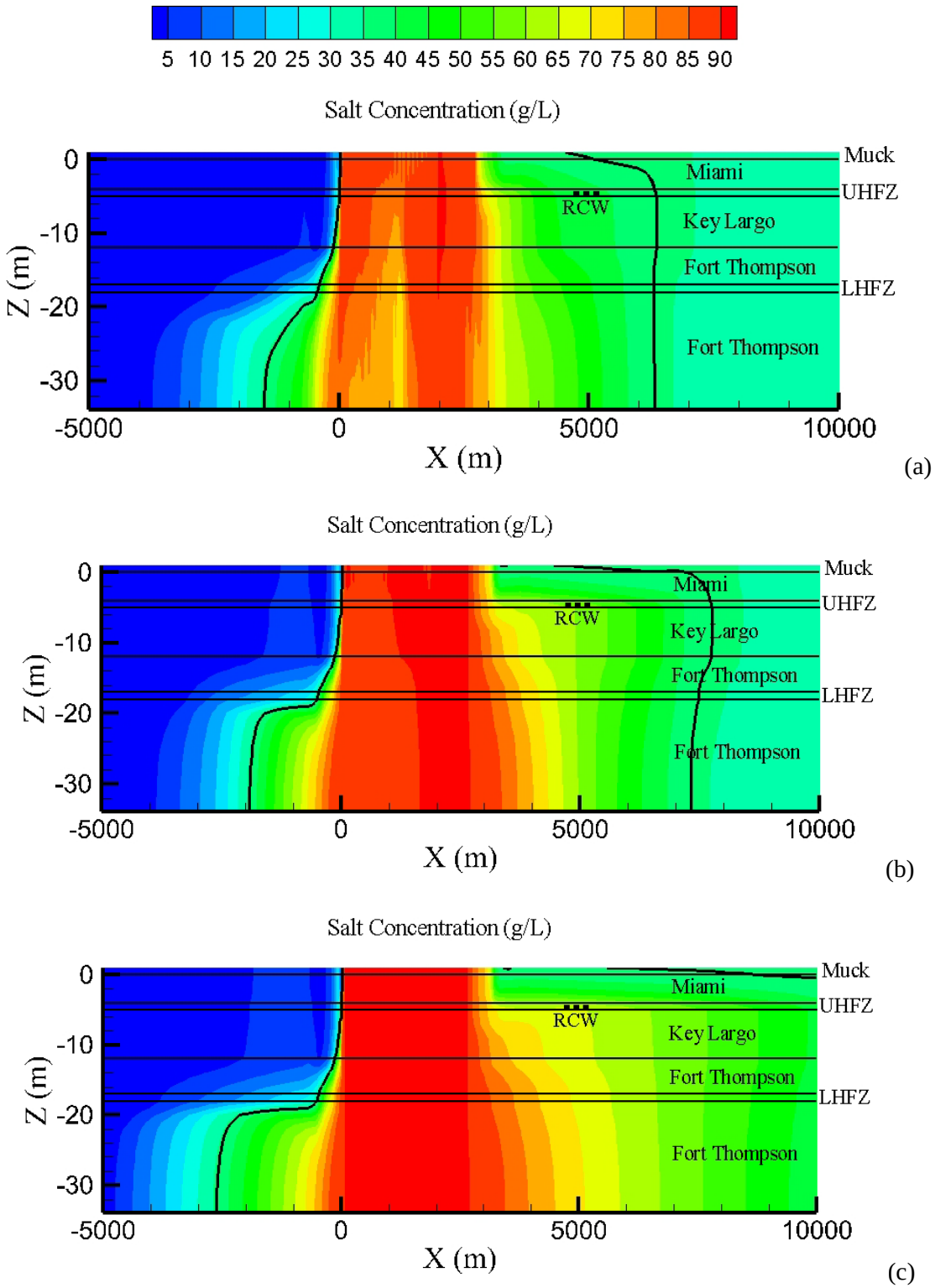


**Figure 8.11**. Salt Concentrations (g/L) over -5,000 < *x* < 10,000 m Range for Case 2D-3 (CCS Salt Concentrations at 90 g/L) at (a) 1 Year, (b) 10 Years, and (c) 40 Years

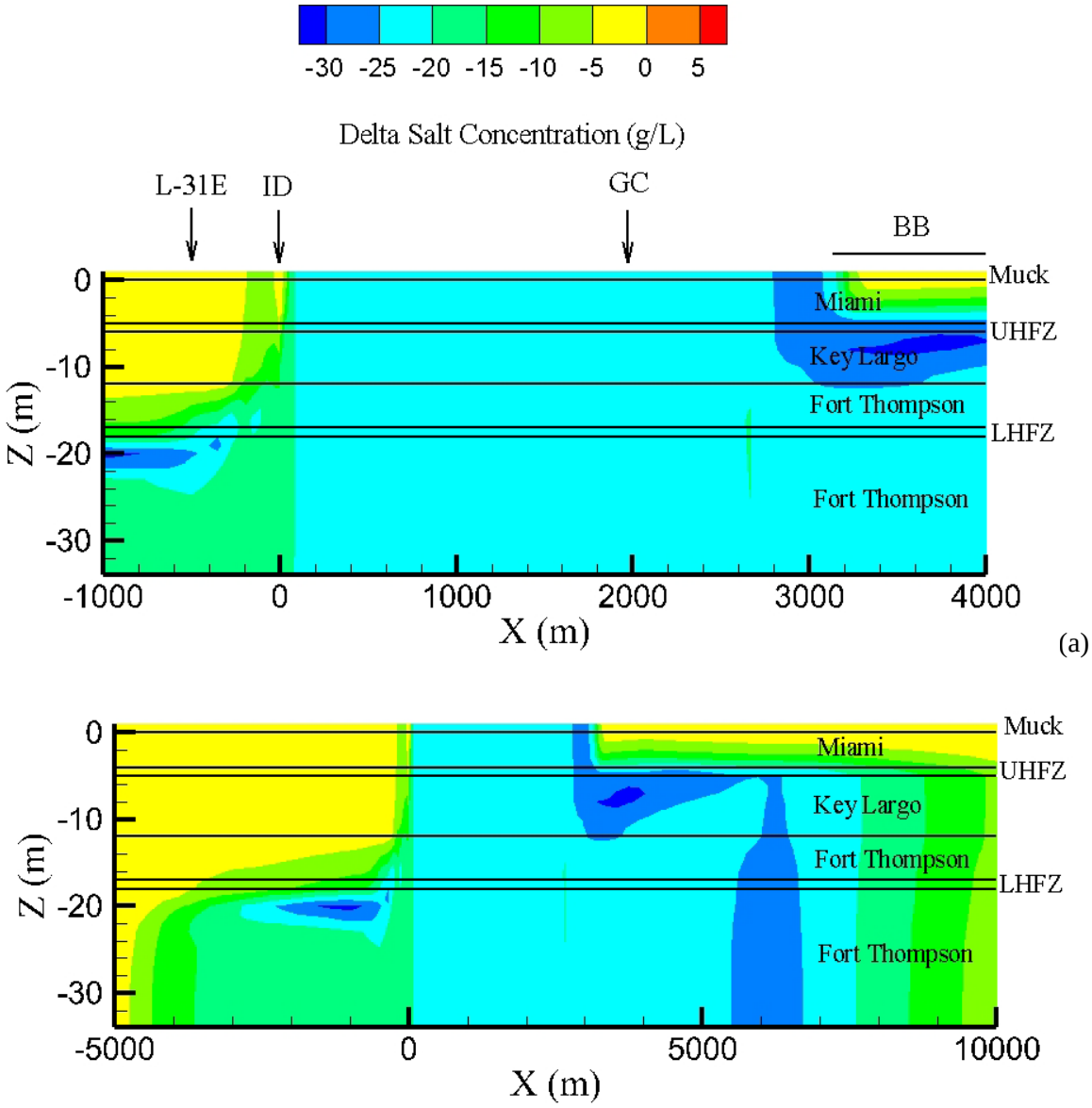


**Figure 8.12**. Differences in Salt Concentrations (g/L) between Base Case and Case 2D-3 at $t$ = 40 Years for (a) -1,000 < $x$ < 4,000 m Range, and (b) -5,000 < $x$ < 10,000 m Range

### 8.2.4 Case 2D-4: Head in CCS Doubled

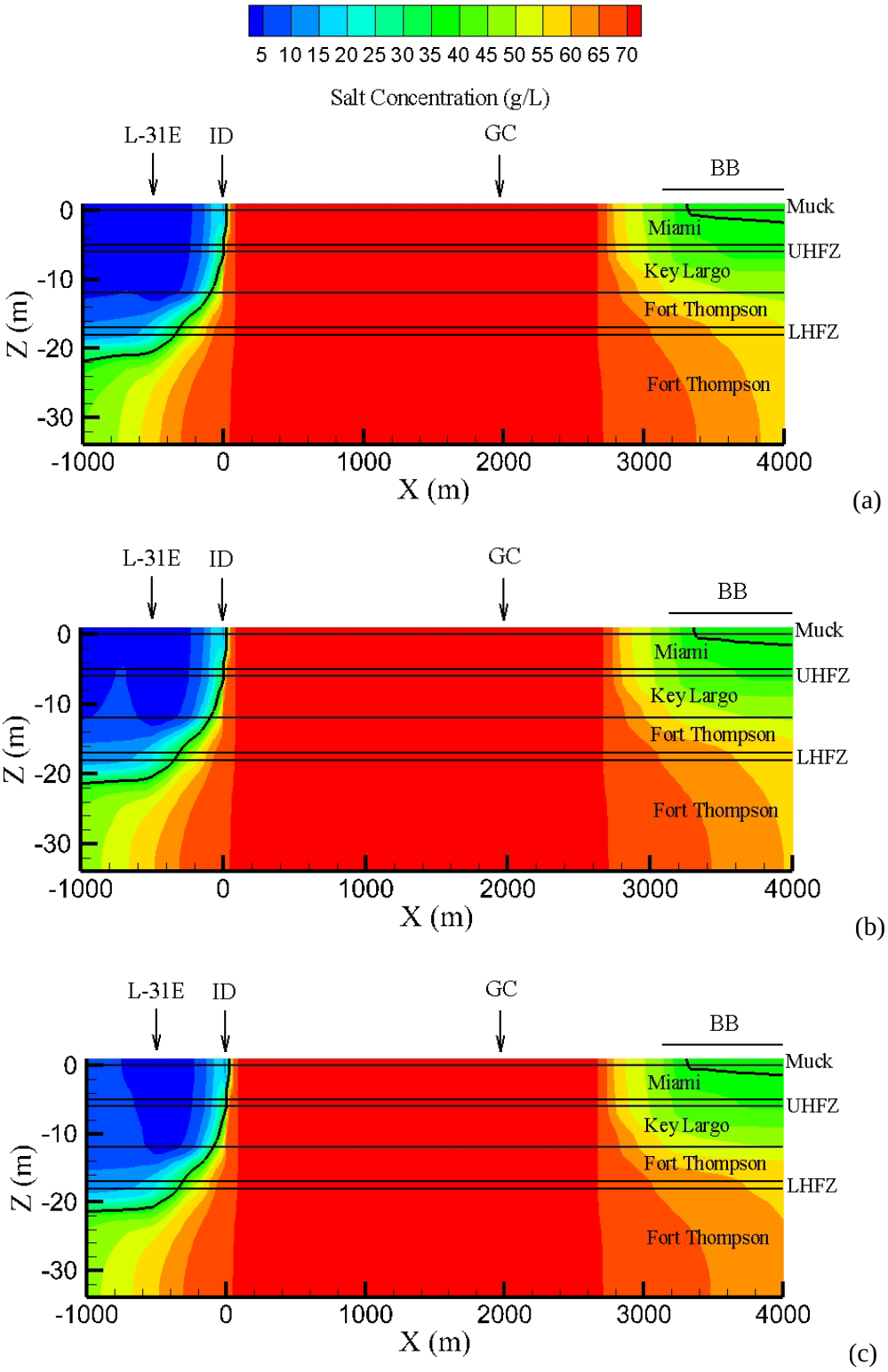


**Figure 8.13**. Salt Concentrations (g/L) over -1,000 < *x* < 4,000 m Range for Case 2D-4 (Double CCS Water Head) at (a) 1 Year, (b) 10 Years, and (c) 40 Years

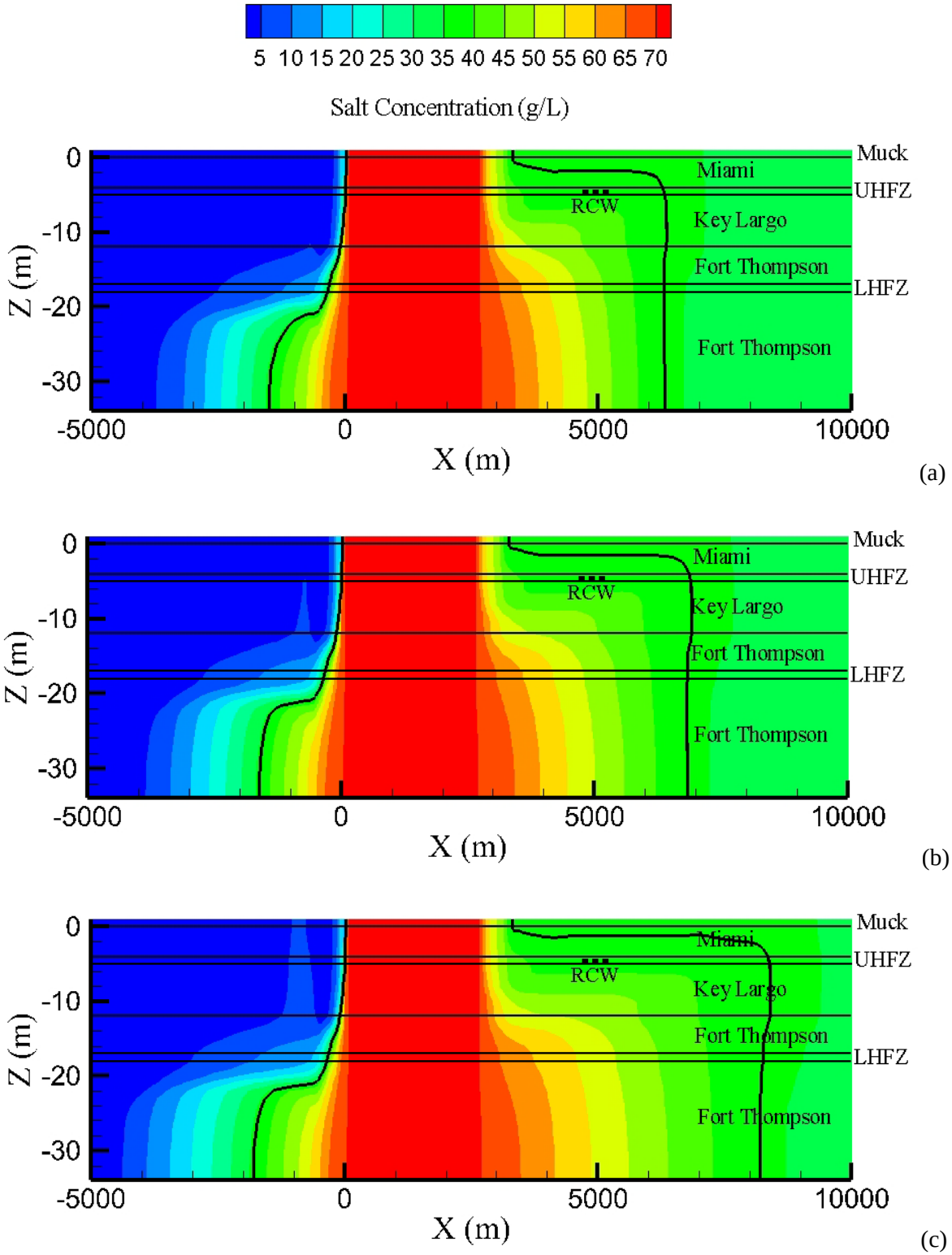


**Figure 8.14**. Salt Concentrations (g/L) over -5,000 < *x* < 10,000 m Range for Case 2D-4 (Double CCS Water Head) at (a) 1 Year, (b) 10 years, and (c) 40 Years

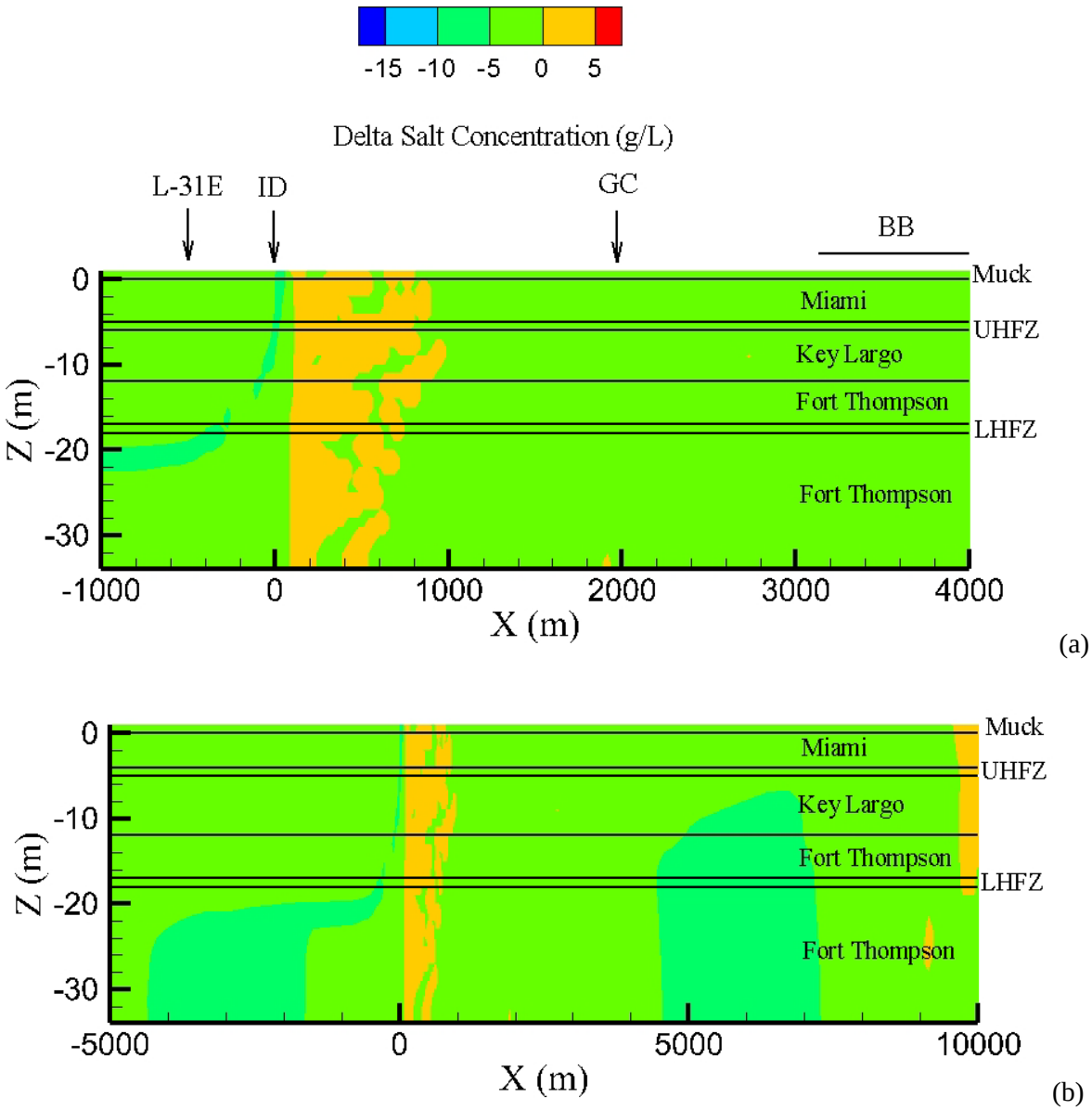


**Figure 8.15**. Differences in Salt Concentrations (g/L) between Base Case and Case 2D-4 at $t$ = 40 Years for (a) -1,000 < $x$ < 4,000 m Range, and (b) -5,000 < $x$ < 10,000 m Range

### 8.2.5 Case 2D-5: Sea Level Rise in Biscayne Bay of 0.5 m over 40 Years

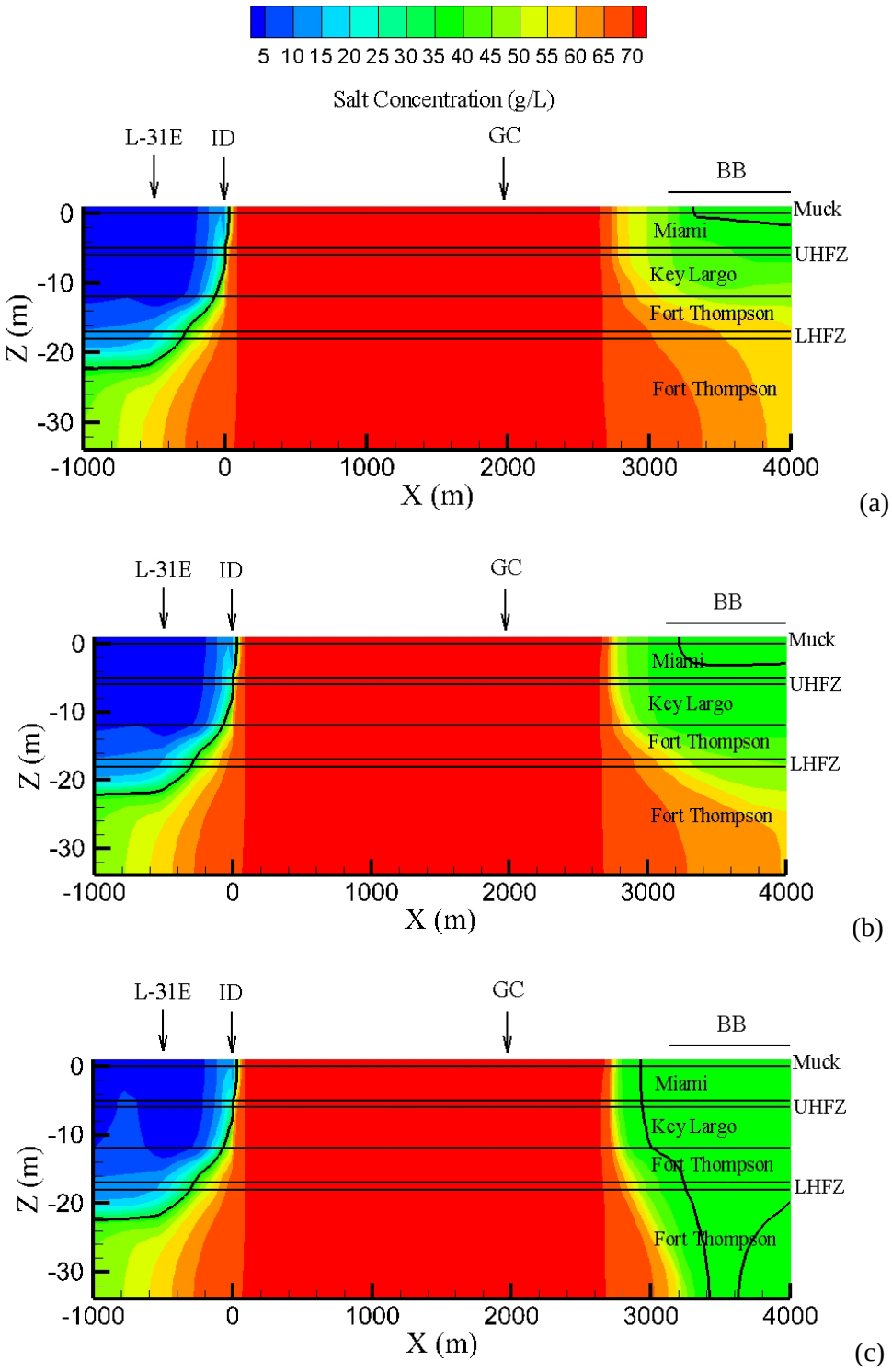


**Figure 8.16**. Salt Concentrations (g/L) over -1,000 < *x* < 4,000 m Range for Case 2D-5 (Seawater Level Increase of 0.5 m over 40 Years) at (a) 1 Year, (b) 10 Years, and (c) 40 Years

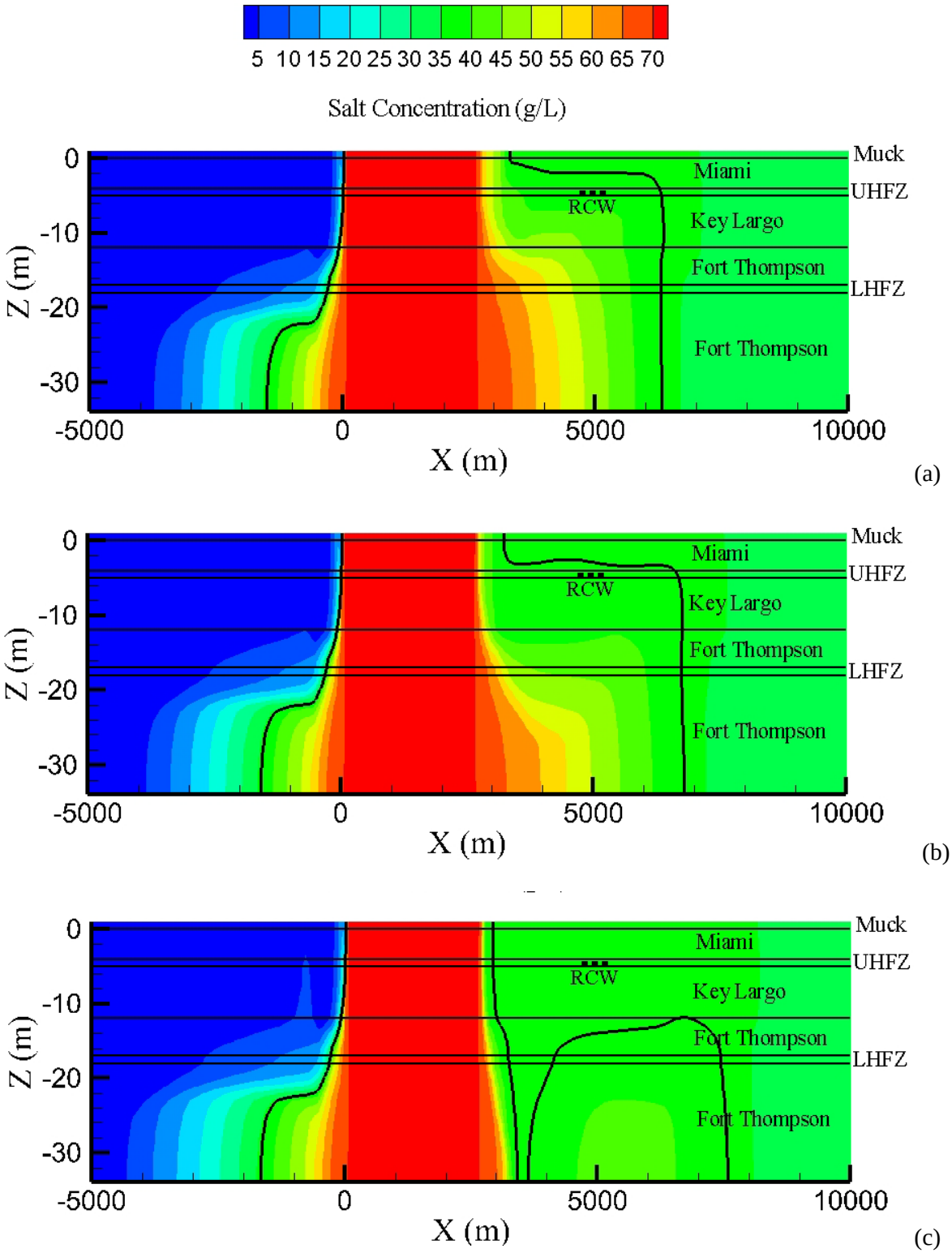


**Figure 8.17**. Salt Concentrations (g/L) over -5,000 < *x* < 10,000 m Range for Case 2D-5 (Seawater Level Increase of 0.5 m over 40 Years) at (a) 1 Year, (b) 10 Years, and (c) 40 Years

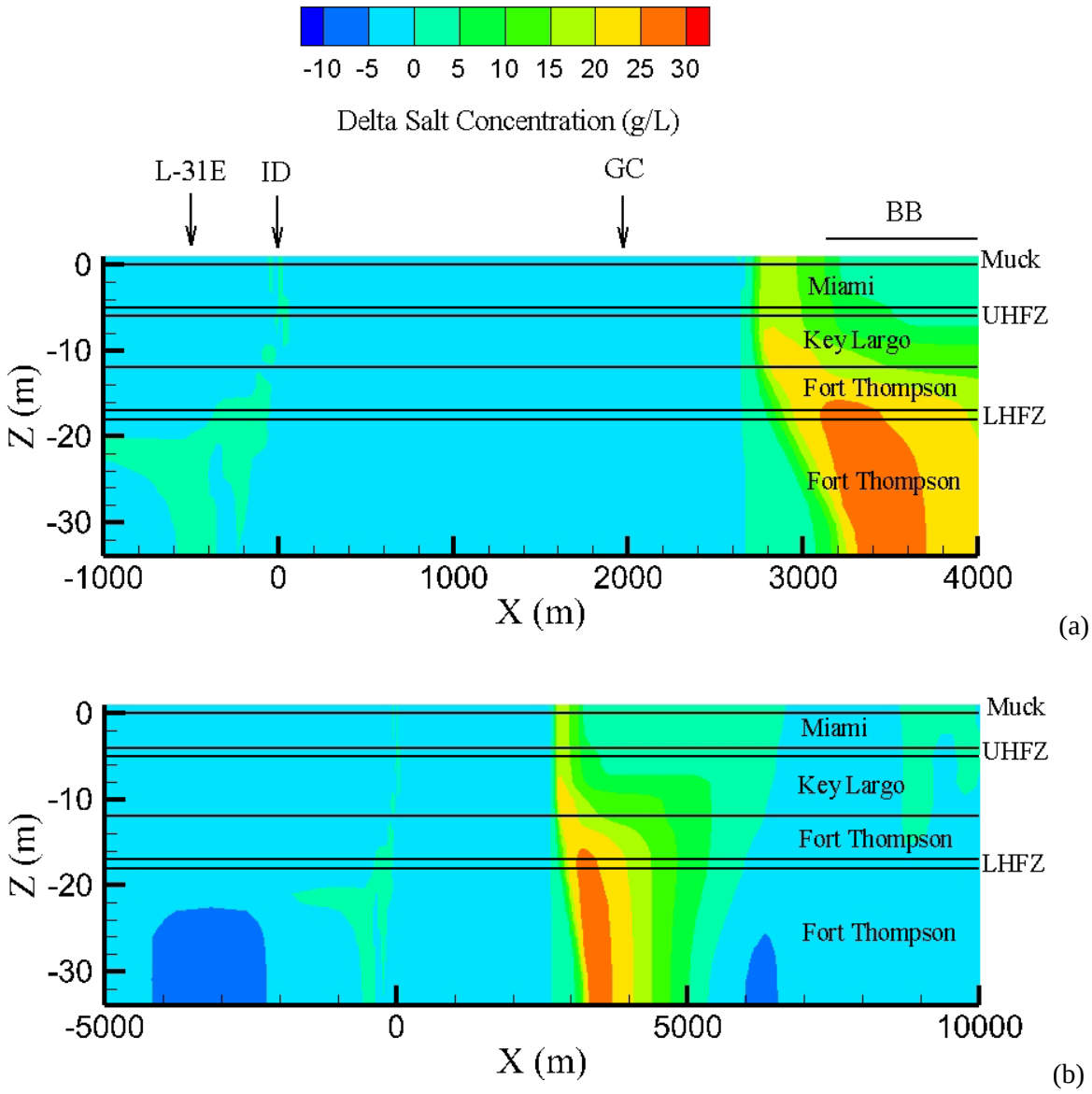


**Figure 8.18**. Differences in Salt Concentrations (g/L) between Base Case and Case 2D-5 at $t$ = 40 Years for (a) -1,000 < $x$ < 4,000 m Range, and (b) -5,000 < $x$ < 10,000 m Range

### 8.2.6 Case 2D-6: Sea Level Rise in Biscayne Bay of 1.5 m over 40 Years

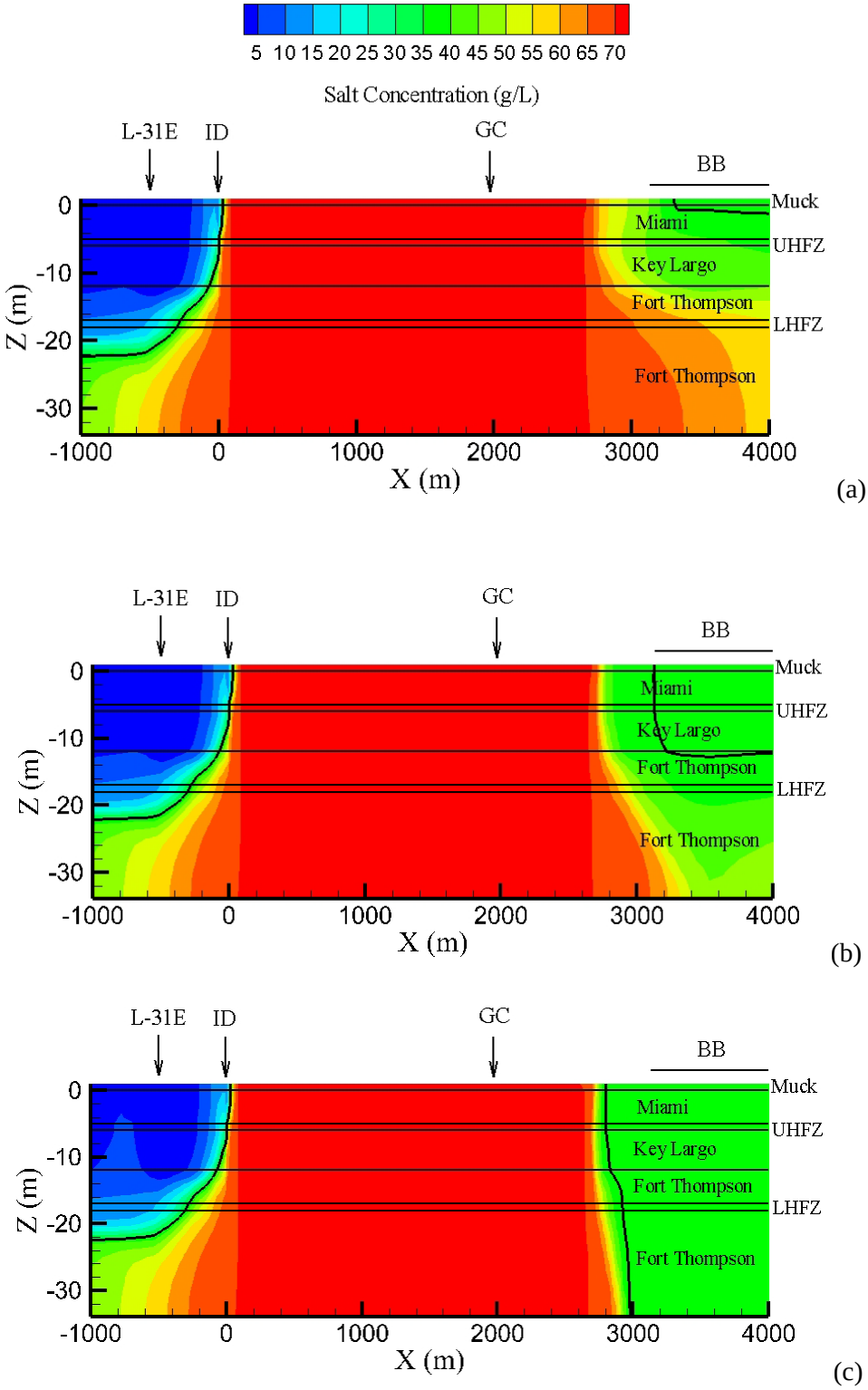


**Figure 8.19**. Salt Concentrations (g/L) over -1,000 < *x* < 4,000 m Range for Case 2D-6 (Seawater Level Increase of 1.5 m over 40 Years) at (a) 1 Year, (b) 10 Years, and (c) 40 Years

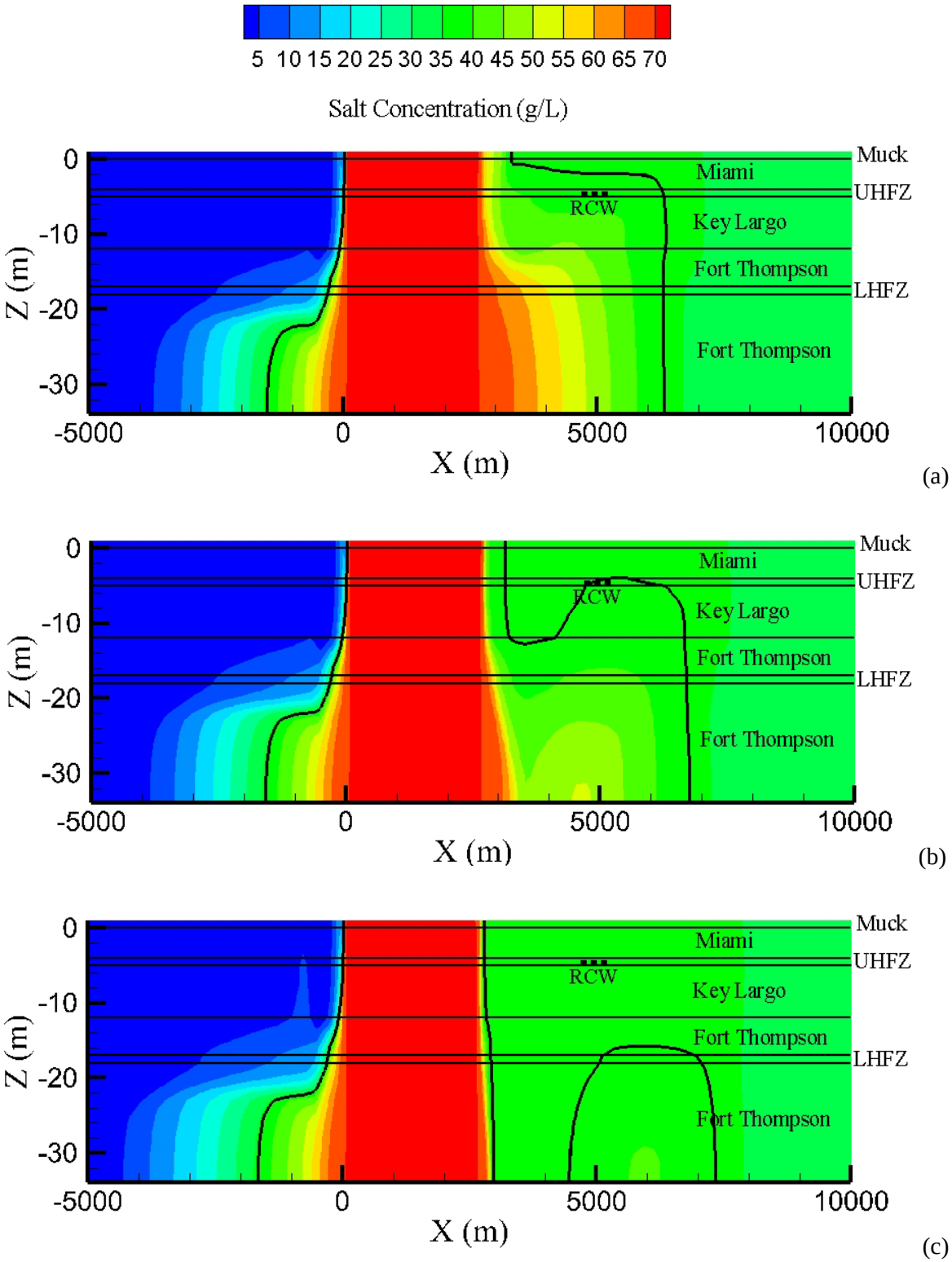


**Figure 8.20**. Salt Concentrations (g/L) over -5,000 < *x* < 10,000 m Range for Case 2D-6 (Seawater Level Increase of 1.5 m over 40 Years) at (a) 1 Year, (b) 10 Years, and (c) 40 Years

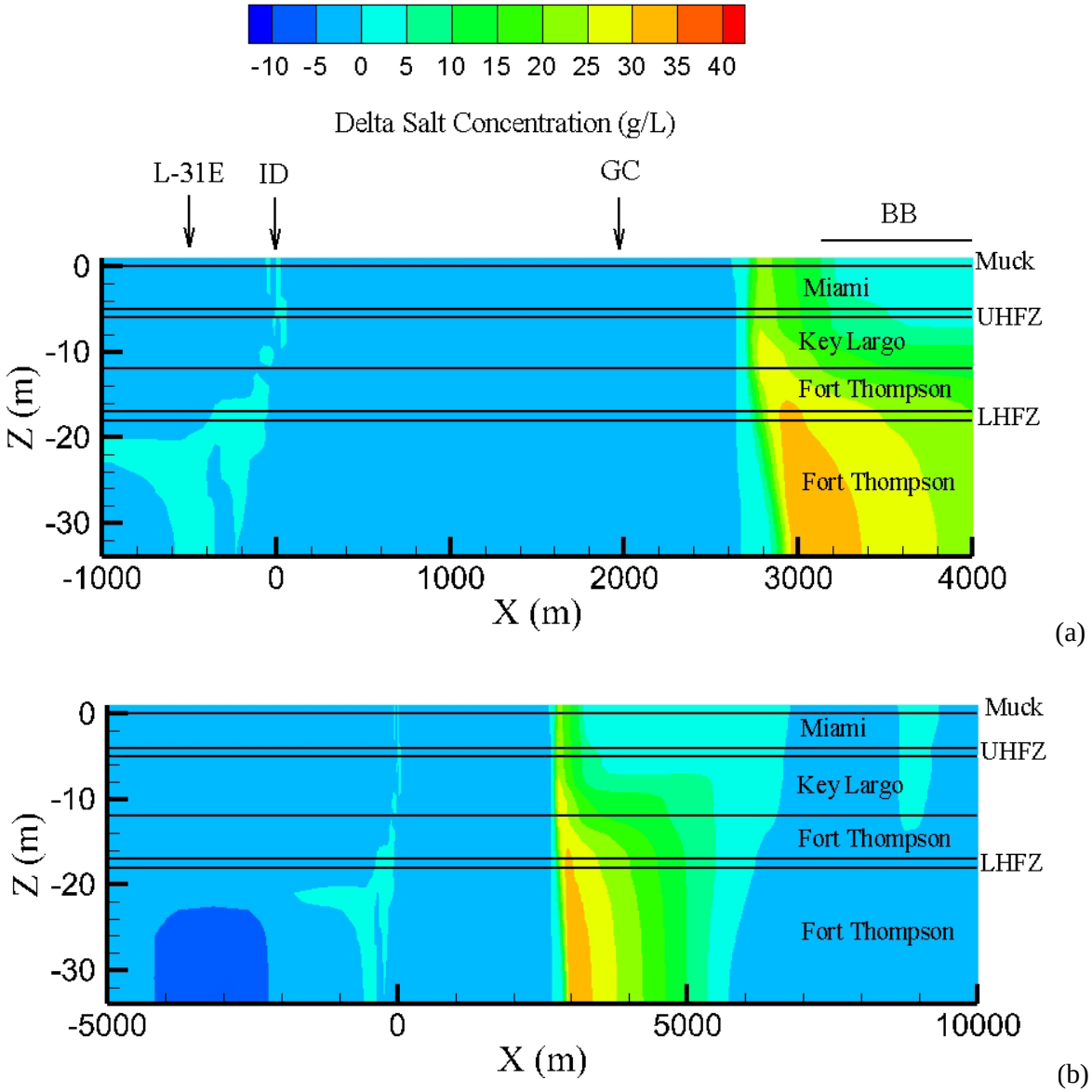


**Figure 8.21**. Differences in Salt Concentrations (g/L) between Base Case and Case 2D-6 at $t$ = 40 Years for (a) -1,000 < $x$ < 4,000 m Range, and (b) -5,000 < $x$ < 10,000 m Range

### 8.2.7 Case 2D-7: Head in L-31E Canal Increased by 0.5 m

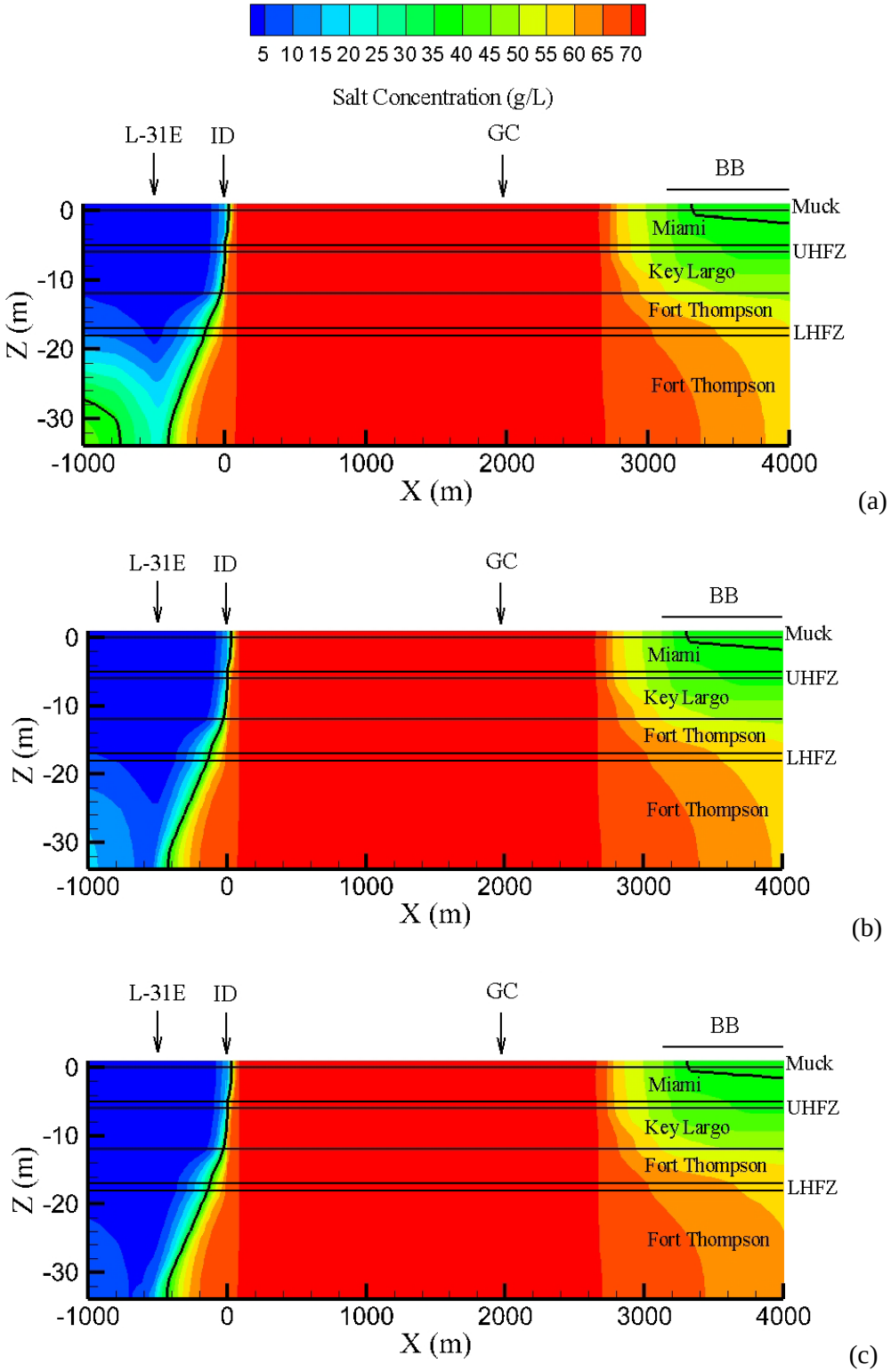


**Figure 8.22**. Salt Concentrations (g/L) over -1,000 < *x* < 4,000 m Range for Case 2D-7 (0.5 m Head Increase in L-31E Canal) at (a) 1 Year, (b) 10 Years, and (c) 40 Years

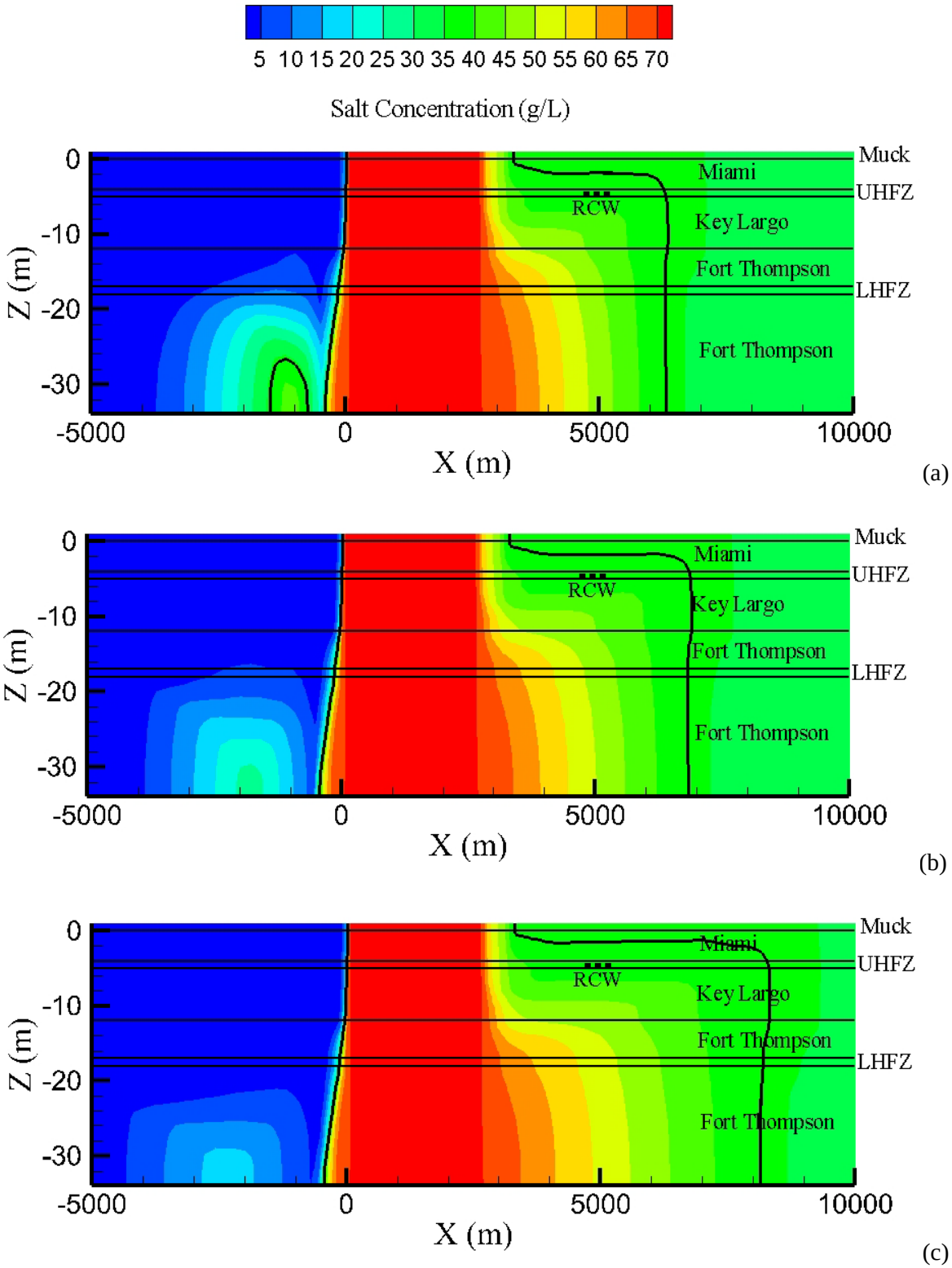


**Figure 8.23**. Salt Concentrations (g/L) over -5,000 < *x* < 10,000 m Range for Case 2D-7 (0.5 m Head Increase in L-31E Canal) at (a) 1 Year, (b) 10 Years, and (c) 40 Years

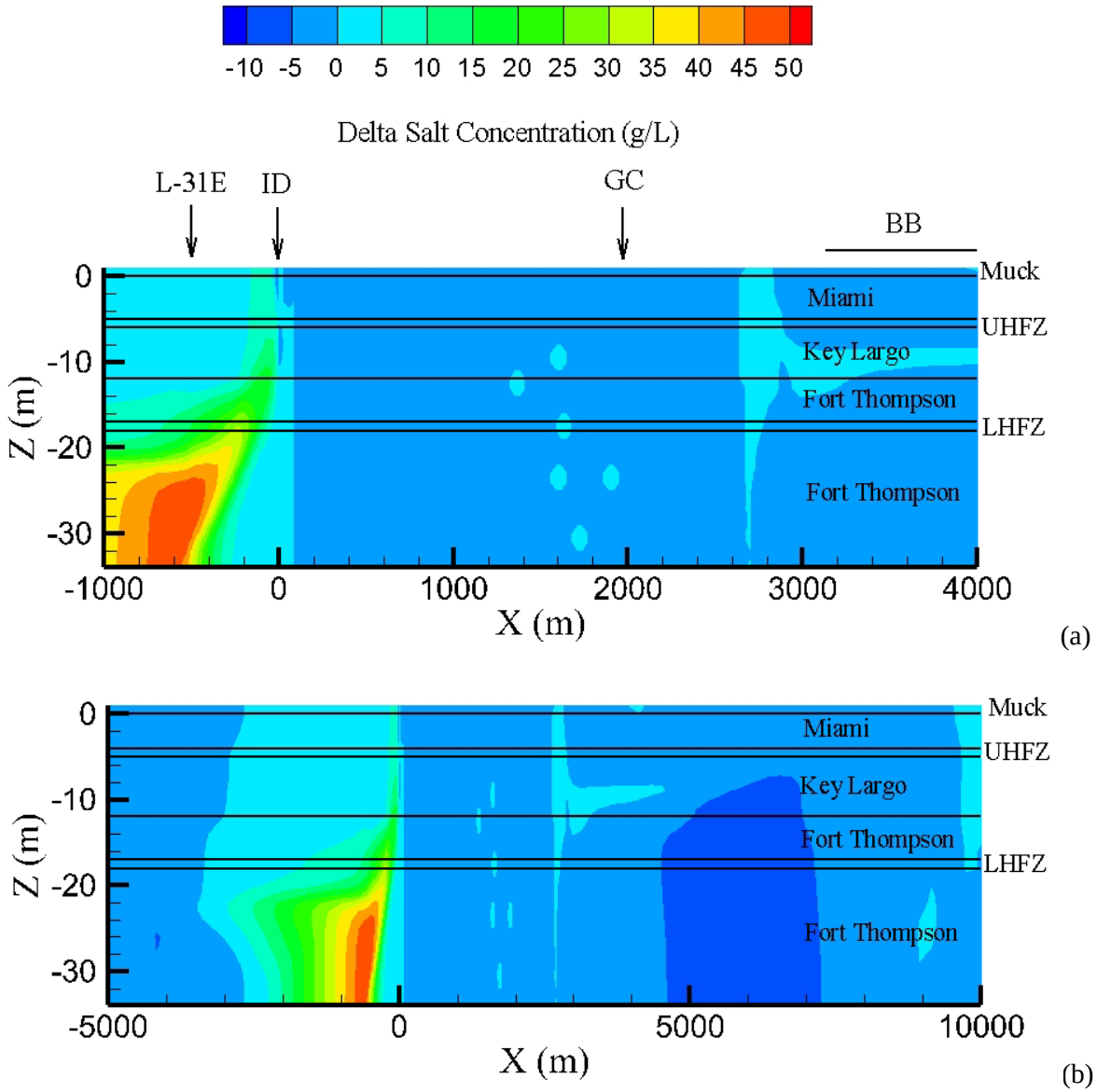


**Figure 8.24**. Differences in Salt Concentrations (g/L) between Base Case and Case 2D-7 at $t$ = 40 Years for (a) -1,000 < $x$ < 4,000 m Range, and (b) -5,000 < $x$ < 10,000 m Range

### 8.2.8 Case 2D-8: 1.0 m Head Increase at West Boundary

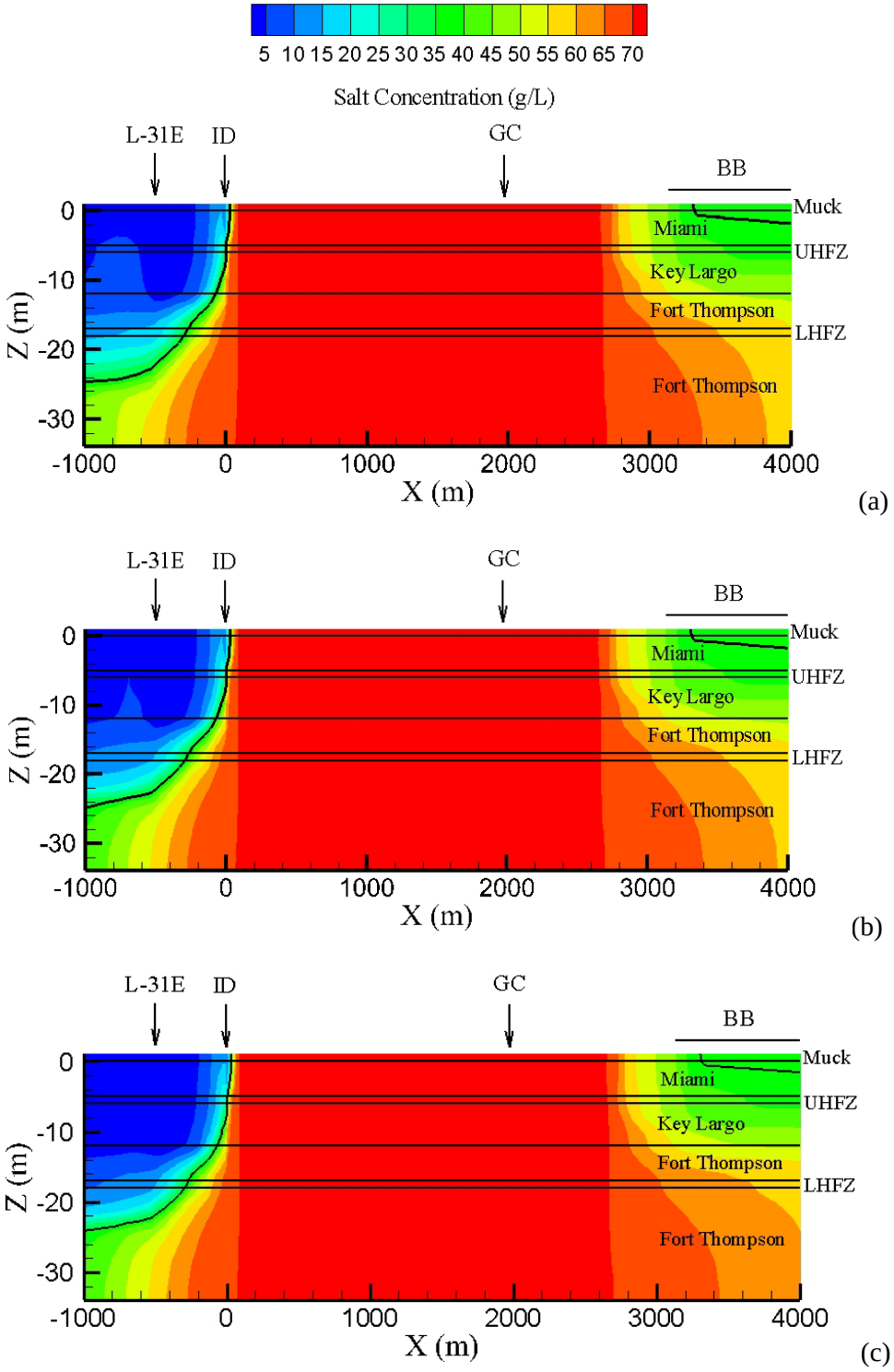


**Figure 8.25**. Salt Concentrations (g/L) over -1,000 < *x* < 4,000 m Range for Case 2D-8 (1.0 m Head Increase at West Boundary) at (a) 1 year, (b) 10 Years, and (c) 40 Years

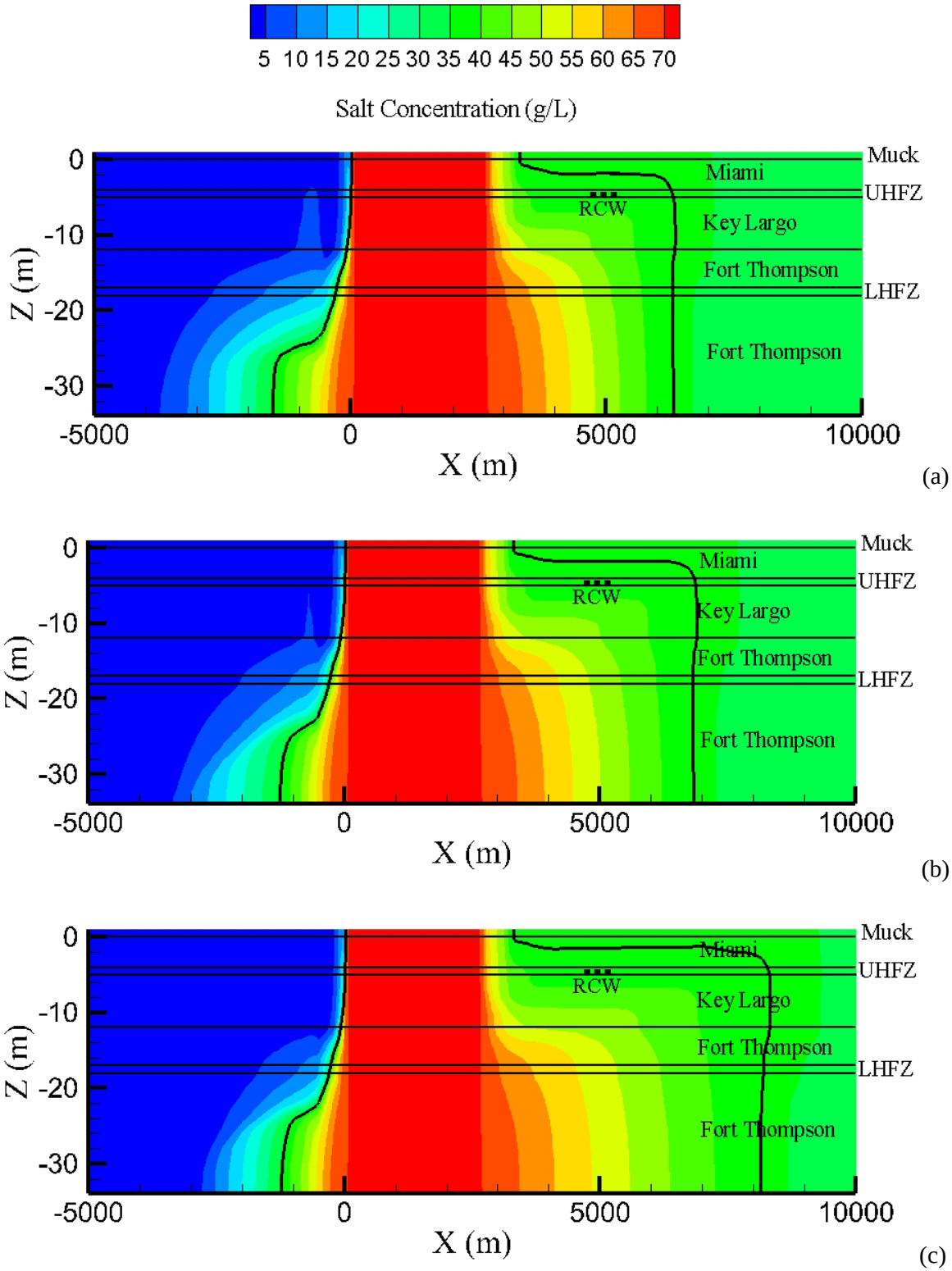


**Figure 8.26**. Salt Concentrations (g/L) over -5,000 < *x* < 10,000 m Range for Case 2D-8 (1.0 m Head Increase at West Boundary) at (a) 1 Year, (b) 10 Years, and (c) 40 Years

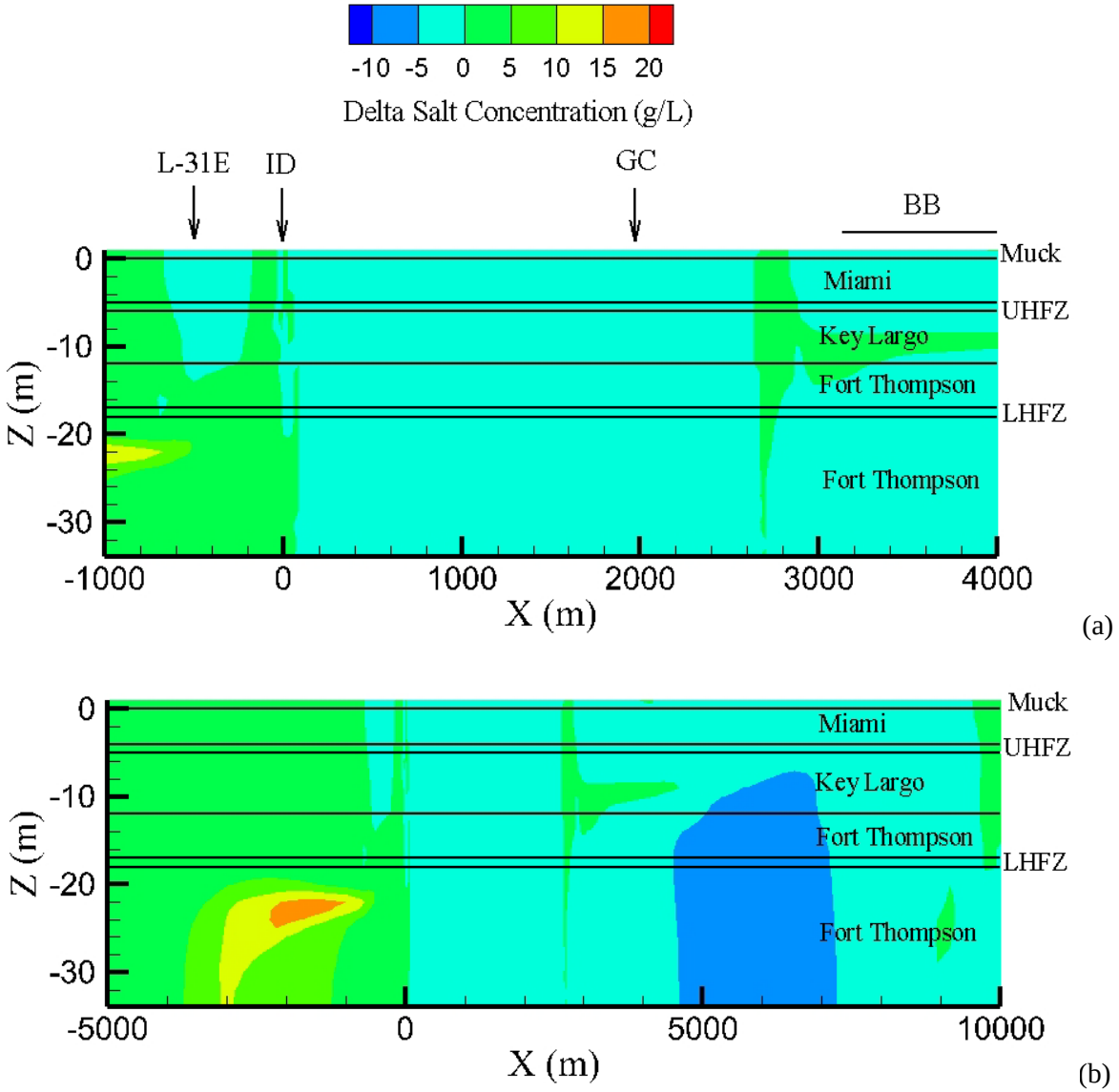


**Figure 8.27**. Differences in Salt Concentrations (g/L) between Base Case and Case 2D-8 at $t$ = 40 Years for (a) -1,000 < $x$ < 4,000 m Range, and (b) -5,000 < $x$ < 10,000 m Range

### 8.2.9 Case 2D-9: 1.0 m Head Decrease at West Boundary

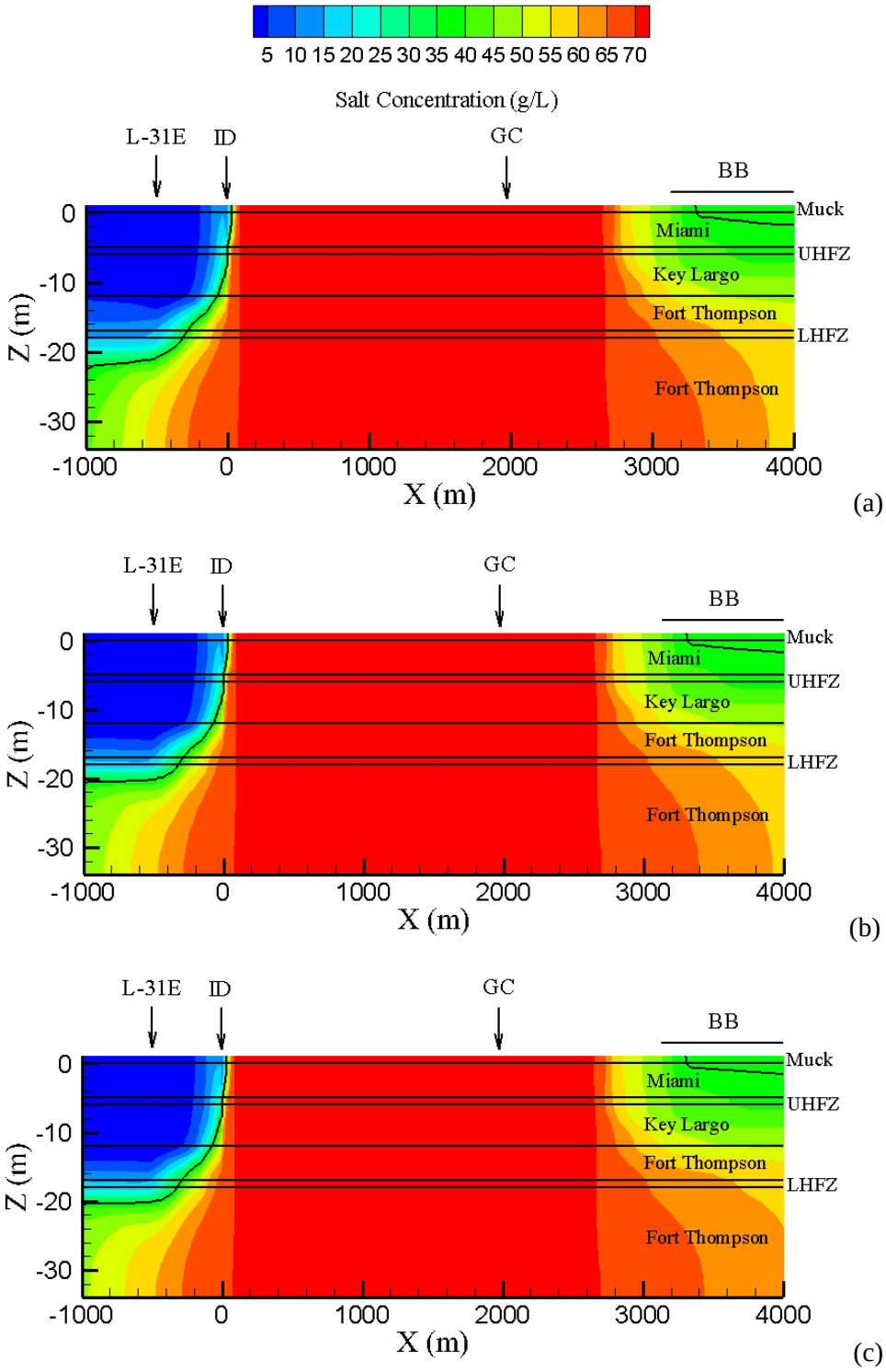


**Figure 8.28**. Salt Concentrations (g/L) over -1,000 < *x* < 4,000 m Range for Case 2D-9 (1.0 m Head Decrease at West Boundary) at (a) 1 Year, (b) 10 Years, and (c) 40 Years

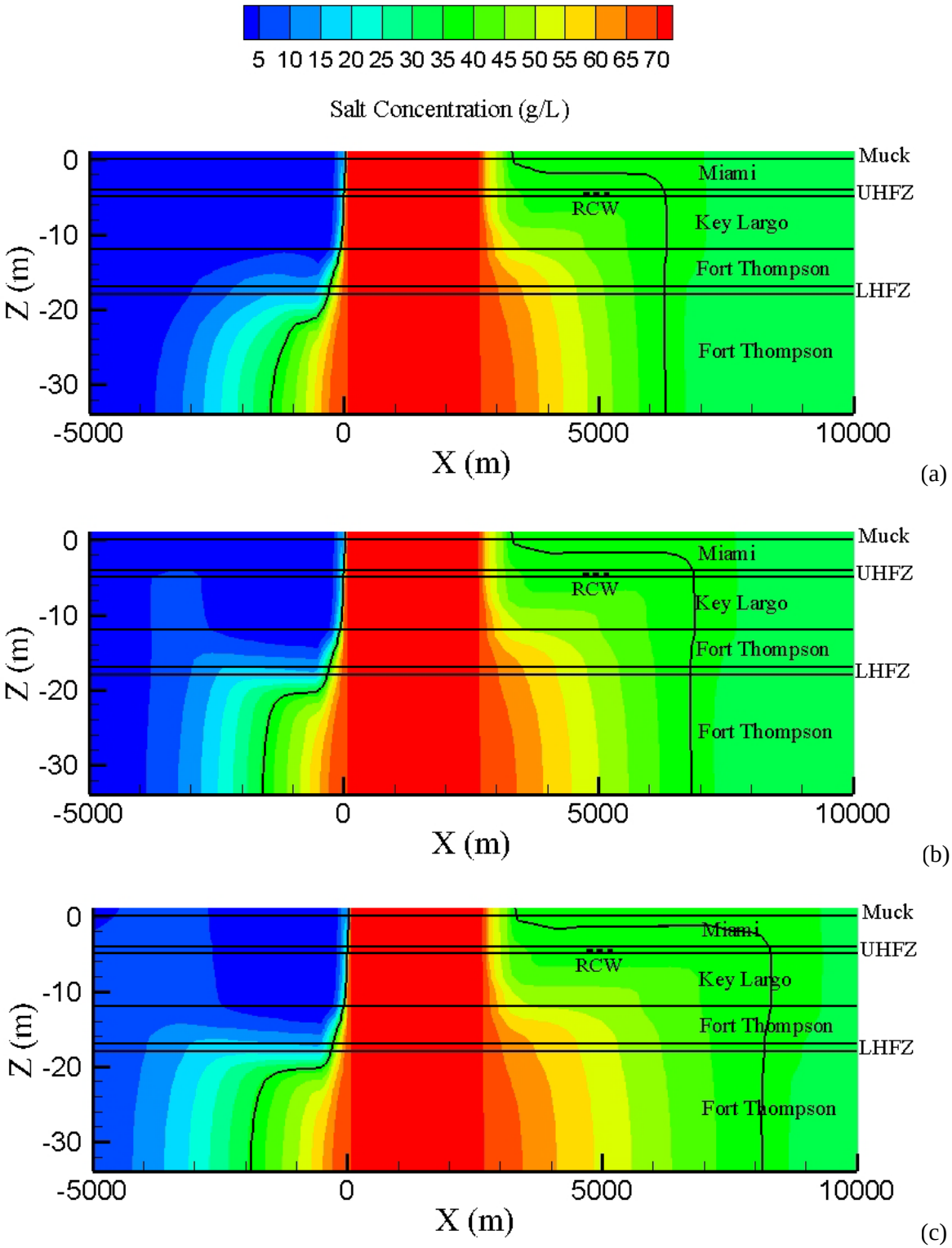


**Figure 8.29**. Salt Concentrations (g/L) over -5,000 < *x* < 10,000 m Range for Case 2D-9 (1.0 m Head Decrease at West Boundary) at (a) 1 Year, (b) 10 Years, and (c) 40 Years

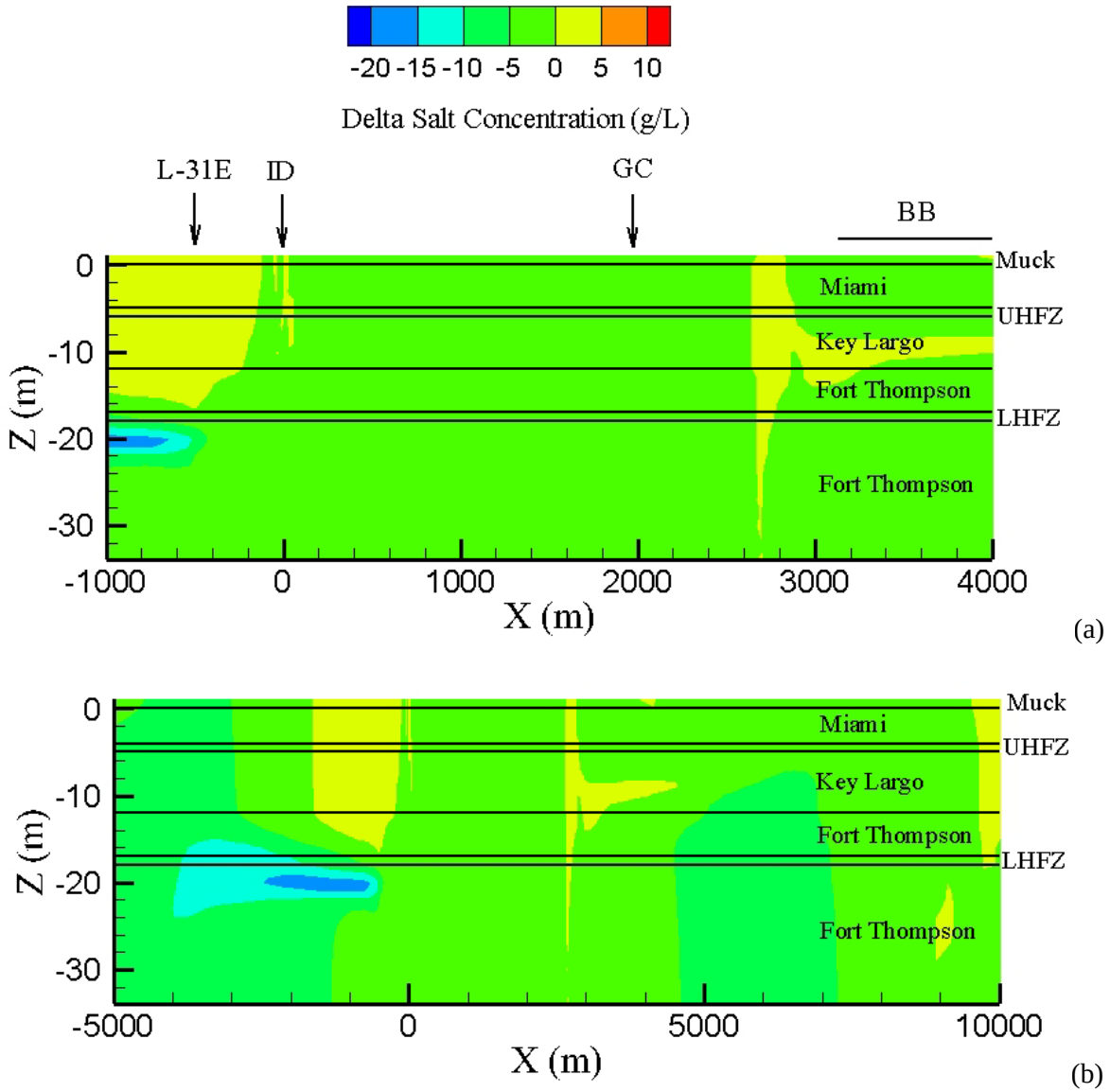


**Figure 8.30**. Differences in Salt Concentrations (g/L) between Base Case and Case 2D-9 at $t$ = 40 Years for (a) -1,000 < $x$ < 4,000 m Range, and (b) -4,000 < $x$ < 10,000 m Range

# 9.0 3D Simulation Results

The results of the 3D simulations are summarized here by case number/name and the associated figures, presented by case number/name, appear in the following sections.

The plots in Figure 9.1 show the fluctuating nature of the salt concentrations in the RCWs. When interpreting these plots, however, it is important to recognize that extraction only takes place for 60 days and that for these extraction periods, the plotted concentrations represent the saltwater that is removed from the subsurface. For the remainder of each year, no water is extracted and the reported salt concentrations only indicate concentrations at the well location. The concentration plots in Figure 9.1a indicate similar responses for each year. When the pumps are turned on, the concentrations quickly increase at all three wells (RCW-1, RCW-2, and RCW-3) due to hypersaline water removal from the UHFZ west of the RCWs and the Key Largo formation below the RCWs. A more detailed view of the individual behavior at each RCW is presented in Figure 9.1b, in which time is plotted on a logarithmic scale. This figure clearly shows the concentration increase during each extraction period when hypersaline water is transported to the RCWs through the highly permeable UHFZ. The increase occurs almost immediately after turning on the wells and lasts for less than a day. Later on during the pumping periods, seawater influx from the Biscayne Bay becomes more prominent and the concentrations start to decrease again. At the end of the extraction episodes, approximately 95% of the pumped water originates from the Biscayne Bay. The second (slight) increase during the extraction periods for RCW-1 is associated with hypersaline migration from the underlying Key Largo formation. During the off-periods, concentrations slowly increase at the well locations primarily due to diffusion processes, mixing saltwater originating from Biscayne Bay and hypersaline water from the UHFZ and the Key Largo. Over the 20-year time frame shown in Figure 9.1, the overall trend indicates a slow concentration decrease in the RCWs. If the RCW were not used (Case 3D-1), the simulations show that the concentrations at the well locations would only have increased slowly as the hypersaline plume slowly migrates to the east (Figure 9.2). Over the 20-year period, the simulated salt concentrations increase less than 1 g/L.

Salt concentration distributions at a cross section through the RCWs are shown in Figure 9.3 for the pumping (3D Base Case) and the no-pumping case (Case 3D-1). The plots show only limited differences, but exclusively at the east side of the hypersaline plume. Although the pumping has reduced salt concentrations in the Key Largo and upper Fort Thompson layers between $x$ = 3,000 and 5,000 m, it has not considerably lowered the 19,000 salinity contour.

The effects of using 50% of the maximum pumping rate of 86,400 gal/min (Case 3D-2) and 10% of that maximum rate (Case 3D-3 are shown in Figure 9.4 and Figure 9.5, respectively. The results show that decreasing the pumping rate has a relatively minor influence on the well concentrations. Over time, the concentrations at the wells are slightly larger than for the 3D-Base Case during and in between well operations. When less water is extracted, less Biscayne Bay saltwater migrates downward, allowing for increased influence of the hypersaline water migrating eastwards primarily as a result of diffusion. When the extraction period is shortened from 60 days to 30 days per year, while extracting at the maximum rate, (Case 3D-4, Figure 9.6) the observed differences in the 3D Base Case are again rather minor and similar salt concentration amplitudes occur during well operation. In general, the three cases (3D-2, 3, and 4) evaluating operations (rate and duration) suggest that the proposed operation with 86,400 gal/min over 60 days is such that it will completely dominate flow and transport in the area next to the RCWs, because reasonable variations in the rate and duration do not considerably influence well concentrations.

The effects of a limited operation period (i.e., two extraction cycles only) are shown in Figure 9.7. After turning off the pumps after the second 60-day extraction, the simulated concentrations slowly rebound to approximately 40.5 g/L before decreasing to slightly over 39 g/L after 20 years. The final concentration

value is close to the concentrations for the no-pumping case (3D-1) shown in Figure 9.2. The results in Figure 9.7 show that during pumping periods, concentration gradients west of the RCW are increasing because of the large influx of Biscayne Bay water at 35 g/L. The increase in these gradients as a result of pumping can be seen in Figure 9.3, for example. When pumping is terminated, these increased gradients cause a larger diffusive flux toward the east and an increase in concentration. Later in time, density-driven transport will become more important and downward salt migration will cause the concentration to slowly decrease.

When the pumps are operating continuously, the simulated concentrations at RCW-1 increase over time until an asymptotic value of ~42 g/L is obtained after about 1 year (Figure 9.8). The other two wells show an initial increase followed by a decrease to levels slightly above the Biscayne Bay saltwater concentration levels. The difference between RCW-1 and the other two wells shows that RCW-1 extracts some hypersaline water originating from the CCS and that RCW-2 and RCW-3 primarily extract Biscayne Bay saltwater.

In sensitivity Cases 3D-7 through 3D-12, a modification was made to the west of the CCS. The results that the three modifications have in common are that the salt concentrations at the RCWs are only slightly affected, as can be seen in Figure 9.9, Figure 9.12, and Figure 9.15 for Cases 3D-7, 3D-9, and 3D-11, respectively. The lack of influence of the L-31E Canal and west boundary heads on the RCW concentrations is also illustrated by the salt concentration distributions shown in Figure 9.10, Figure 9.13, and Figure 9.16. East of the CCS, these distributions are similar for all the three cases. These three salt distribution figures also show the similar effects of pumping on the hypersaline plume behavior by comparing the pumping with the non-pumping scenario for the same boundary condition modification. For all of these cases, pumping increases the concentration gradients between the hypersaline plume and Biscayne Bay saltwater in the upper parts of the aquifer and removes some of the hypersaline water from the Fort Thompson formation. For each of the three imposed modifications, salt concentration differences from the Base Case are shown in Figure 9.11a, Figure 9.14a, and Figure 9.17a, respectively. As expected, common to each of the three figures is the fact that the salinity differences primarily occur at the west side of the CCS and limited effects occur on the east side. Differences between the pumping and no-pumping cases for the three modifications are shown in Figure 9.11b, Figure 9.14b, and Figure 9.17b, respectively. The plots show that the RCW pumping removes hypersaline water from the east side of the plume but that the concentrations impacts at the location at wells are small, which is consistent with the simulated concentration over time plots shown in Figure 9.9, Figure 9.12, and Figure 9.15.

The effects of sea level rise on RCW behavior are illustrated by Cases 3D-13 and 3D-14 (1.5 m rise), and 3D-15 and 3D-16 (0.5 m rise). Both case sets show that the extracted salt concentrations decrease over time (Figure 9.18 and Figure 9.21) as because the increasing Biscayne Bay head results in displacement of the hypersaline plume toward the CCS. After 20 years of periodic pumping, the extracted water concentration is only slightly larger greater than that of the Biscayne Bay salt water during the pumping period due to extraction of some hypersaline water from the UHFZ. During the non-pumping periods between extractions, the concentrations are reduced to Biscayne Bay salt water levels. Similar to what was observed for the 2D sea level rise simulations, the displacement of the hypersaline water occurs faster for the higher sea level rise case. Differences between the Base Case and the two sea level rise scenarios with pumping show that the enhanced seawater migration toward the west is clearly the dominating process (Figure 9.20a and Figure 9.23a). Differences between the pumping and no- pumping cases for both scenarios near the RCW system are small after 20 years of operation (Figure 9.20b and Figure 9.23b), illustrating the limited effect pumping has on extracted salt water concentrations during sea level rise scenarios.

As is shown in Case 3D-17 Figure 9.24, turning on 4 of the 10 remediation wells, located in the LHFZ, at the total capacity available in the deep injection well proposed to dispose of pumped water (12,000,000

gal/day) does not influence the RCW concentrations. The plots in this figure are identical to the 3D Base Case (Figure 9.1). This result is consistent with the other simulations in which a boundary condition was modified to the west of the CCS (Cases 3D-7 through 3D-12). The concentrations at the remediation wells (Figure 9.25) show that within a year, the extracted concentrations increase to the maximum hypersaline level of 70 g/L (i.e., CCS salt concentration). This result indicates that although the remediation wells extract the maximum possible salt mass after a relatively short amount of time, the hypersaline plume is pulled toward the wells in the LHFZ.

Cases 3D-18 through 3D-21 evaluate RCW behavior after refreshing of the original hypersaline plume with 34 g/L water emanating from the CCS. The initial conditions of these simulations are equal to the final results of the 34 g/L 2D simulations shown in Figure 8.7c and Figure 8.8c. The salt concentration results of these simulations, shown in Figure 9.26 through Figure 9.29, indicate small and diminishing pumping effects over time and constant concentrations for the no-pumping scenarios. The results are as expected because of the major refreshing that occurs before the pumps were activated. The concentrations of the extracted saltwater are greater than the Biscayne Bay concentrations because some of the extracted water originates from the hypersaline plume.

The final case (Case 3D-22) investigates RCW pumping with simultaneous CCS operation (34 g/L saltwater), starting with a pristine aquifer with only saltwater intrusion. The results show that during pumping, a limited amount of water originating from the CCS is extracted, thereby slightly reducing the extracted salt concentration below the Biscayne Bay level (Figure 9.30). This observation is sustained over the simulated period of 20 years.

## 9.1 3D Base Case

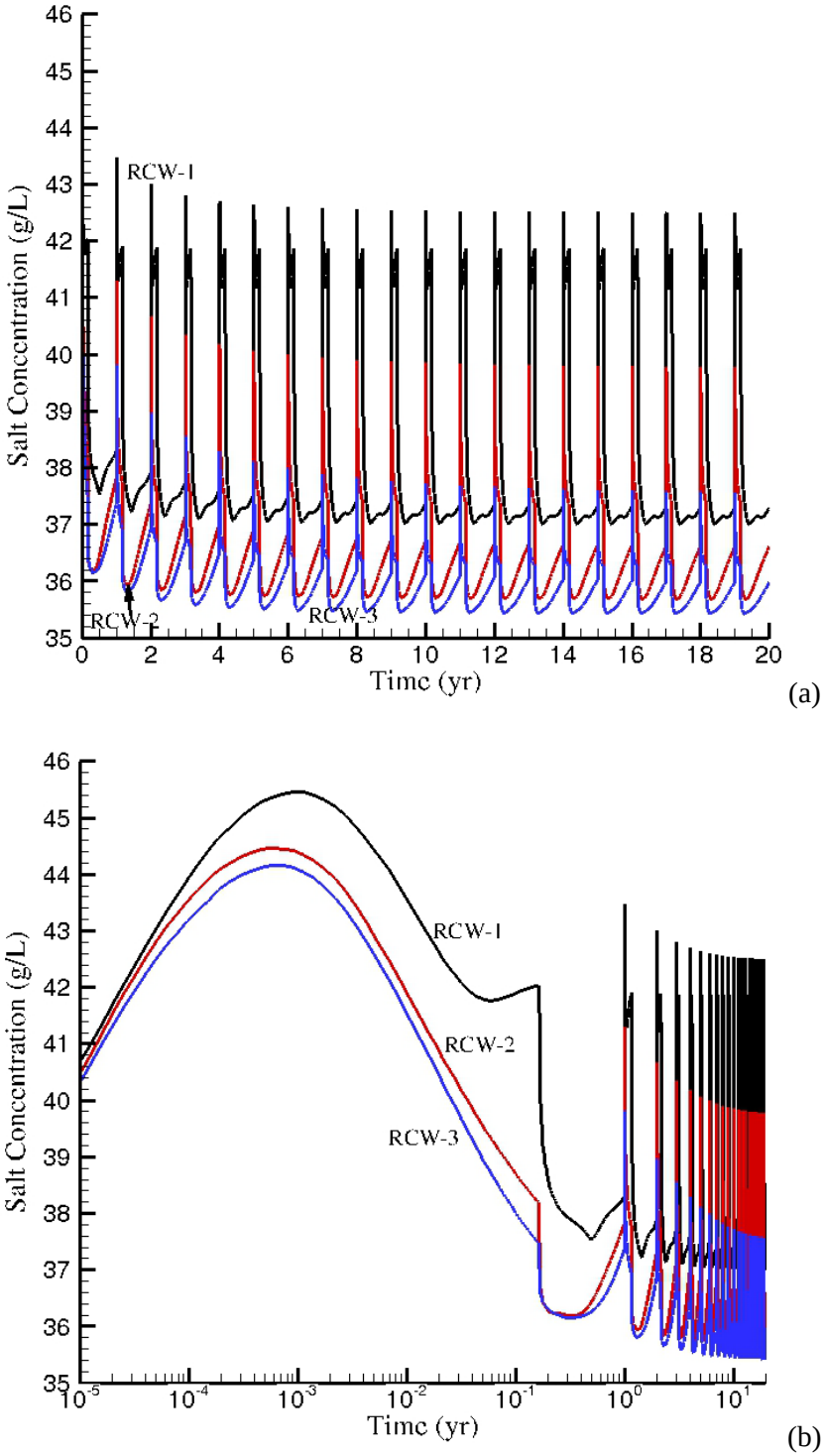


**Figure 9.1**. Salt Concentrations (g/L) over (a) Linear and (b) Logarithmic Time at RCW-1 (black), RCW-2 (red), and RCW-3 (blue) for the Base Case

## 9.2 Case 3D-1: Base Case without Pumping

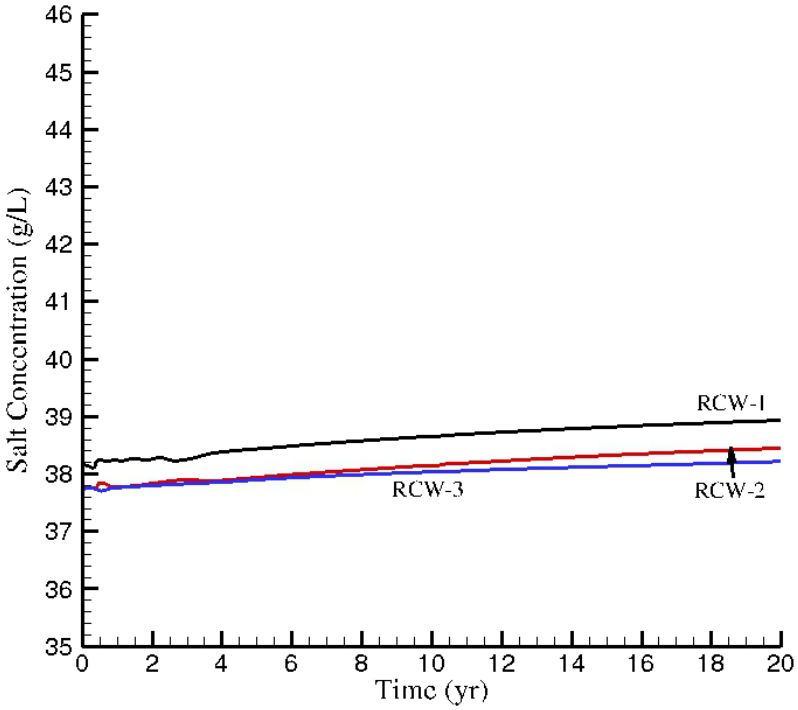


**Figure 9.2**. Salt Concentrations (g/L) over Time at RCW-1 (black), RCW-2 (red), and RCW-3 (blue) for Case 3D-1 (No RCW Pumping)

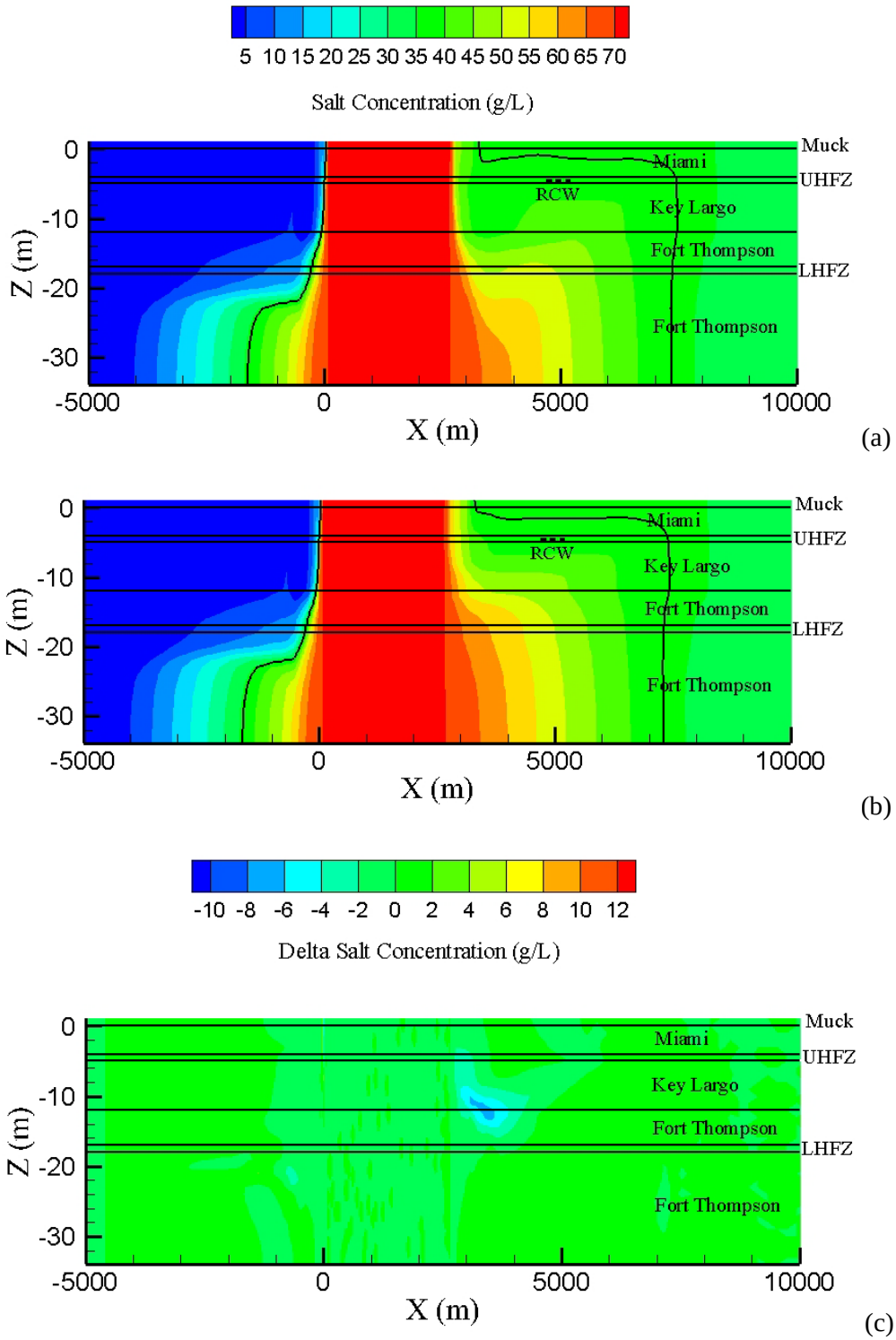


**Figure 9.3**. Salt Concentrations (g/L) for Domain Cross Section at $y$ = 0 m at $t$ = 20 Years for (a) RCW Pumping (3D Base Case) and (b) No RCW Pumping (Case 3D-1). The differences are shown in (c).

## 9.3 Case 3D-2: Half the Extraction Rate

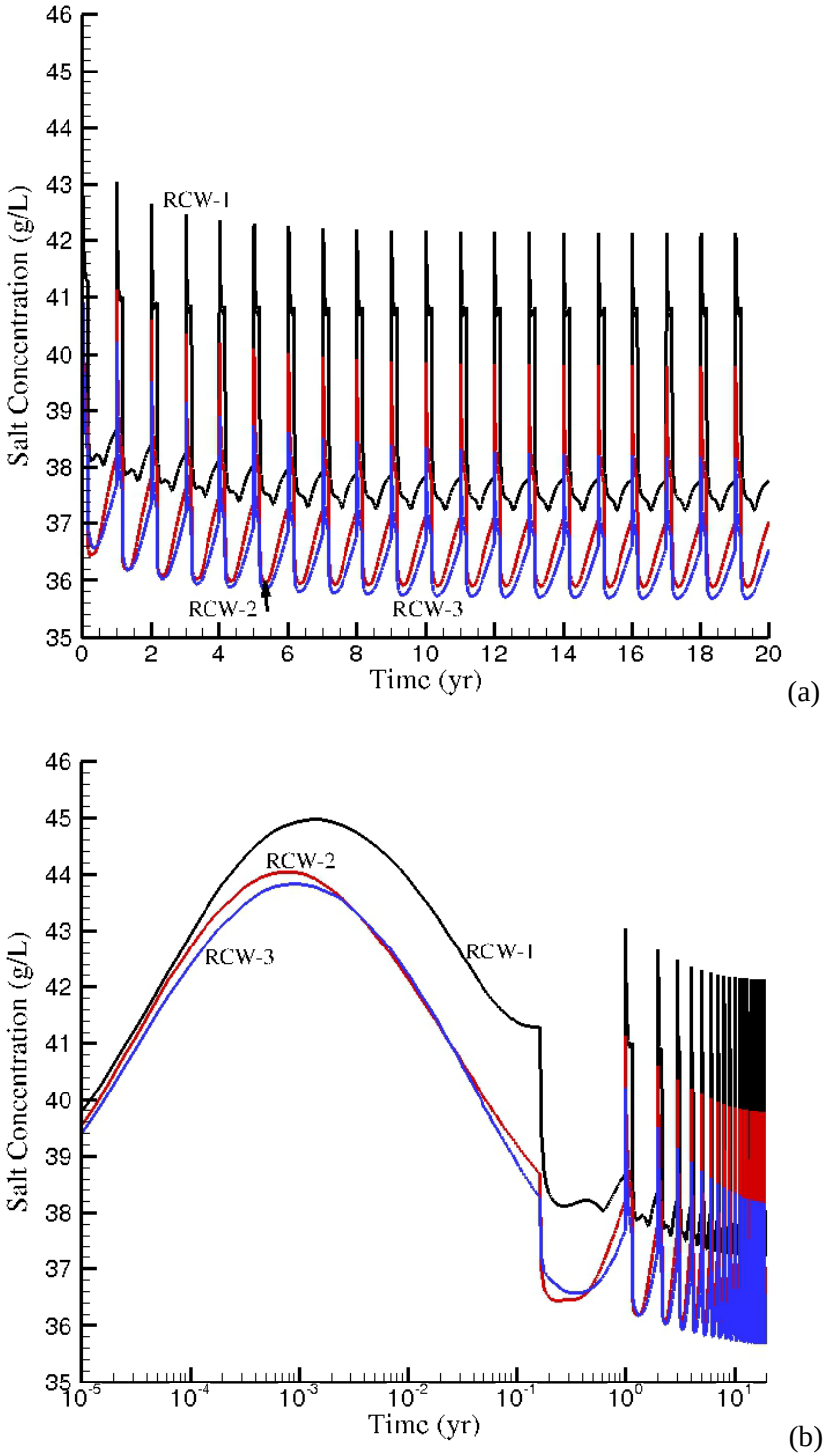


**Figure 9.4**. Salt Concentrations (g/L) over (a) Linear and (b) Logarithmic Time at RCW-1 (black), RCW-2 (red), and RCW-3 (blue) for Case 3D-2 (half the extraction rate)

## 9.4 Case 3D-3: One-Tenth of the Extraction Rate

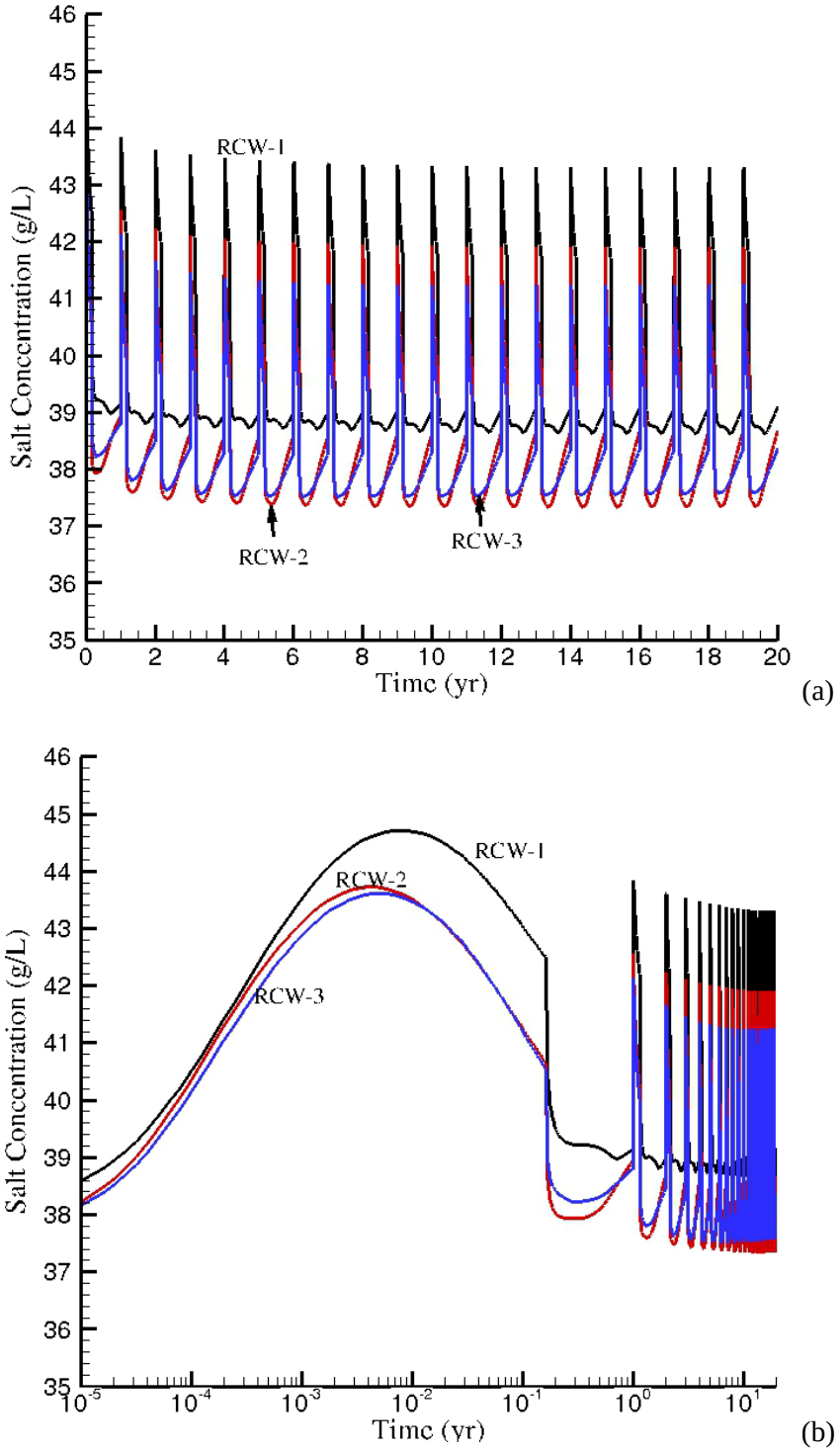


**Figure 9.5**. Salt Concentrations (g/L) over (a) Linear and (b) Logarithmic Time at RCW-1 (black), RCW-2 (red), and RCW-3 (blue) for Case 3D-3 (one-tenth of the extraction rate)

## 9.5 Case 3D-4: 30 Days per Year Operation

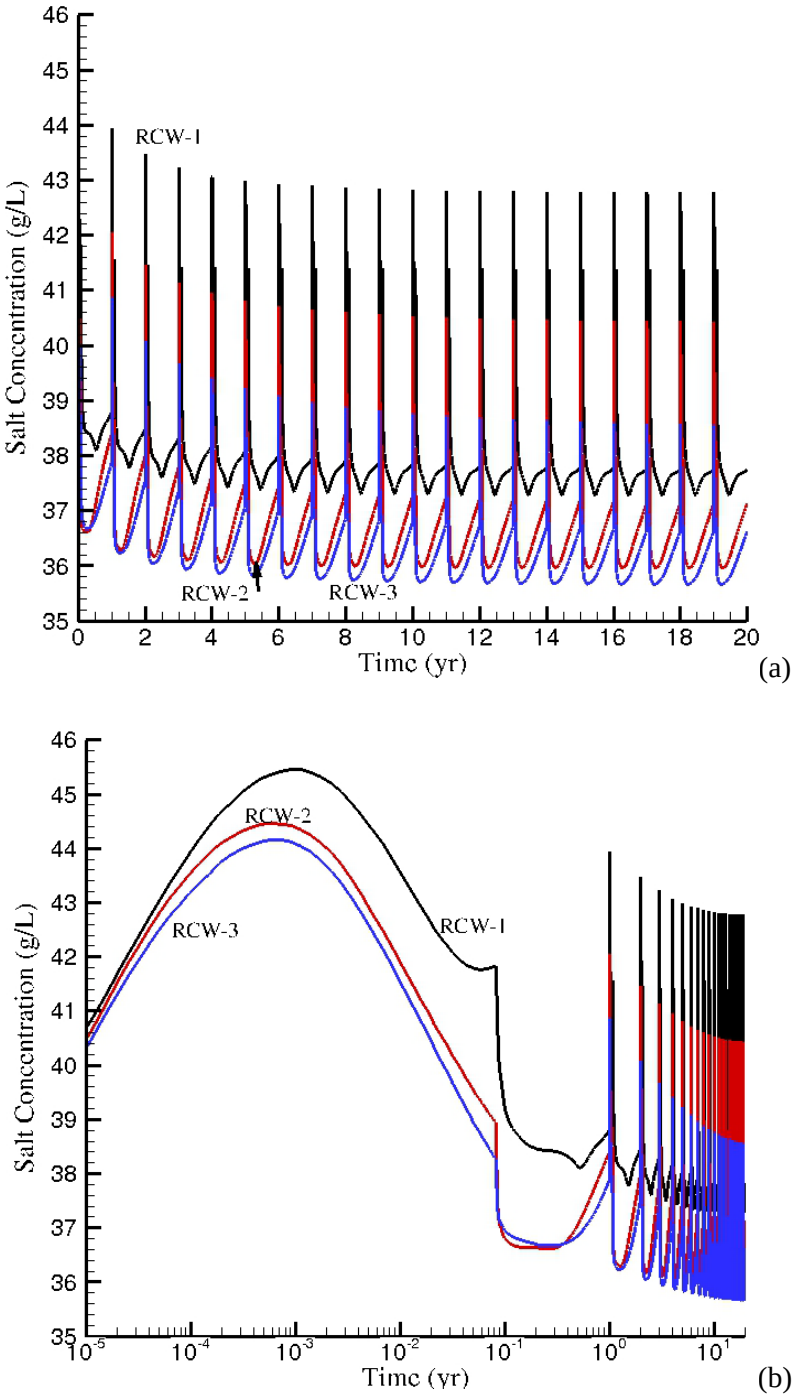


**Figure 9.6**. Salt Concentrations (g/L) over (a) Linear and (b) Logarithmic Time at RCW-1 (black), RCW-2 (red), and RCW-3 (blue) for Case 3D-4 (30 days per year extraction periods)

## 9.6 Case 3D-5: Two Operation Cycles Only

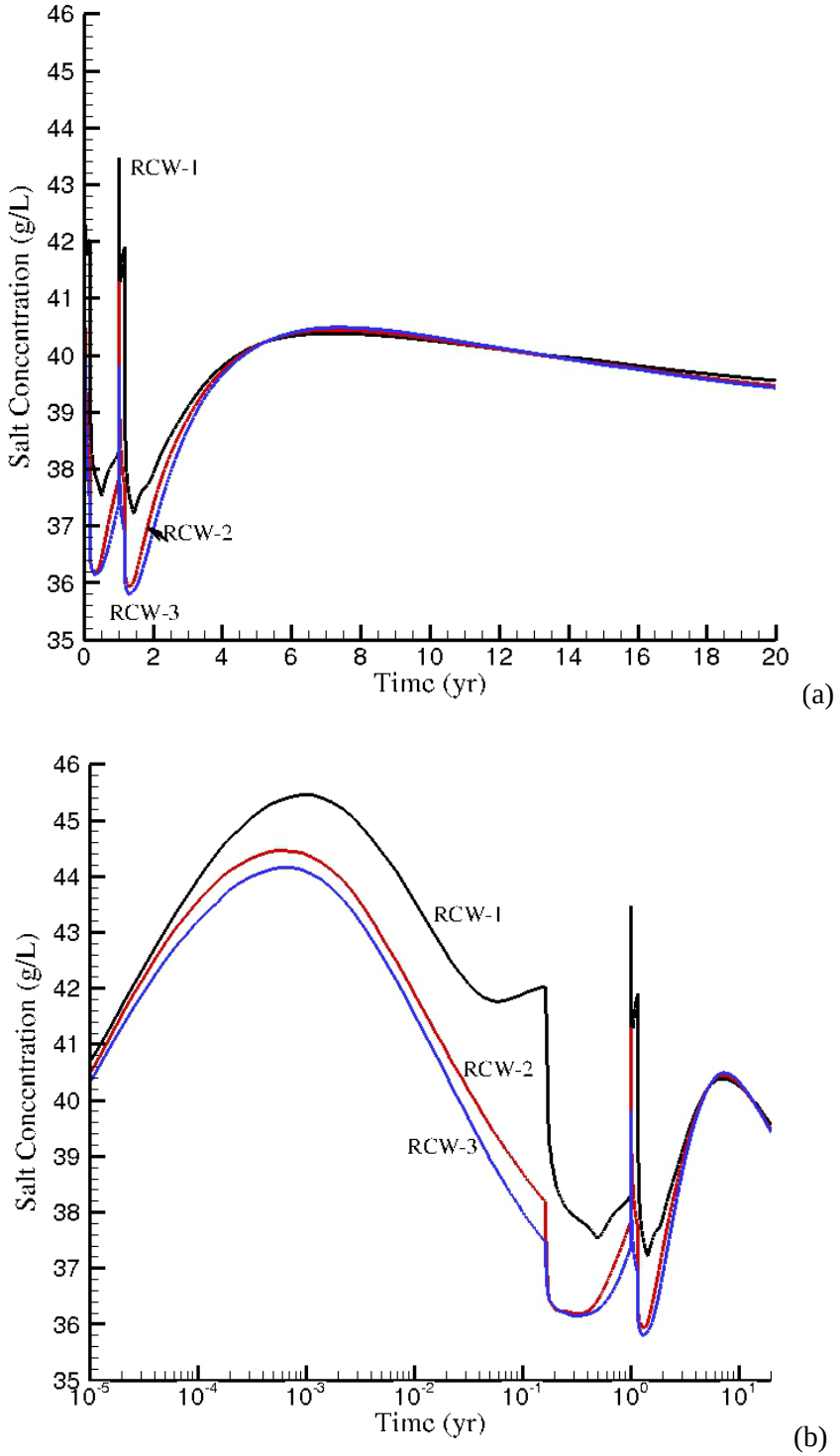


**Figure 9.7**. Salt Concentrations (g/L) over (a) Linear and (b) Logarithmic Time at RCW-1 (black), RCW-2 (red), and RCW-3 (blue) for Case 3D-5 (two operation cycles only)

## 9.7 Case 3D-6: Continuous Operation

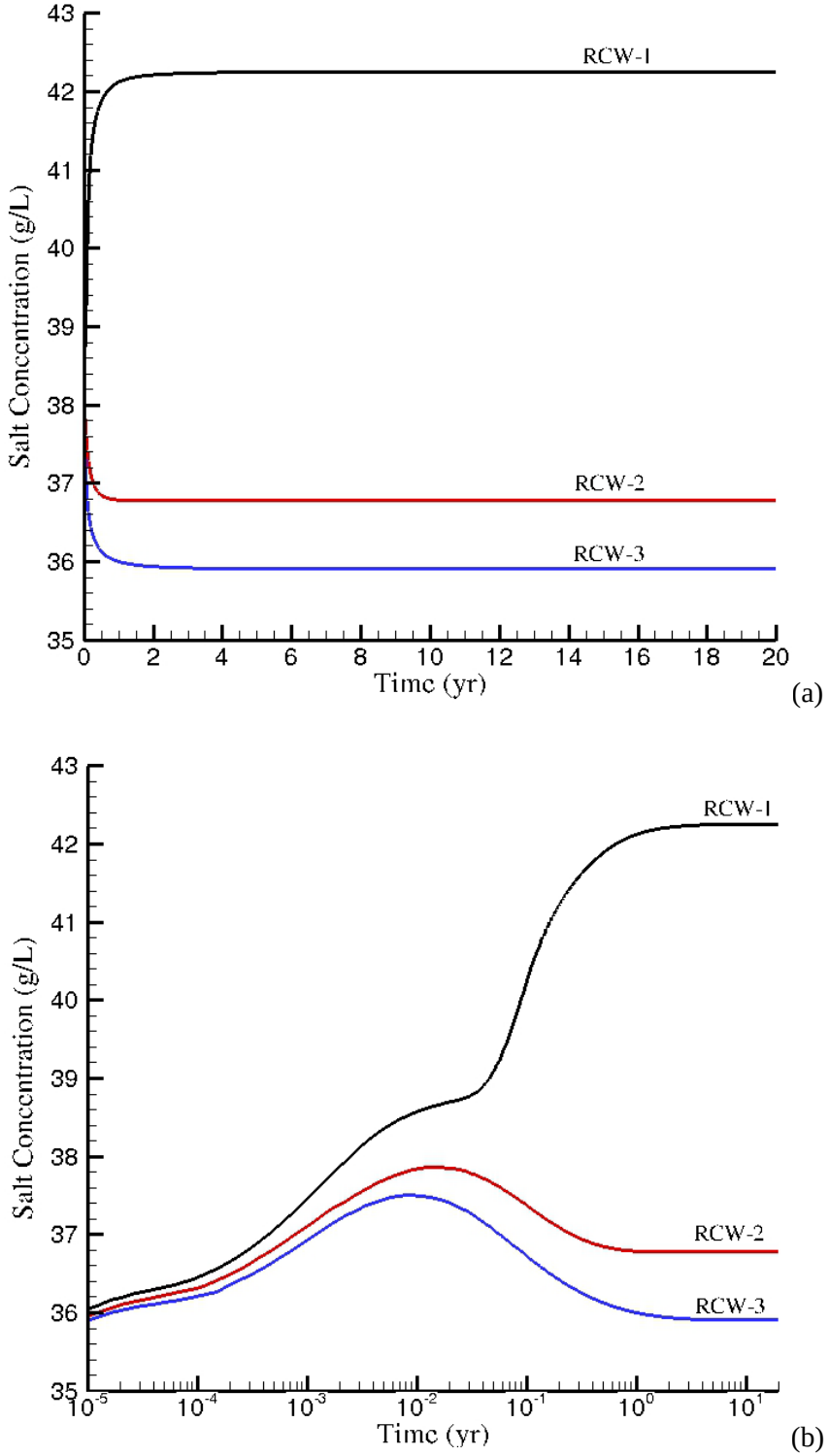


**Figure 9.8**. Salt Concentrations (g/L) over (a) Linear and (b) Logarithmic Time at RCW-1 (black), RCW-2 (red), and RCW-3 (blue) for Case 3D-6 (continuous operation)

## 9.8 Cases 3D-7 and 3D-8: Increased Head in L-31E Canal

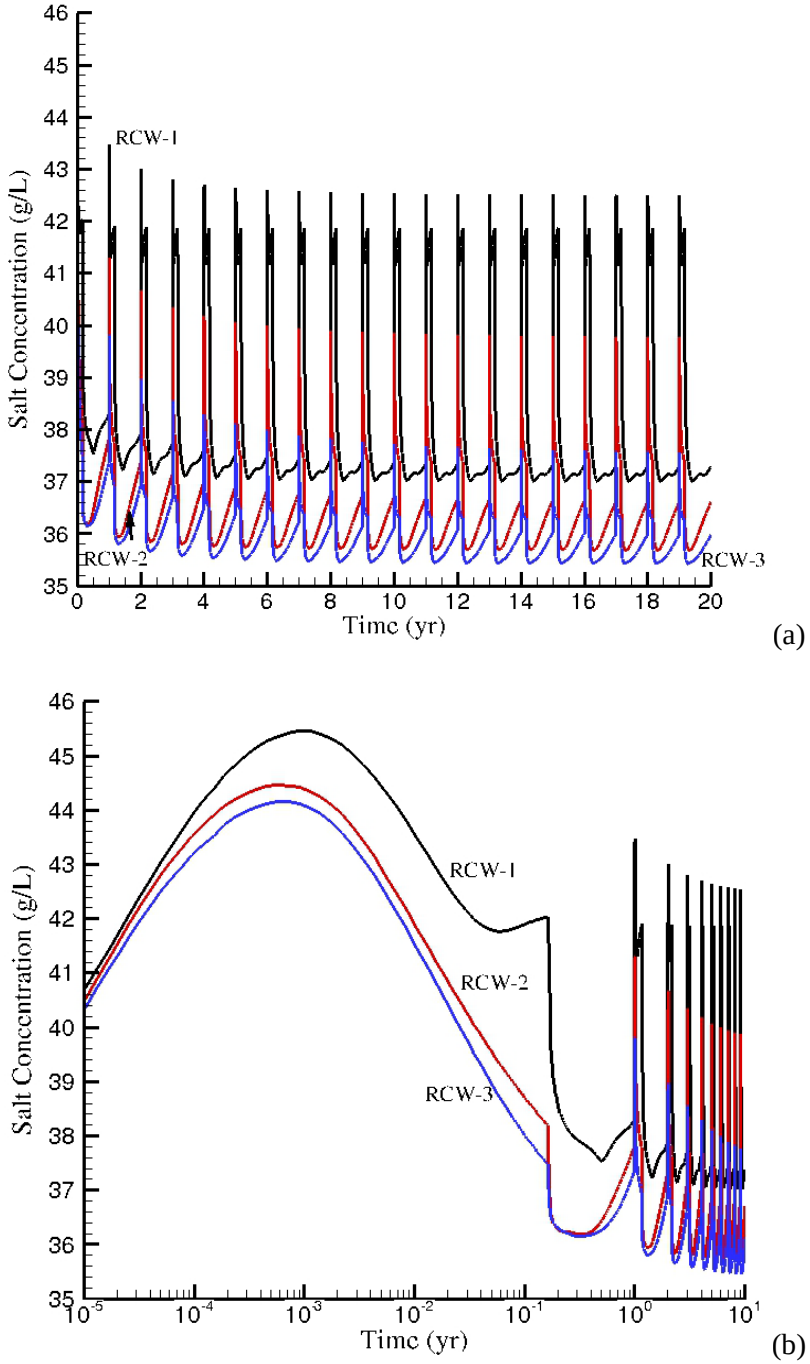


**Figure 9.9**. Salt Concentrations (g/L) over (a) Linear and (b) Logarithmic Time at RCW-1 (black), RCW-2 (red), and RCW-3 (blue) for Case 3D-7 (increased head in L-31E Canal)

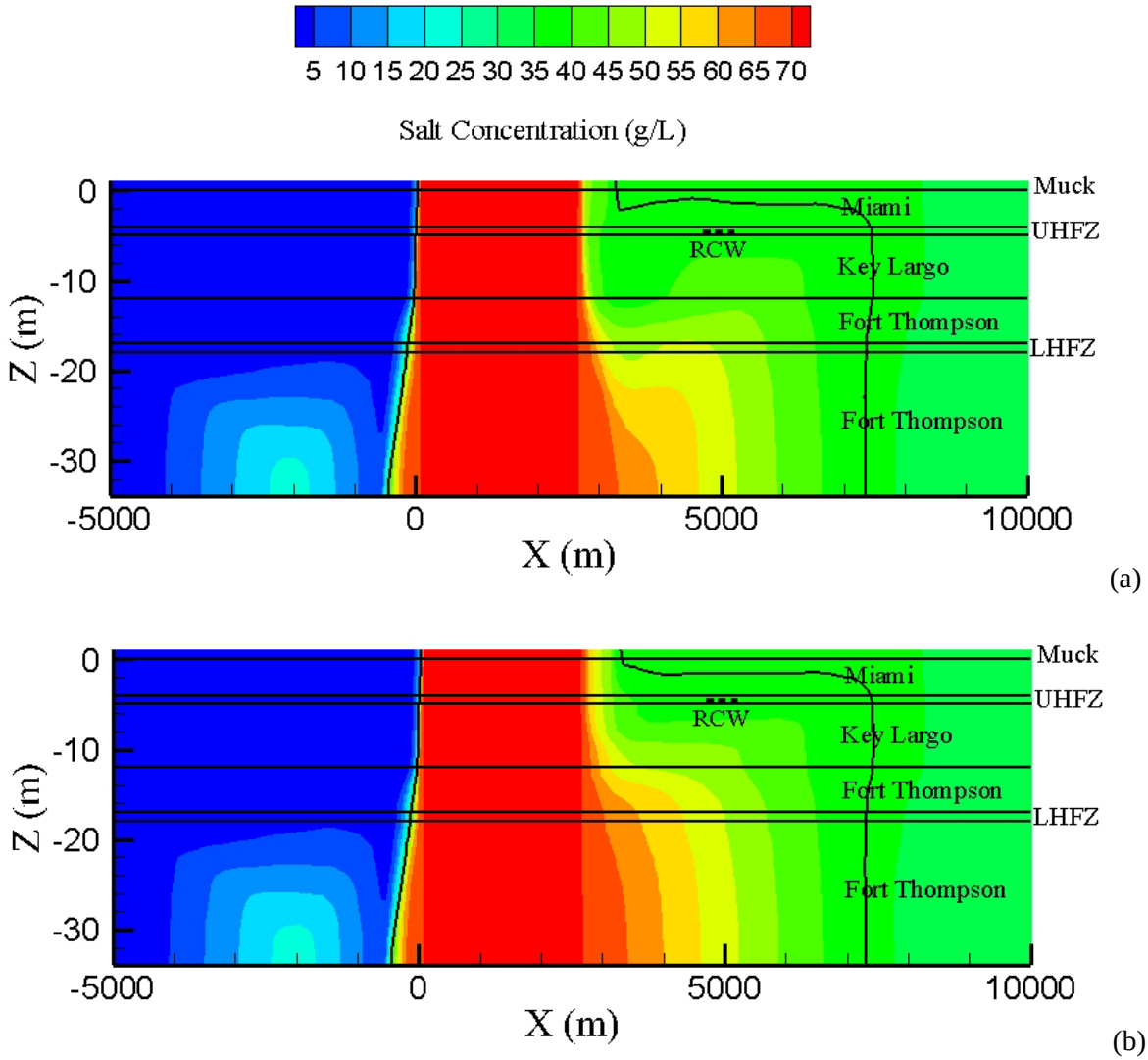


**Figure 9.10**. Salt Concentrations (g/L) for Domain Cross Section at $y$ = 0 m at $t$ = 20 Years for (a) Case 3D-7 (increased head in L-31E Canal with RCW pumping) and (b) Case 3D-8 (without pumping)

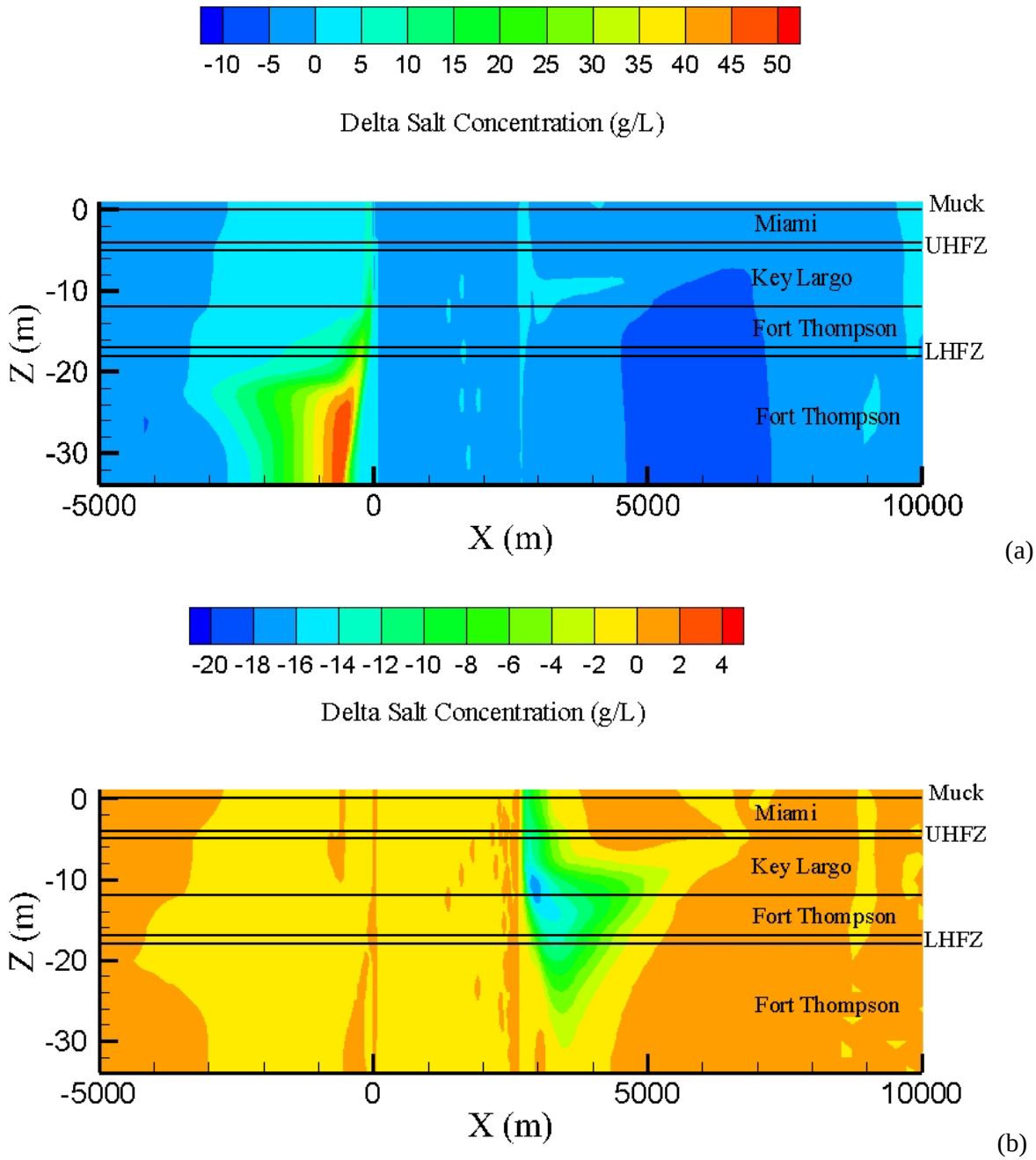


**Figure 9.11**. Differences in Salt Concentrations (g/L) between (a) Base Case (Figure 9.3a) and Case 3D-7 (Figure 9.10a) and (b) Pumping (Case 3D-7) and No Pumping (Case 3D-8) for Elevated Head in L-31E Canal.

## 9.9 Cases 3D-9 and 3D-10: Increased Head at West Boundary

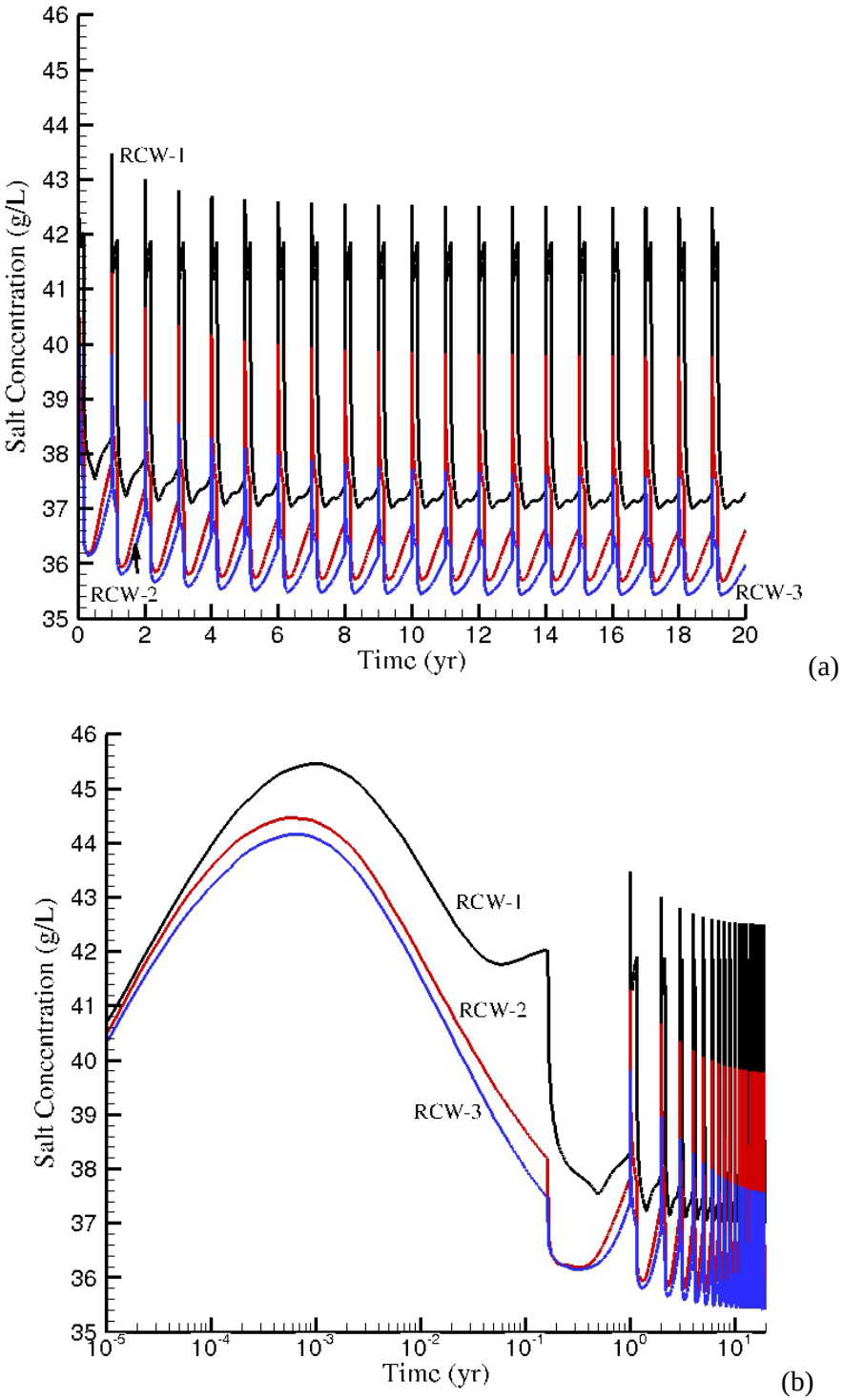


**Figure 9.12**. Salt Concentrations (g/L) over (a) Linear and (b) Logarithmic Time at RCW-1 (black), RCW-2 (red), and RCW-3 (blue) for Case 3D-9 (increased head at west boundary)

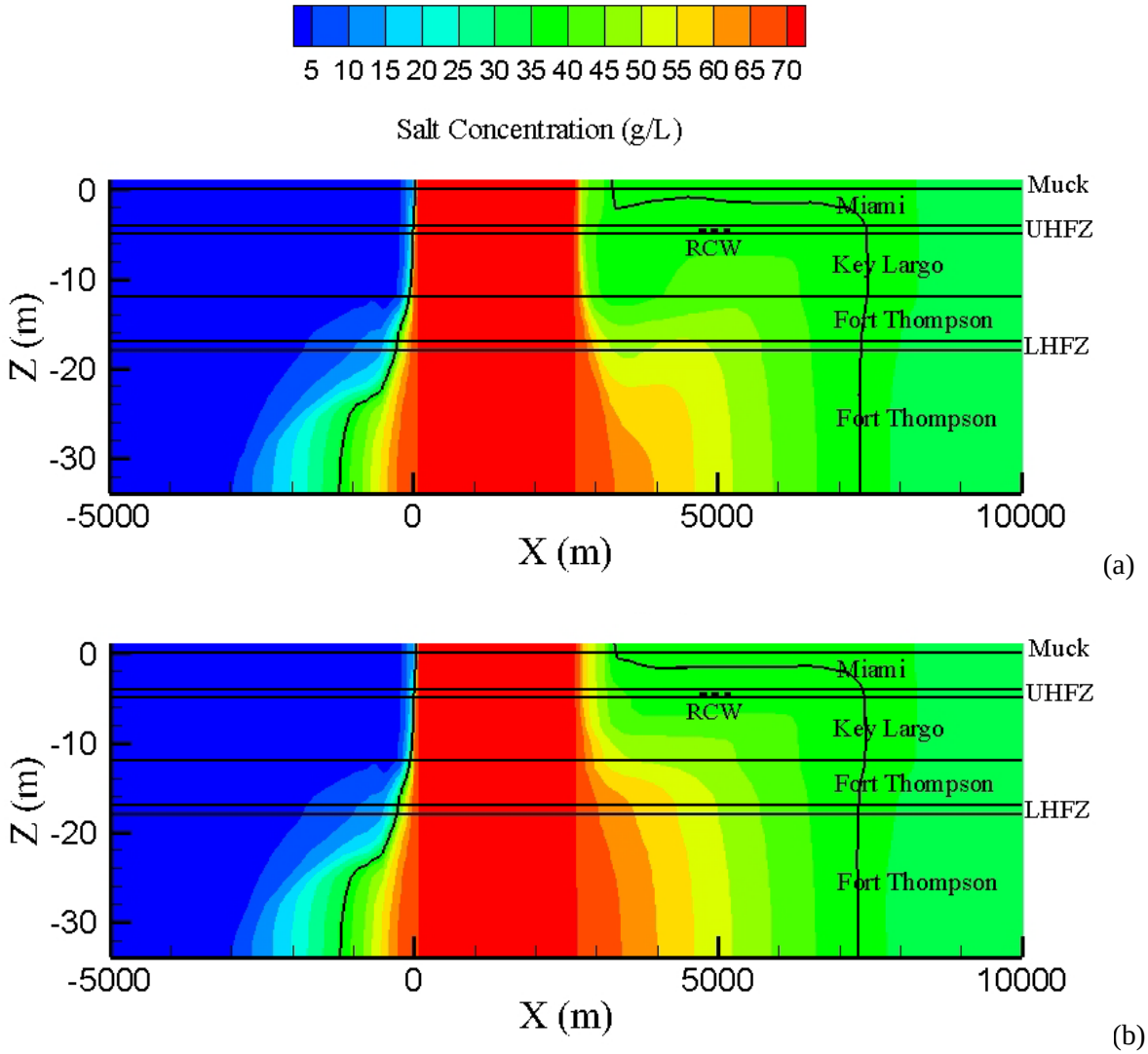


**Figure 9.13**. Salt Concentrations (g/L) for Domain Cross Section at $y$ = 0 m at $t$ = 20 Years for (a) Case 3D-9 (increased head at west boundary with RCW pumping) and (b) Case 3D-10 (without pumping)

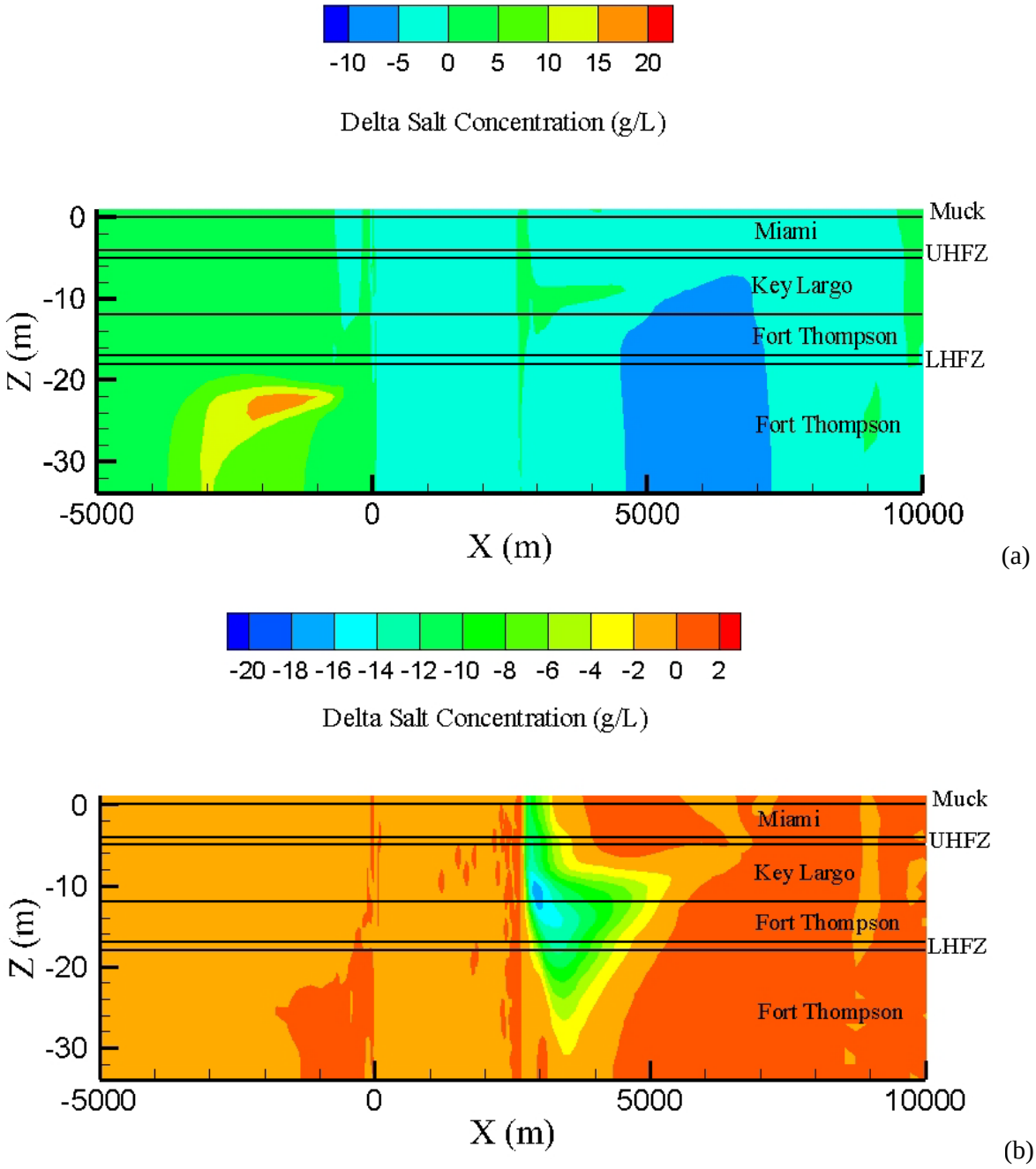


**Figure 9.14**. Differences in Salt Concentrations (g/L) between (a) Base Case (Figure 9.3a) and Case 3D-9 (Figure 9.13a) and (b) Pumping (Case 3D-9) and No Pumping (Case 3D-10) for Increased Head at the West Boundary

## 9.10 Cases 3D-11 and 3D-12: Decreased Head at West Boundary

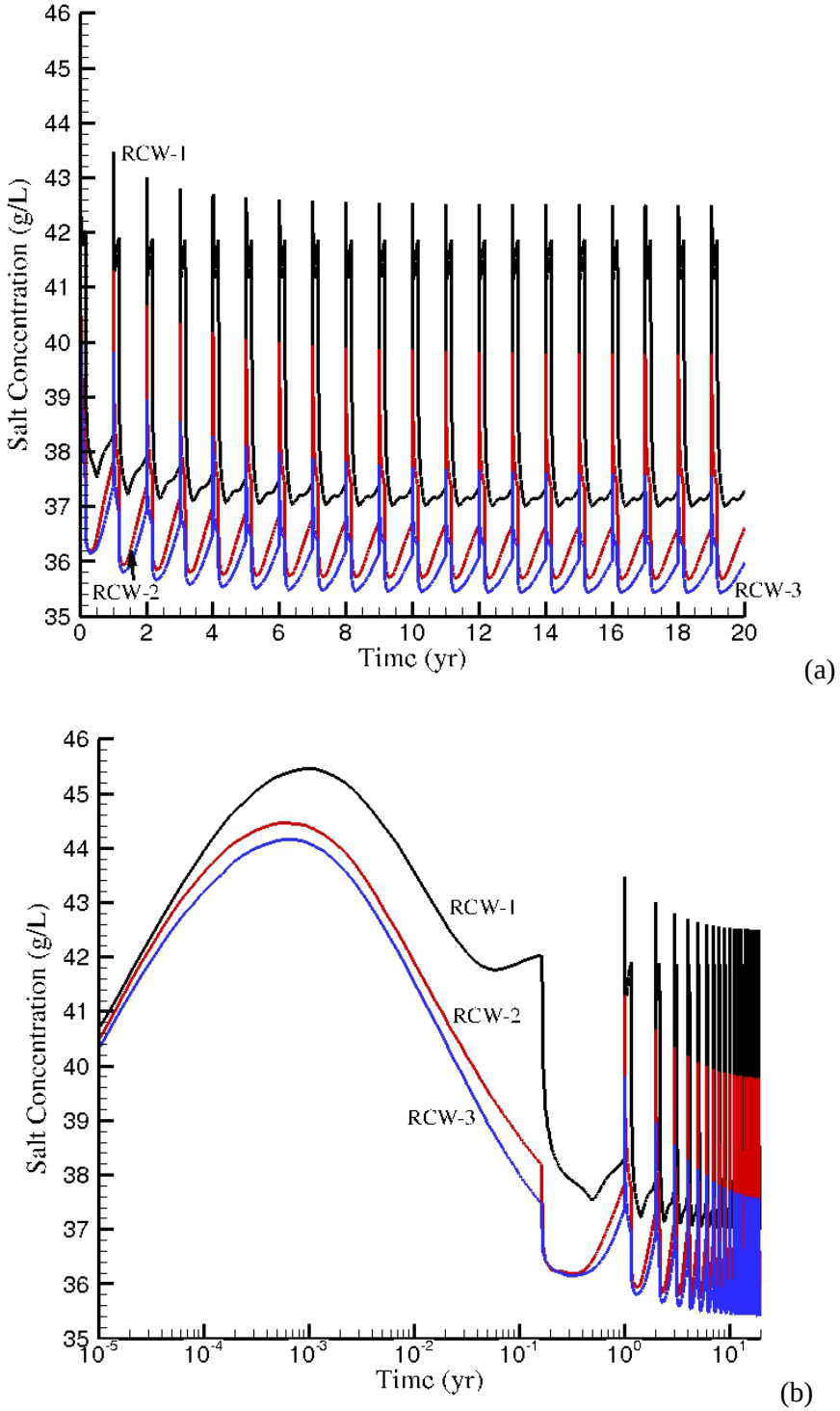


**Figure 9.15**. Salt Concentrations (g/L) over (a) Linear and (b) Logarithmic Time at RCW-1 (black), RCW-2 (red), and RCW-3 (blue) for Case 3D-11 (decreased head at west boundary)

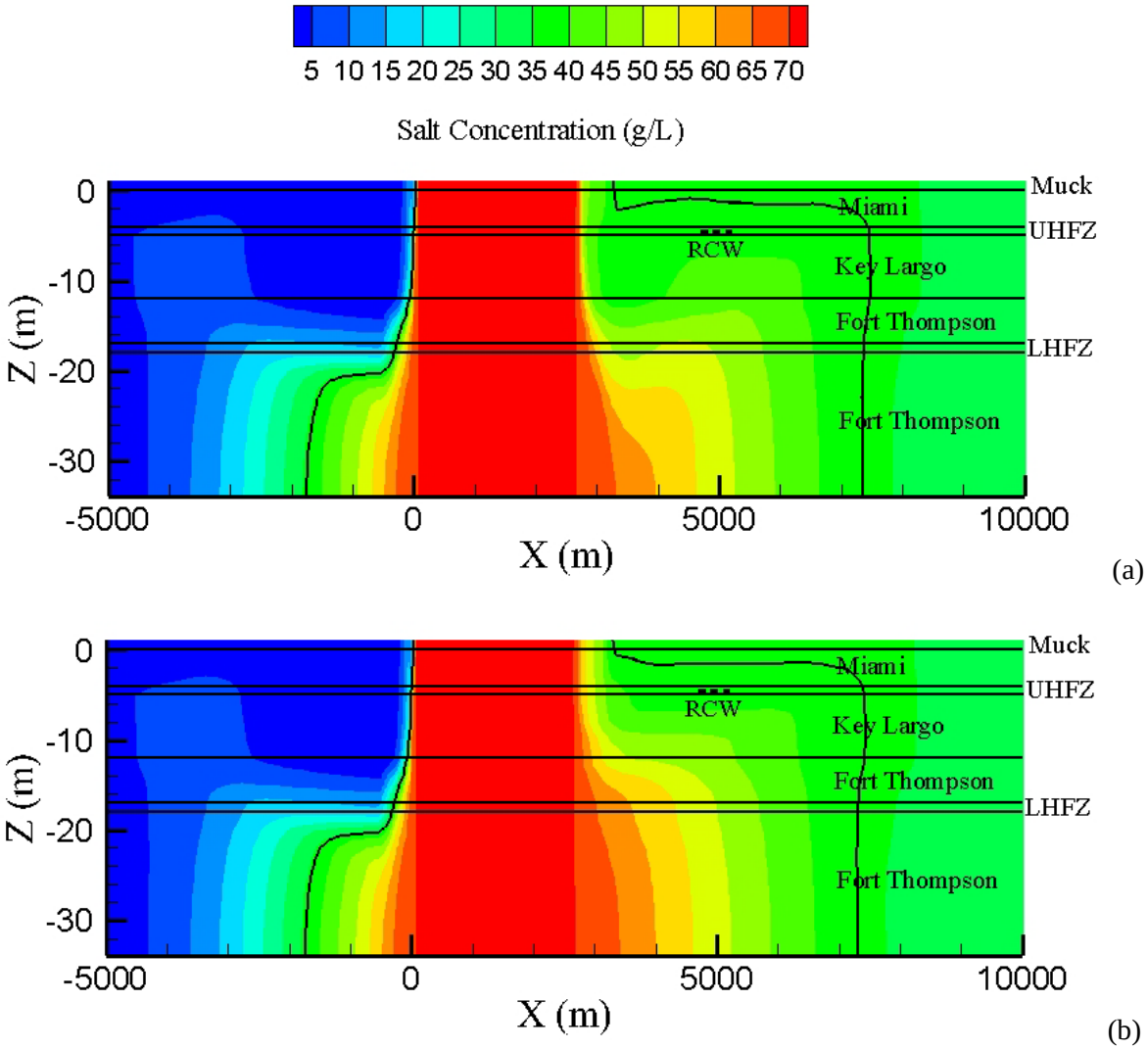


**Figure 9.16**. Salt Concentrations (g/L) for Domain Cross Section at $y$ = 0 m at $t$ = 20 Years for (a) Case 3D-11 (decreased head at west boundary with RCW pumping) and (b) Case 3D-12 (without pumping)

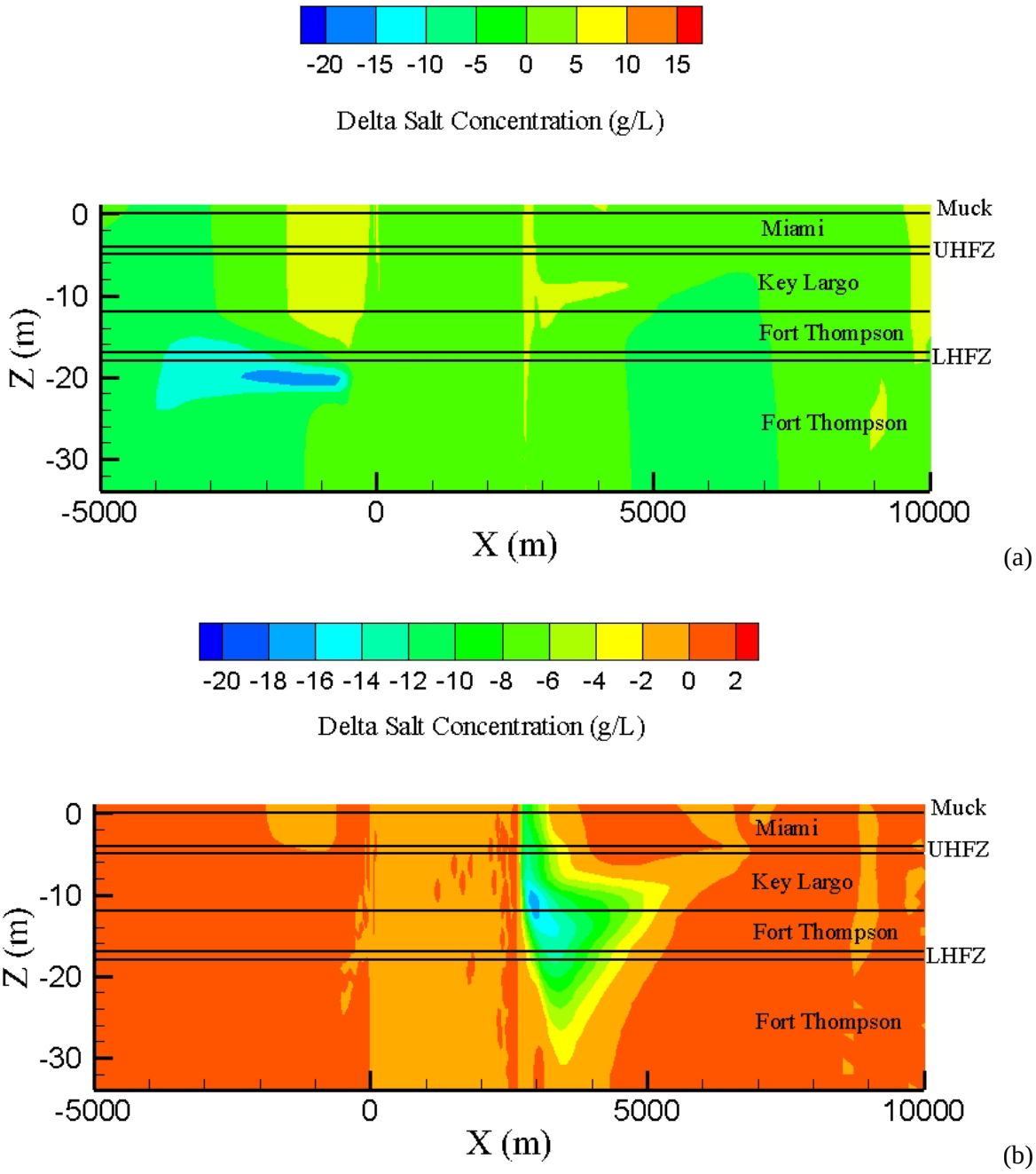


**Figure 9.17**. Differences in Salt Concentrations (g/L) between (a) Base Case (Figure 9.3a) and Case 3D-11 (Figure 9.16a) and (b) Pumping (Case 3D-11) and No Pumping (Case 3D-12) for Decreased Head at the West Boundary

## 9.11 Cases 3D-13 and 3D-14: 1.5 m Sea Level Rise

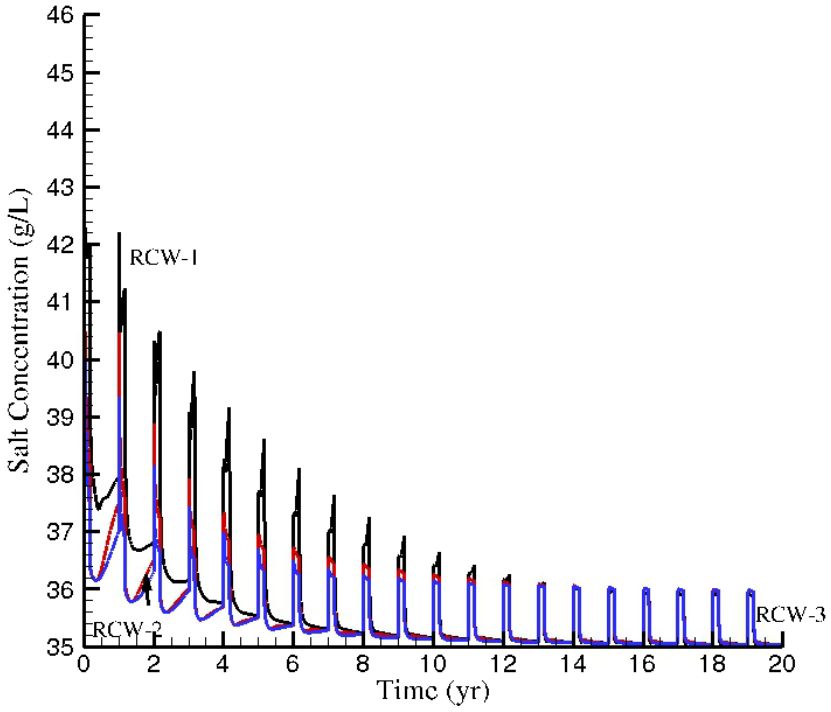


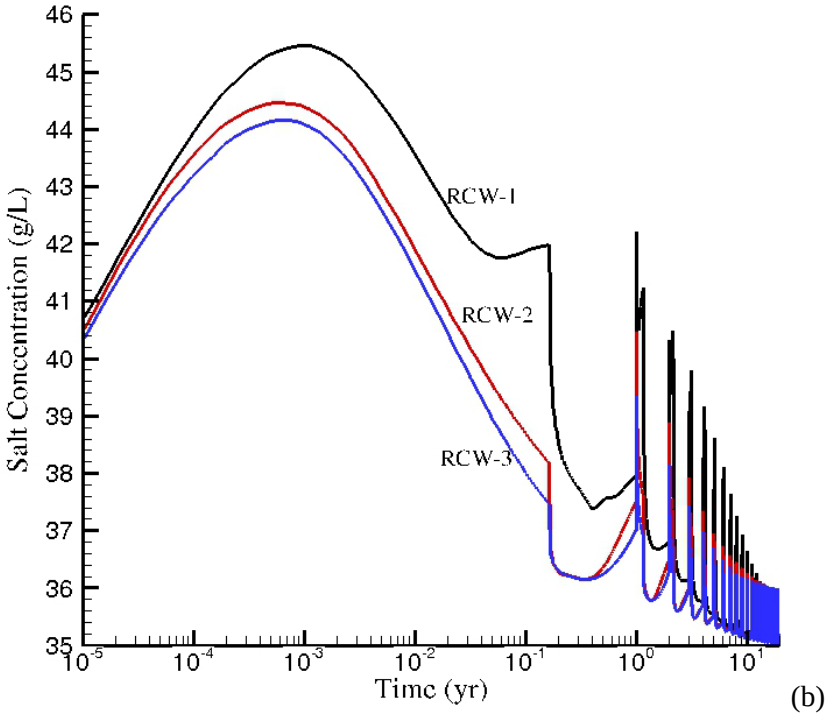


**Figure 9.18**. Salt Concentrations (g/L) over (a) Linear and (b) Logarithmic Time at RCW-1 (black), RCW-2 (red), and RCW-3 (blue) for Case 3D-13 (1.5 m sea level rise)

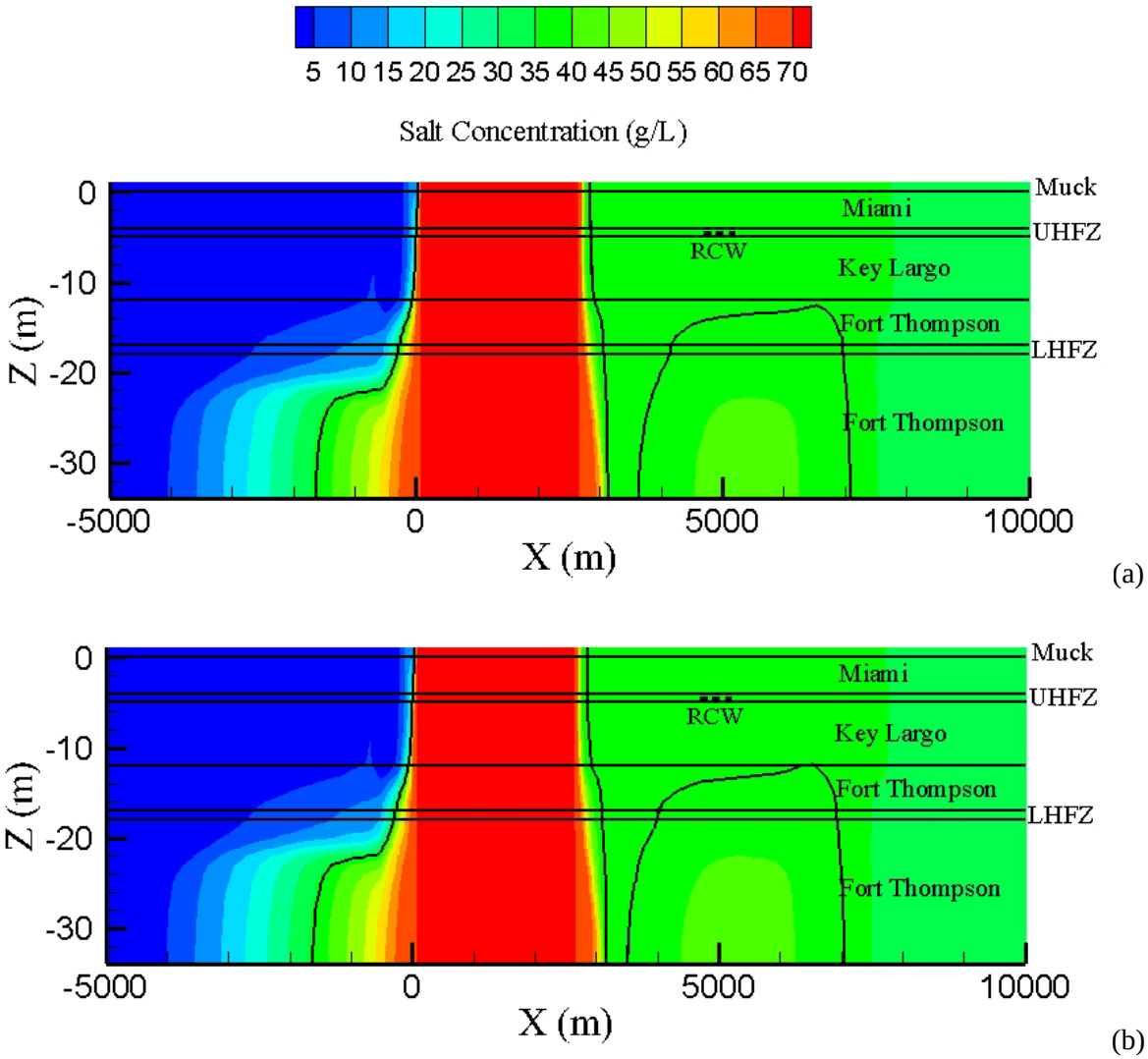


**Figure 9.19**. Salt Concentrations (g/L) for Domain Cross Section at $y$ = 0 m at $t$ = 20 Years for (a) Case 3D-13 (1.5 m sea level rise with RCW pumping) and (b) Case 3D-14 (without pumping)

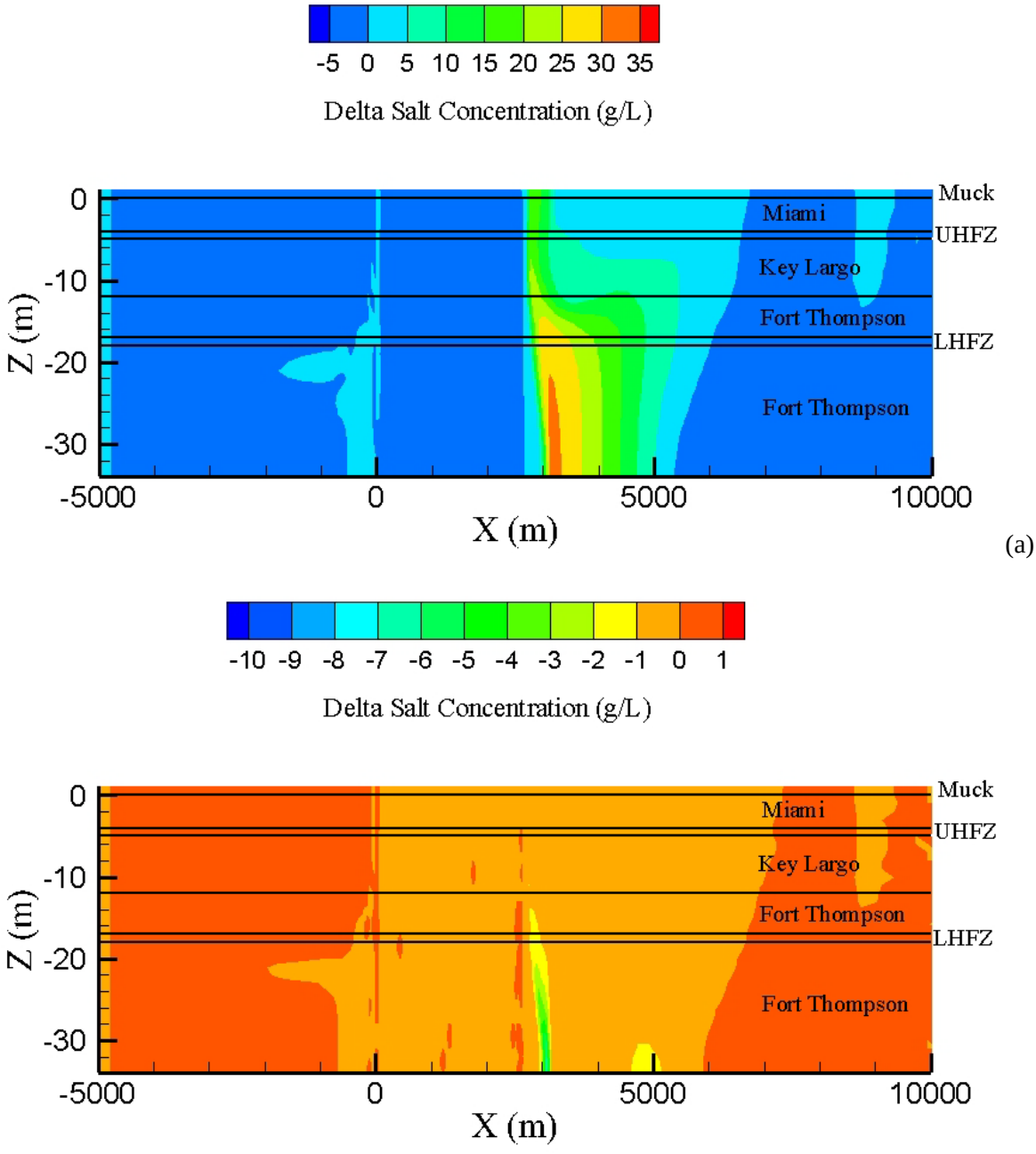


**Figure 9.20**. Differences in Salt Concentrations (g/L) between (a) Base Case (Figure 9.3a) and Case 3D-13 (Figure 9.19a) and (b) Pumping (Case 3D-13) and No Pumping (Case 3D-14) for 1.5 m sea level rise

## 9.12 Cases 3D-15 and 3D-16: 0.5 m Sea Level Rise

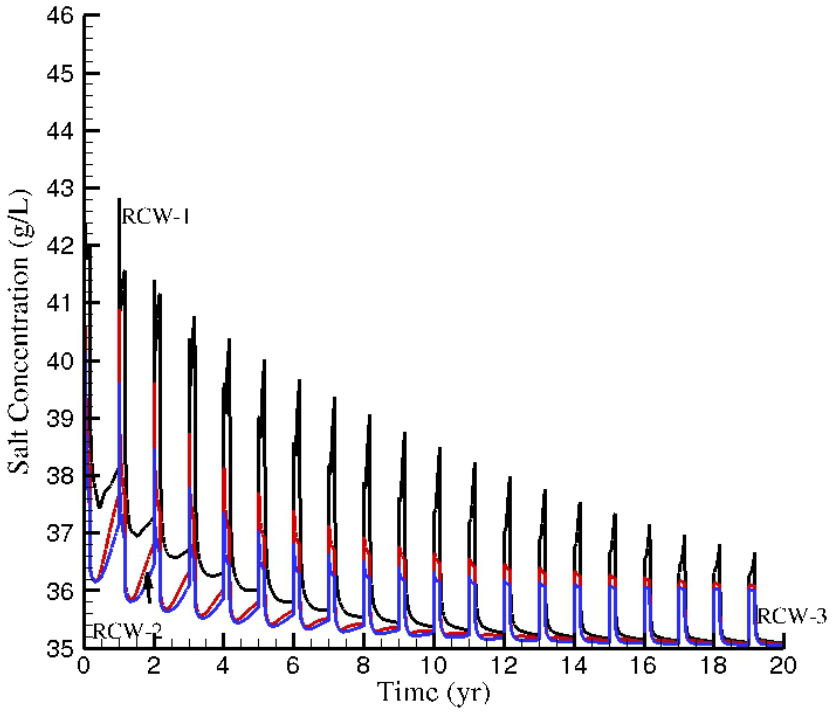


(a)

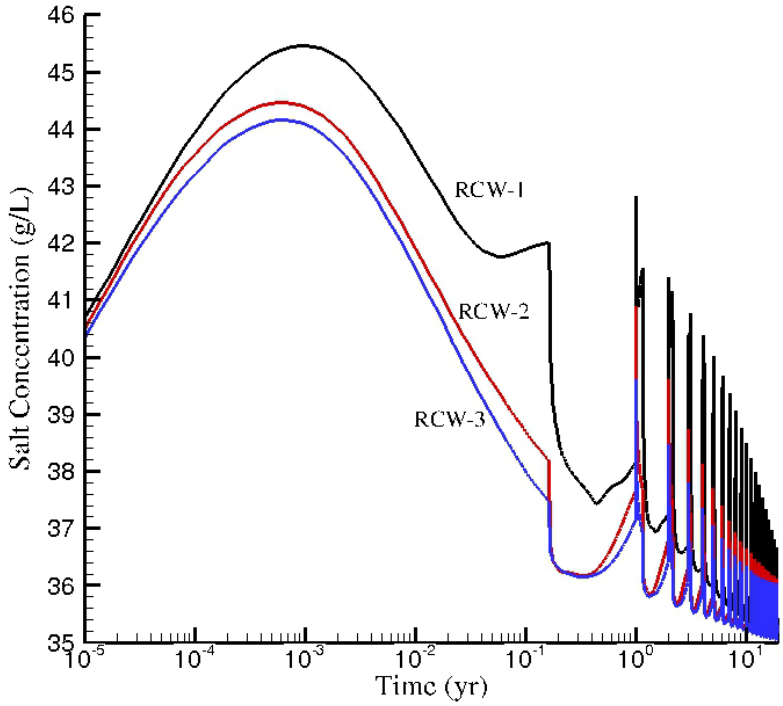


(b)

**Figure 9.21**. Salt Concentrations (g/L) over (a) Linear and (b) Logarithmic Time at RCW-1 (black), RCW-2 (red), and RCW-3 (blue) for Case 3D-15 (0.5 m sea level rise)

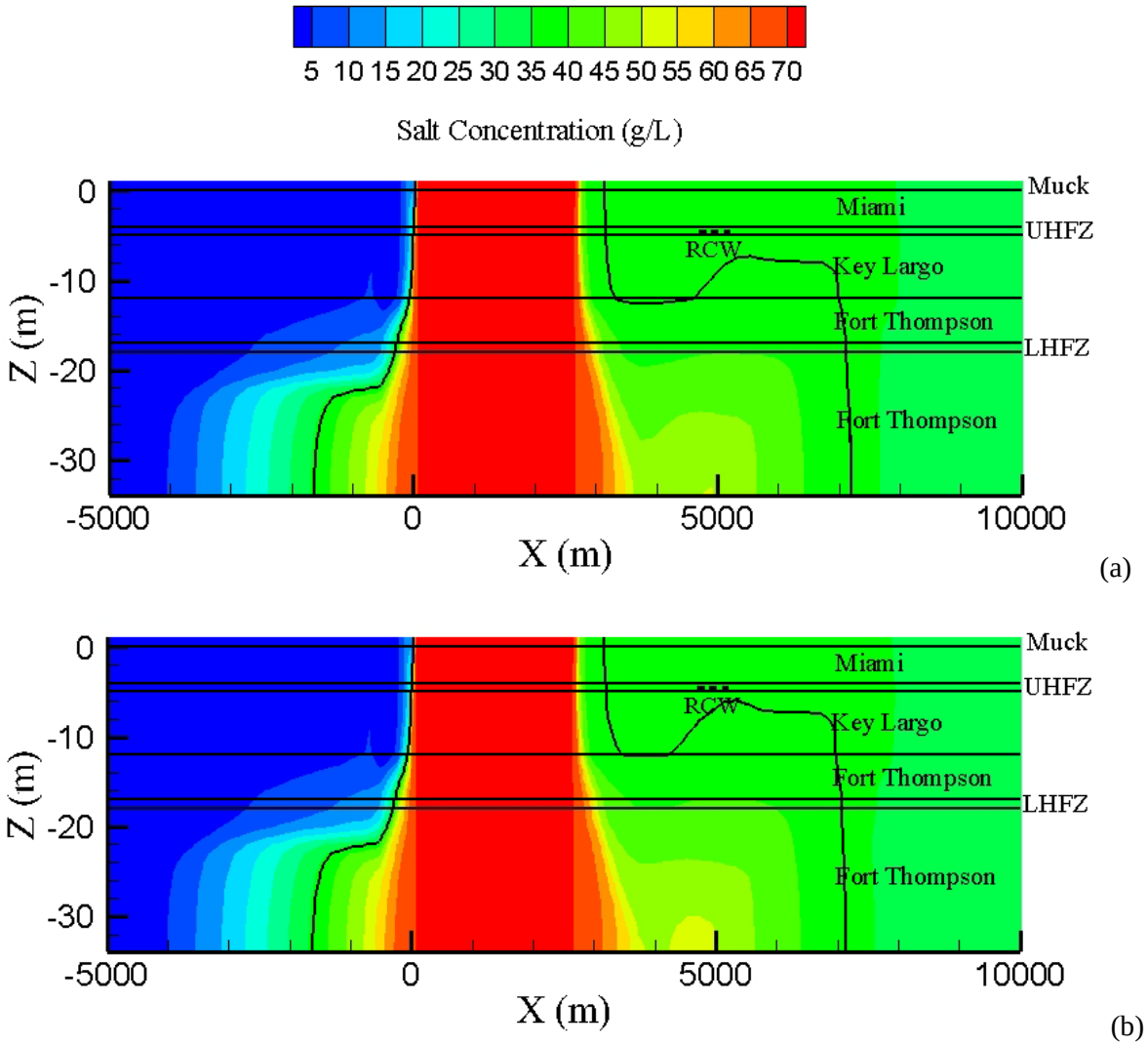


**Figure 9.22**. Salt Concentrations (g/L) for Domain Cross Section at $y$ = 0 m at $t$ = 20 Years for (a) Case 3D-15 (0.5 m sea level rise with RCW pumping) and (b) Case 3D-16 (without pumping)

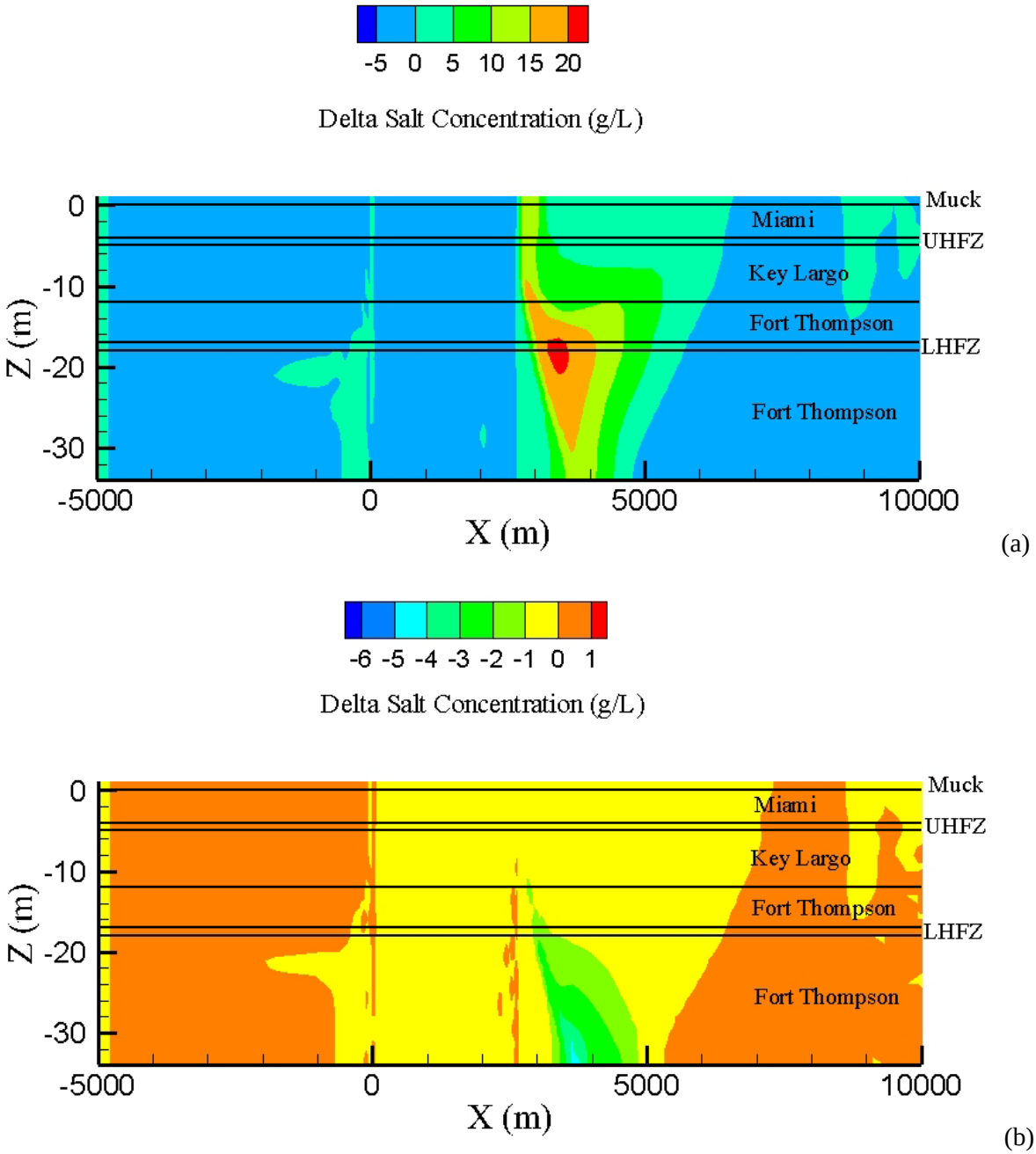


**Figure 9.23**. Differences in Salt Concentrations (g/L) between (a) Base Case (Figure 9.3a) and Case 3D-15 (Figure 9.22a) and (b) Pumping (Case 3D-15) and No Pumping (Case 3D-16) for 0.5 m sea level rise

## 9.13 Case 3D-17: Base Case but with 4 Remediation Wells Continuously Operating at 12,000,000 gal/day

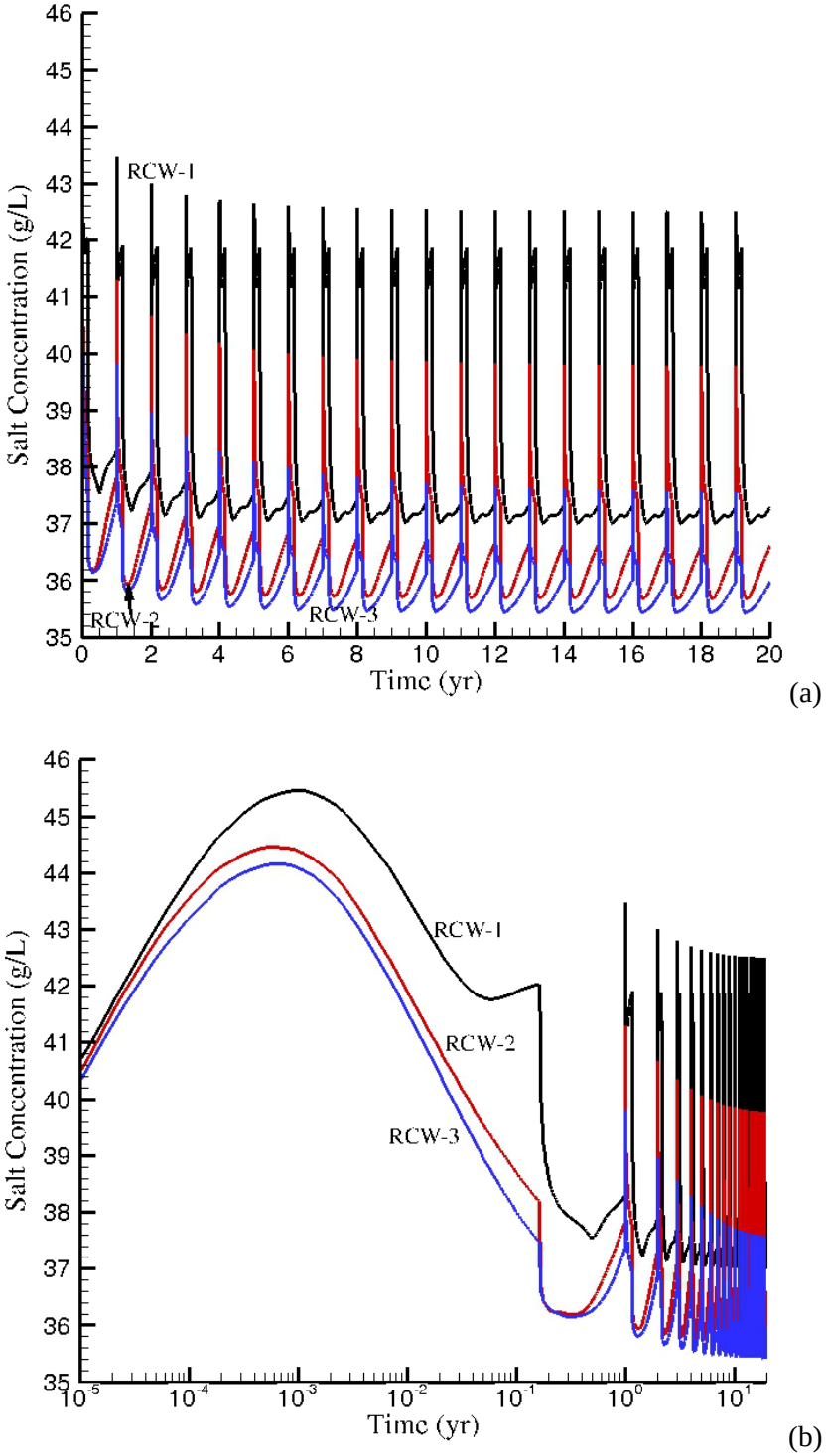


**Figure 9.24**. Salt Concentrations (g/L) over (a) Linear and (b) Logarithmic Time at RCW-1 (black), RCW-2 (red), and RCW-3 (blue) for Case 3D-17 (remediation wells turned on)

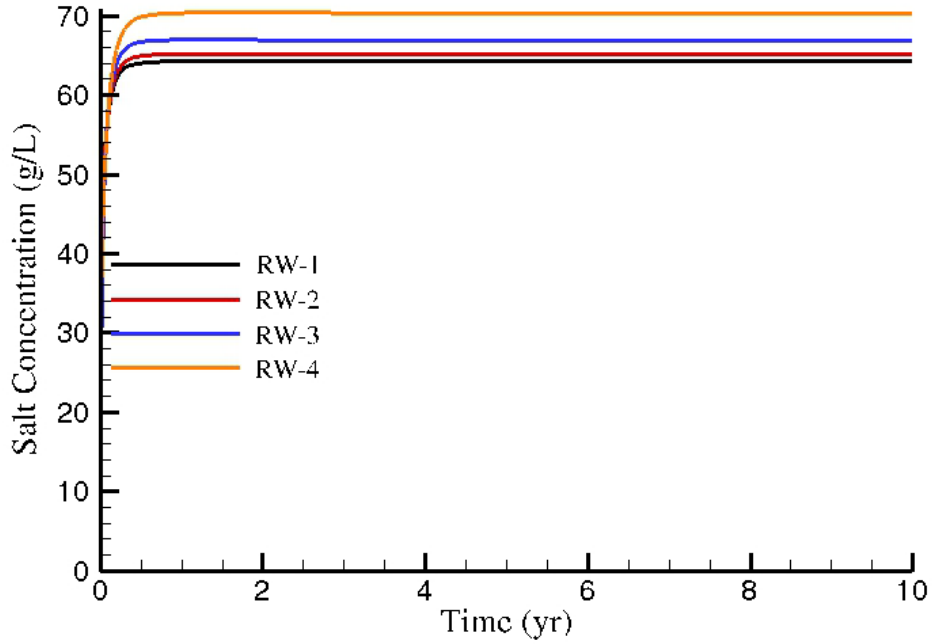


(a)

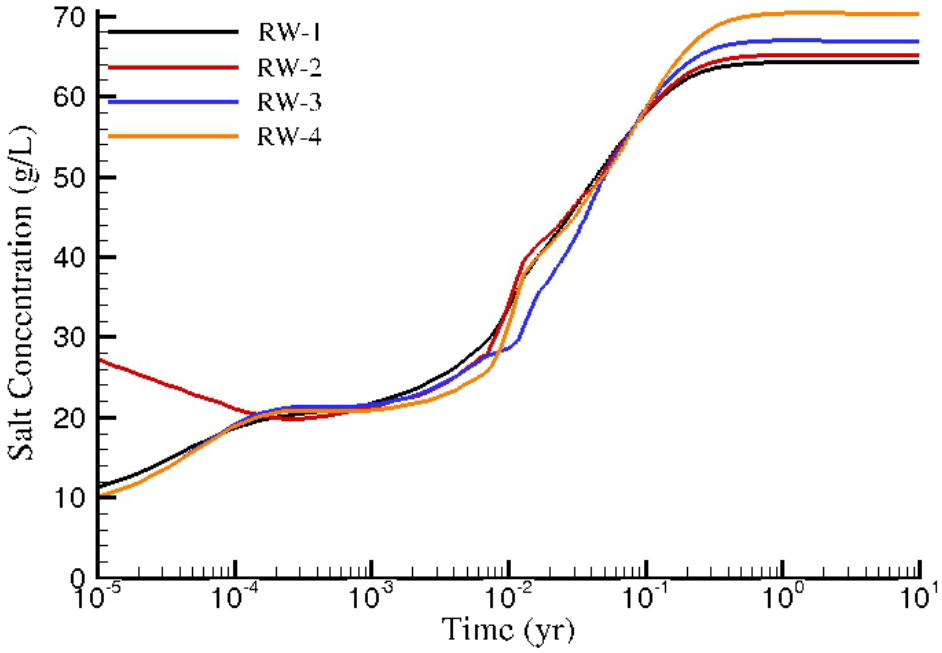


(b)

**Figure 9.25**. Salt Concentrations (g/L) over (a) Linear and (b) Logarithmic Time at Active Remediation Wells for Case 3D-17 (remediation wells turned on)

## 9.14 Case 3-18: Pumping after Refreshing

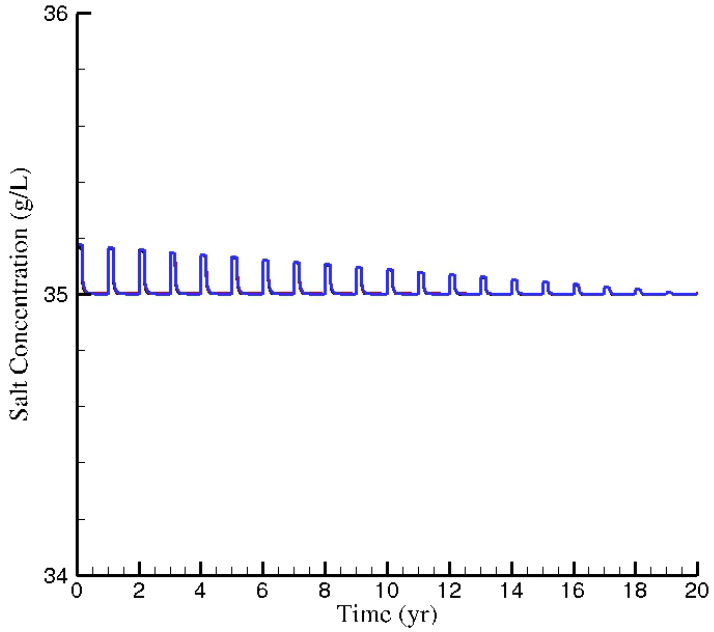


**Figure 9.26**. Salt Concentrations (g/L) over Time at RCW-1 (black), RCW-2 (red), and RCW-3 (blue) for Case 3D-18 (pumping after refreshing)

## 9.15 Case 3D-19: No Pumping after Refreshing

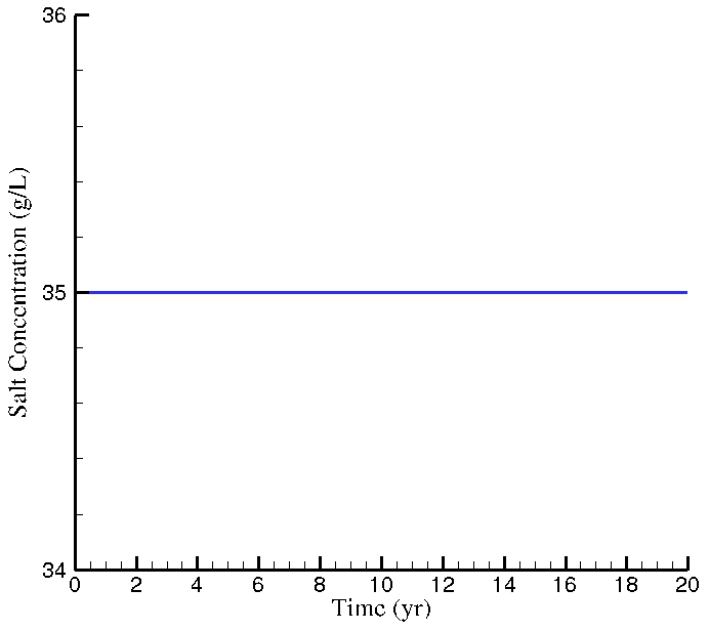


**Figure 9.27**. Salt Concentrations (g/L) over Time at RCW-1 (black), RCW-2 (red), and RCW-3 (blue) for Case 3D-19 (no pumping after refreshing)

## 9.16 Case 3D-20: Pumping and Sea Level Rise after Refreshing

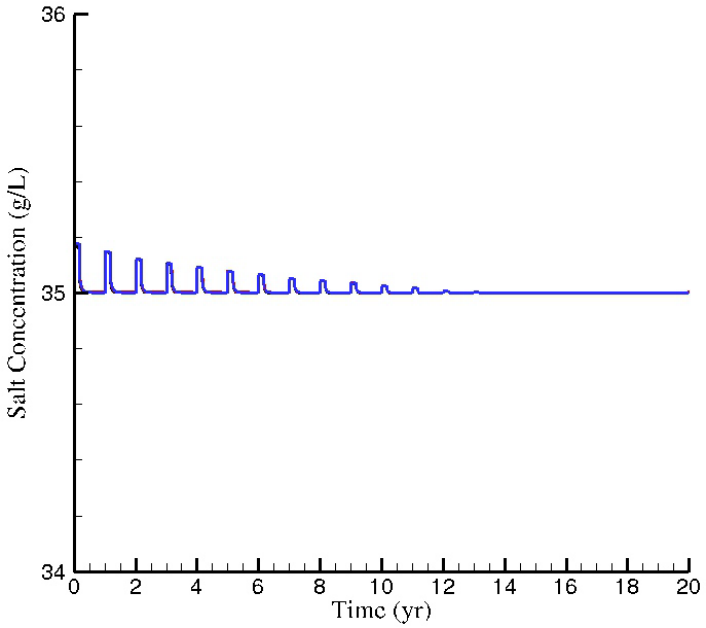


**Figure 9.28**. Salt Concentrations (g/L) over Time at RCW-1 (black), RCW-2 (red), and RCW-3 (blue) for Case 3D-20 (pumping and sea level rise after refreshing)

## 9.17 Case 3D-21: Pumping with Decreased West Boundary and L-31E Canal Heads, and Sea Level Rise

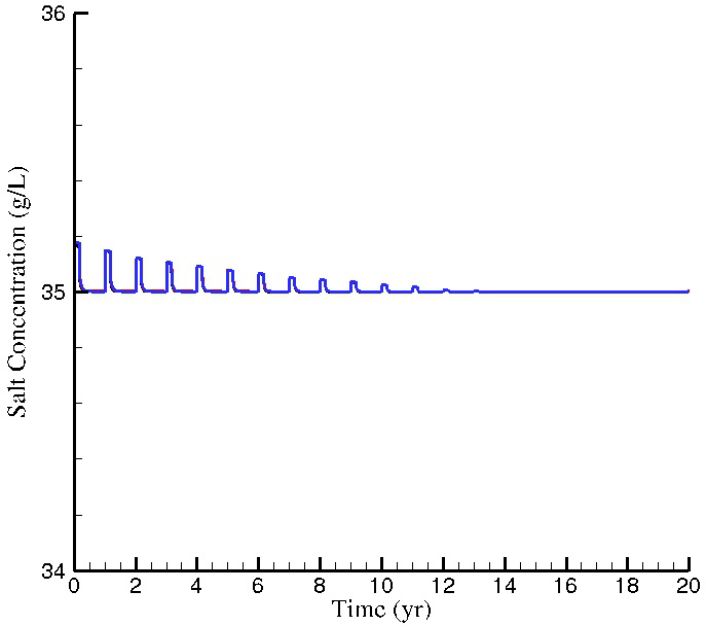


**Figure 9.29**. Salt Concentrations (g/L) over Time at RCW-1 (black), RCW-2 (red), and RCW-3 (blue) for Case 3D-21 (pumping, sea level rise, decreased west boundary head, increased CC head, after refreshing)

## 9.18 Case 3D-22: Pumping and CCS Operation with 34 g/L in Pristine Aquifer

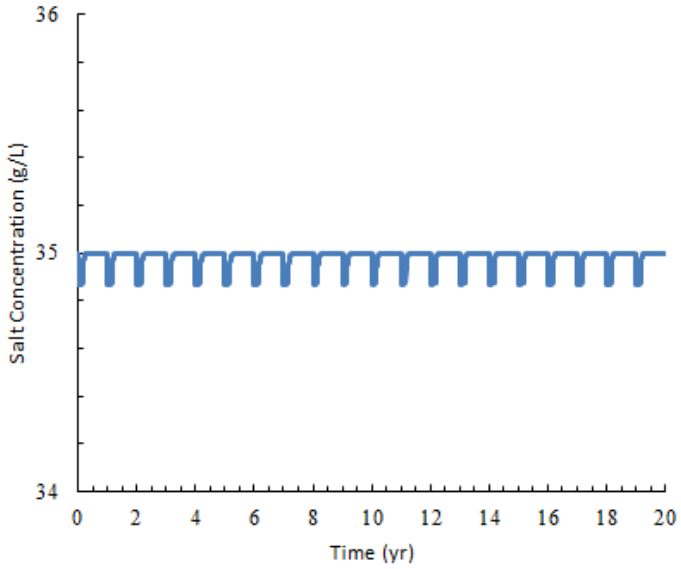


Figure 9.30.Salt Concentrations (g/L) over Time at RCW-1 (black),RCW-2 (red), and RCW-3 (blue) for Case 3D-22 (pumping and CCS operation with 34 g/L in pristine aquifer)

# 10.0 Discussion

Numerical models are mathematical representations of complex processes occurring in three dimensions over time. As discussed in the introduction of this report, the appropriate role of a numerical model is to test assumptions of the behavior of complex systems. Even running a numerical model numerous times with different parameters cannot compensate for all uncertainties.

Reclaimed water would be the primary source of cooling water for the proposed reactors. Saline water from the RCWs beneath Biscayne Bay would only be used when reclaimed water is not available in sufficient quantity or quality, and its use would likely be limited to a maximum of 60 days per year under the State of Florida Conditions of Certification (COCs; State of Florida 2014). Neither the reclaimed water nor the RCWs water provides a safety function. Therefore, the proposed units would be able to remain safe if both sources of water were lost. The review team determined that the primary reclaimed water source is reliable because of the need for Miami-Dade County to dispose of large volumes of treated water that now go to the ocean. Therefore, it is likely that the RCWs would be used less than the 60 days per year. Based on the modeling efforts described in the draft EIS, more than 90% of the water pumped when the RCWs are operating is expected to come from Biscayne Bay, and small amounts are expected to come from the hypersaline plume beneath the cooling canals, the inland part of the Biscayne aquifer, and the drainage canals.

2D and 3D simulations of the Turkey Point CCS subsurface were conducted to assess hypersaline saltwater behavior emanating from the CCS. The 2D simulations were conducted to investigate the effects of CCS salinity, L-31E Canal head, Interceptor Ditch head, boundary conditions, and sea level rise. The 3D simulations were completed to evaluate potential impacts of RCW pumping on the movement of water between the CCS, the underlying Biscayne aquifer, and the Biscayne Bay.

The main observations derived from conducting the 2D simulations are as follows:

- CCS operation with warm 70 g/L hypersaline water leads to the development of a large subsurface plume. The shape of the plume is affected by unstable density-driven flow as the plume extends farther west and east in the Fort Thompson formation at the bottom of the aquifer.
- Temperature effects are less pronounced than the concentration effects because of energy transfer from the infiltrating fluid with to the subsurface matrix and thermal diffusion. Further, for the range of temperatures and salinities considered, salinity not temperature is the dominate factor in the density of the water.
- Reducing the CCS salt concentration leads to a stable displacement of hypersaline water from the CCS to the subsurface. Some of the original hypersaline water migrates to the west and east primarily in the Fort Thompson formation.
- Increasing the hydraulic head in the L-31E Canal limits westward migration of the hypersaline plume. The effects are visible throughout the depth of the aquifer.
- Increasing the west boundary hydraulic head (indicative of increased recharge) results in a compression of the hypersaline plume at the west side of the CCS. Decreasing the west boundary hydraulic head (indicative of reduced recharge) has the opposite effect and leads to additional migration of the hypersaline plume in the western direction.
- During sea level rise, infiltrating saltwater from the Biscayne Bay pushes the hypersaline water toward the CCS subsurface. Over time, the interface between hypersaline water originating from the CCS and seawater becomes sharper and more vertical.

The main observations derived from conducting the 3D simulations are as follows:

- Periodic extraction using the RCW system leads to fluctuating salt concentrations in the wells. During pumping, the concentrations initially increase because of advective transport of hypersaline water through the UHFZ. The concentrations then decrease with continued pumping because of the influence of extracted Biscayne Bay saltwater. Between pumping episodes, the concentrations at RCW location in the UHFZ slightly increase because of diffusion of hypersaline water eastward. The well salt concentrations do not change significantly from year to year.
- RCW pumping increases the concentration gradients between the hypersaline plume below the CCS and Biscayne Bay saltwater in the upper parts of the aquifer and removes some of the hypersaline water from the Fort Thompson formation.
- The extracted volumes originate largely from the Biscayne Bay (>95%).
- Pumping rate reduction (up to 10% of maximum) and duration reduction (50%) do not considerably influence well concentrations. This result indicates that the proposed RCW operation with a 86,400 gal/min withdrawal rate over 60 days per year completely dominates flow and transport adjacent to the RCWs.
- Boundary condition modifications (i.e., L-31E Canal head and west boundary head increases) applied to the west of the CCS do not influence RCW extraction behavior.
- Seawater rise in the Biscayne Bay leads to decreasing RCW saltwater concentration over time because the increasing Biscayne Bay hydraulic head displaces hypersaline water toward the CCS subsurface.
- Operation of remediation wells in the LHFZ below the Interceptor Ditch does not influence extracted RCW salt concentrations. Salt concentrations in the remediation wells are predicted to increase to CCS levels within a year.
- Freshening of the CCS surface water results in reduced RCW salt concentrations with relatively minor (<1 g/L) fluctuations.

The numerical modeling described in this report provides sufficient evidence that limited pumping of the RCWs as a backup water supply is unlikely to cause a noticeable change in the existing extent of saltwater intrusion or to reduce the flow of water that is relatively fresh into Biscayne Bay compared to the variability that occurs under current conditions. However, the review team recognizes that uncertainties remain in the impact analysis because it is impossible to have complete knowledge of the hydrologic system and because future operational and environmental conditions are not known with certainty. A virtually limitless number of future scenarios are plausible. The sources of uncertainty in the RCW analysis include heterogeneity in subsurface parameters, lack of experience with RCW systems in carbonate strata, and uncertainty in the potential need for using the backup water supply. Uncertainties in the future site environment include possible freshening of the IWF cooling canals, possible remediation of the subsurface hypersaline plume, and the magnitude and rate of future sea level rise.

These uncertainties require the review team analyst to be circumspect about relying solely on numerical models, and lead to the fact that even the general conservatism adopted in the analysis does not ensure that the analysis is bounding for all future conditions. Because of this, the review team does not rely solely on the output of one or more numerical model(s). In this assessment, the analyst used models to test possible effects of changes in the affected environment and uncertainty in some subsurface parameters. This information was combined with the geography of the RCW field (such as the relatively short distance from the laterals to the bottom of Biscayne Bay relative to the distance from the laterals to

the Homestead well fields), the conceptual model of key processes (e.g., density impacts on potentiometric surface from salinity differences), and the reasonably foreseeable requirement of a monitoring program with mitigation options. The review team determined that the monitoring proposed in the initial COCs related to the RCW construction and operation would be sufficient to detect unexpected behavior in a timely manner. While all possible mitigations are not detailed at this time, in accordance with the COC, the review team considers the ultimate mitigation of ceasing operation of the RCWs to be a practice that would ensure prevention of any impacts in a timely manner. "When harm occurs, or is imminent, SFWMD [South Florida Water Management District] will require Licensee to modify withdrawal rates or mitigate the harm" (State of Florida 2014). If reclaimed water is not available and the 60-day limitation on RCW pumping is exhausted, the plant can be safely shut down. There is no safety function provided by either cooling water source.

# 11.0 Conclusion

Some perturbations of the baseline boundary conditions can result in significantly altered environmental baselines. However, although the operation of the RCWs would change the incremental impacts of the RCWs on the salinity distribution of the aquifer, the alterations all would remain at levels that may not be detectable except within the immediate vicinity of the RCWs. The numerical model analysis confirms the slight eastward movement of hypersalinity assumed in the conceptual model caused by the operation of the RCWs, but it does not demonstrate any plausible upward impelling force above the RCWs that would result in hypersalinity moving into Biscayne Bay as a result of the RCWs. As the review team has acknowledged in the EIS, when the water surface elevation in the cooling canals exceeds the elevation in the Bay, the water will follow the gradient of the impelling force into the Bay and may contribute to salinity there. Both of these effects also apply for other tracers, including nutrients and tritium.

Although the primary focus of this review is on the incremental impacts of the RCWs on the Biscayne Bay and the Biscayne aquifer, the review team acknowledges the cumulative impacts of other changes including those from sea level rise and possible future regulatory actions. While the scenarios considered in this analysis tended to be bounding for sea level rise and possible regulatory actions, the analysis also provides a basis for assessing cumulative impacts. The review team has no jurisdiction over the proposed regulatory actions considered and assumes that mitigation actions proposed by the state and county agencies would improve the baseline environment. As long as the incremental effect of the RCWs remains minor, the cumulative effects will also be minor.

The minor localized alterations in salinity distribution allow the review team to infer that the operation of the RCWs is unlikely to interfere with any of the proposed mitigation actions.

# 12.0 Literature Cited

Cunningham KJ, MC Sukoop, H Huang, PF Alvarez, HA Curran, RA Renken, and JF Dixon. 2009. Prominence of ichnologically influenced macroporosity in the karst Biscayne aquifer: stratifrom “super-K” zones. *Geological Society of America Bulletin* 121:164–180.

FPL (Florida Power& Light Company). 2014a. Letter from M.K. Nazar to NRC, dated October 29, 2014, regarding "Proposed Turkey Point Units 6 and 7 Combined License Application Submittal 13, Submittal of the Annual Update of the COL Application—Revision 6 and the Semi-Annual Update of the Departures Report." L-2014-316, Juno Beach, Florida.

FPL (Florida Power& Light Company). 2014b. Turkey Point Plant, Units 6 and 7 COL Application, Part 3 – Environmental Report. Revision 6, Juno Beach, Florida.

FPL (Florida Power & Light Company). 2015. Turkey Point Plant Units 6 and 7 COL Application, Part 2 – Final Safety Analysis Report. Revision 7, Juno Beach, Florida. Accession No. ML15301A339.

Hughes JD, CD Langevin, and L Brakefield-Goswani. 2010. Effect of hypersaline cooling canals on aquifer salinization. *Hydrogeology Journal* 18:25–38.

Millero FJ and F Huang. 2009. The density of seawater as a function of salinity (5 to 70 g/kg) and temperature (273.15 to 363.15K). *Ocean Science* 5: 91–100.

National Environmental Policy Act of 1969, as amended. 42 U.S.C. § 4321 et seq.

NRC (U.S. Nuclear Regulatory Commission). 2016. Final Environmental Impact Statement for Combined Licenses (COLs) for Turkey Point Nuclear Plant Units 6 and 7. (In preparation)

State of Florida. 2014. "Final Order on Certification, In Re: Florida Power & Light Company Turkey Point Units 6 & 7 Power Plant Siting Application No. PA 03–45A3." State of Florida Siting Board, OGC Case No. 09–3107, Division of Administrative Hearings, Case No. 09–03575–EPP, Tallahassee, Florida.

White MD and M Oostrom. 2006. *STOMP – Subsurface Transport Over Multiple Phases, Version 4.0 – User’s Guide*. PNNL-15782, Pacific Northwest National Laboratory, Richland, Washington.

Pacific Northwest
NATIONAL LABORATORY

*Proudly Operated by* **Battelle** *Since 1965*

U.S. DEPARTMENT OF
ENERGY

902 Battelle Boulevard
P.O. Box 999
Richland, WA 99352
**1-888-375-PNNL** (7665)

***www.pnnl.gov***